LASER-INDUCED FLUORESCENCE AND SYNTHETIC JET FUEL ANALYSIS IN THE ULTRA COMPACT COMBUSTOR

THESIS

Aaron C. Drenth, Captain, USAF

AFIT/GAE/ENY/09-D03

DEPARTMENT OF THE AIR FORCE
AIR UNIVERSITY

AIR FORCE INSTITUTE OF TECHNOLOGY

Wright-Patterson Air Force Base, Ohio

AFIT/GAE/ENY/09-D03

LASER-INDUCED FLUORESCENCE AND SYNTHETIC JET FUEL ANALYSIS IN THE ULTRA COMPACT COMBUSTOR

THESIS

Presented to the Faculty

Department of Aeronautics and Astronautics

Graduate School of Engineering and Management

Air Force Institute of Technology

Air University

Air Education and Training Command

In Partial Fulfillment of the Requirements for the

Degree of Master of Science in Aeronautical Engineering

Aaron C. Drenth

Captain, USAF

December 2009

AFIT/GAE/ENY/09-D03

LASER-INDUCED FLUORESCENCE AND SYNTHETIC JET FUEL ANALYSIS IN THE ULTRA COMPACT COMBUSTOR

Aaron C. Drenth

Captain, USAF

December 2009

Approved:

_____	_____
LtCol Richard D. Branam, USAF (Chairman)	date
_____	_____
Dr. Paul King (Member)	date
_____	_____
Dr. Mark Reeder (Member)	date

Abstract

The Ultra-Compact Combustor (UCC) is currently under investigation at the Air Force Institute of Technology (AFIT) and Air Force Research Laboratory's Propulsion Directorate. The combustor is a small-scale, axi-symmetric, atmospheric pressure, laboratory combustor with an outer circumferential cavity in which the flame is stabilized by a highly accelerated swirled flow. UCCs will enable aero gas turbine reheat cycle engines and significantly shorten conventional aero gas turbine engines. The experiments of this work utilized the AFIT small-scale combustion diagnostics facility, investigating a sector model of the UCC. The research objectives were to perform an addition to the COAL lab laser diagnostic system, validation of this system, and characterization of a small-scale UCC sector model using hydrogen, propane and traditional as well as synthetic jet fuel. Two-line planar laser induced fluorescence (PLIF) of a laminar premixed hydrogen-air flame validated the laser system. OH species concentrations were measured. Flame temperatures between 1650 and 2400 K were measured with a two-line fluorescence technique using different transitions in the (1,0) band of the OH (A-X) electronic transition system with 5-8% error achievable. Comparisons to existing research prove accuracy. Instantaneous temperature measurements were determined with lower confidence in results. Flame location studies revealed swirl within the UCC main channel increasing mixing. UCC and Hencken burner operational procedures were updated and improved where necessary. A UCC sectional model re-design is needed to equalize cavity exit areas for curved and straight sections. An initial comparison of synthetic jet fuel and traditional jet fuel emissions data shows higher combustion efficiency with synthetic fuel. Future work will involve using PLIF to further study the cavity-vane interactions of the UCC.

Acknowledgements

I would like to thank my wife for all her love and support and also my family and friends for their support and encouragement during my graduate program.

Thanks to my excellent advisor, Lieutenant Colonel Richard Branam - he taught me a great deal about combustion and kept me on track with my research. Without him, my early graduation may not have been possible. I am greatly indebted to lab technician John Hixenbaugh, laser diagnostic expert Jacob Schmidt and COAL lab intern Michael Boehler for all of their hard work and their assistance in my research.

Finally and above all, I want to thank the Lord - my guide through this great adventure!

Aaron Drenth

Table of Contents

Page

List of Figures

Page

List of Tables

Page

List of Symbols

Symbol	
A	Einstein A Coefficient (s^{-1})
A_e	Exit Area (mm^2)
$\mathring{A}$	Angstrom (1×10^{-10} meters)
CO	Carbon Monoxide
CO_2	Carbon Dioxide
C_2H_4	Ethylene
C_3H_8	Propane
$C_{12}H_{26}$	n-dodecane
C_xH_y	hyrdrocarbon
g	Gravitational constant (m/s^2)
H_2	Hydrogen
H_2O	Water
H_C	Lower heater value (J/kg)
H_Z	Hertz
k	Boltzmann's Constant $\left(\frac{m^2 kg}{s^2 K}\right)$
M	Molecular Mass (kg/kmol)
N_2	Nitrogen
NO	Nitric Oxide
NO_X	Oxides of Nitrogen
NO_2	Nitrogen Dioxide
OH	Hydroxyl Radical
O_2	Oxygen
Q	Quenching Rate (s^{-1}), heat (J)
ρ	Density (kg/m^3)
S	Entropy (J/(kg K))
S_B	Buoyant flame speed (m/s)
ϕ	Equivalence Ratio

σ	molecule cross section $\left(\overset{o}{A}^{2} \right)$
x	number of carbon atoms
y	number of hydrogen atoms
μm	micrometer

List of Abbreviations

Abbreviation	
AFIT	Air Force Institute of Technology
AFRL	Air Force Research Laboratory
AR	Antireflective
CAI	California Analytical Instruments
CARS	Coherent Anti-Stokes Raman Spectroscopy
CFD	Computational Fluid Dynamics
COAL	Combustion Optimization and Laser
CT	Constant Temperature
DOD	Department of Defense
DOE	Department of Energy
EI	Emissions Index
f	focal length
F	Fahrenheit
FCU	Frequency Conversion Unit
FDU	Frequency Doubling Unit
FT	Fischer-Tropsch
FWHM	Full-Width, Half-Maximum
HPT	High Pressure Turbine
IHPTET	Integrated High Performance Turbine Engine Technology
ICCD	Intensifying Charge Couple Device
IGV	Inlet guide vanes
ISSI	Innovative Scientific Solutions Inc.
ITB	Inter-stage turbine burner
JP	Jet Propellant
K	Kelvin
kg	Kilogram
LDV	Laser Doppler Velocimetry
LIF	Laser-Induced Fluorescence
LII	Laser-Induced Incandescence

LPT	Low Pressure Turbine
m	meter
min	minute
ml	milliliter
mm	millimeter
msec	millisecond
mJ	milli-Joule
MW	Molecular Weight
NASA	National Aeronautics and Space Administration
Nd:YAG	Neodymium-doped yttrium aluminum garnet
nm	nanometer
nsec	nanosecond
PI	Princeton Instruments
PIV	Particle Imaging Velocimetry
PLIF	Planar Laser Induced Fluorescence
ppm	parts per million
ROI	Region of interest
RVC	Radial Vane Cavity
S	Synthetic
SAE	Society of Automotive Engineers
SLPM	Standard Liter Per Minute
ST	Specific thrust
T	Temperature
TDLAS	Tunable Diode-Laser-Based Absorption Spectroscopy
TSFC	Thrust specific fuel consumption
TVC	Trapped Vortex Combustion
UCC	Ultra Compact Combustor
UHC	Unburned Hydrocarbons
UV	Ultraviolet
UVT	Ultraviolet Tracking
VAATE	Versatile Affordable Advanced Turbine Engines

VI	Virtual Instrument
2-D	Two dimensional
3-D	Three dimensional

LASER-INDUCED FLUORESCENCE AND SYNTHETIC JET FUEL ANALYSIS IN THE ULTRA COMPACT COMBUSTOR

I. Introduction

I.1 Motivation

As the world's use, demand, and cost of energy in terms of economic and environmental impact steadily increase, the efficient use of energy is more desirable than ever. Competition for the world's energy will also increase. In 2007 the world's energy consumption increased by 2.4%, with China's share of the world energy consumption growth at 52%.[1] The U.S. military is the single largest consumer of energy in the world with the Air Force accounting for more than 50% of the energy consumed, spending more than $7 billion per year on energy with more than 80% for aviation fuel.[2] The profound dependence on these fuels whose cost continues to rise shows no sign of dissipating in the near future. As a result, it is imperative future gas turbine engine development focus on technological advancements quantified by increased thrust-to-weight ratio as well as combustion efficiency and decreased thrust specific fuel consumption (TSFC). In addition, environmental concerns demand decreased exhaust noise and pollutant emissions. If the U.S. military is to maintain global air superiority and the commercial aircraft industry is to remain economically stable, a focus must be on the advancement of gas turbine engine technology.

Even though the need for greater advancements in propulsion technology is high, the investment in gas turbine engine research has considerably declined over the past years.[3] A continued decline in research could jeopardize the military's capability to remain air dominant in the future. To reverse the decline, the Versatile Affordable

Advanced Turbine Engines (VAATE) initiative, modeled after the highly successful Integrated High Performance Turbine Engine Technology (IHPTET) program, seeks specific improvements in turbine engine technology such as a 200% increase in engine thrust-to-weight ratio, a 25% reduction in engine fuel consumption, and a 60% reduction in engine development, procurement, and life cycle maintenance cost.[3] To promote continued advancement in gas turbine engine technology research, VAATE will be modeled after a prominent characteristic that made IHPTET so successful – an integrated technology plan between the Department of Defense (DOD), National Aeronautics and Space Administration (NASA), Department of Energy (DOE), academia and industry.

One engine advancement currently in development as part of the VAATE initiative is the Ultra-Compact Combustor (UCC), potentially a partial problem solution. By making significant changes in airflow direction and fuel mixing in the combustor of a gas-turbine engine, the UCC will greatly reduce the axial length required for efficient combustion. This has the potential for two major advantages: First, the shortened combustor placed after the compressor section of the engine circumferentially over the turbine increases the thrust-to-weight ratio. More specifically, it makes use of the inter-stage turbine burner (ITB) concept. The ITB is a reheat cycle concept locating an additional combustor between the high and low-pressure turbine stages improving thermodynamic cycle efficiencies. Secondly, the UCC as a standard combustor positioned between the compressor and turbine reduces the weight and length of the engine. Another benefit is the circumferential design of the UCC features a trapped vortex combustor (TVC), enhanced airflow capability, and greater fuel mixing to increase combustion efficiency.[4]

As a parallel to the research towards the advancement of engine technology, the U.S. Air Force has sought other ways to reduce its dependence on foreign sources of petroleum. The Air Force is currently midway through a certification process of new Fischer-Tropsch (FT) process fuels.[5] Various jet fuels produced from synthesis gas ($CO+H_2$) via FT technology are currently under close study for their suitability for aircraft. Production of synthesis gas can be from coal, natural gas, or other carbon-containing materials. These new fuels will provide a reliable domestic source of alternative fuel choices for the engines of tomorrow.

I.2 Problem Statement

The UCC is in its early stages of design and development. Theoretically, various designs of the UCC have shown potential in accomplishing these improvements through extensive research using computational fluid dynamics (CFD). Experimental research is needed to accurately prove what interactions actually occur inside the cavity-vane section of the UCC to facilitate these improvements.

One way to quantify these advancements is with state-of-the-art, non-intrusive laser diagnostic techniques such as planar laser-induced fluorescence (PLIF). PLIF can be used to analyze species concentrations, flame temperatures and locations. Before using the PLIF setup on the UCC, a validation of the system should be performed through the study of a laminar premixed flame. A Hencken burner was used for this purpose. Once the laser diagnostic system was validated, it was used to take measurements of interactions inside the small-scale UCC through optically clear quartz windows. Another way to quantify these improvements is through emissions data. Emissions data was captured using a portable emissions analyzer and the data used to calculate combustion

efficiency. Hydrogen, propane, traditional jet propellant (JP-8) fuel and one variant of FT synthetic jet fuel (S-8) was used in the UCC and the results were. Research was performed in the Combustion Optimization and Analysis Laser (COAL) lab located at the Air Force Institute of Technology (AFIT).

I.3 UCC Research Focus Areas

The UCC study being conducted by AFRL and AFIT has three main focus areas. The first is to investigate the effect of body forces on the combustion process in a true UCC design. As mass flow in the cavity is increased, the turbulent Reynolds number in the main flow path has been shown to decrease. Research in this area intends to discover whether the behavior is an effect of body forces or flow shear by holding velocity constant while altering the radius of curvature, thus the G-load. The effects of altering air jet geometry, equivalence ratio, and main airflow velocity will all be investigated.

The second purpose is to investigate the effectiveness of performing Trapped Vortex Combustion in the UCC. Using CFD models supported by experimental data, the best conditions for extracting mass from the cavity into the main flow will be determined. The effect of trapping a vortex in the cavity on performance and range of operation will also be investigated.

Finally, the reactions between the vortex cavity and vane cavity must be observed and understood in order to ensure optimal mass transfer from the vortex cavity to the main flow. CFD studies have focused on variations of the geometry of the radial vanes and their cavities and the effects on combustor performance parameters. These experimental models are based on optimum geometries found using CFD analysis.

I.4 Thesis Objectives

This thesis will focus on advancing the second and third research areas by investigating combustor performance and the cavity-vane interactions. The three objectives of this research was First: Develop a two-line PLIF laser diagnostic tool for the COAL lab that will allow species concentrations and flame temperatures be calculated simultaneously from the collected data. A Hencken burner producing a laminar, pre-mixed hydrogen-air flame was used to calibrate the two-line PLIF diagnostic tool. Once the system was working, results were validated against data collected by previous researchers. Second: Study the UCC using two-line PLIF thermometry and to perform a flame location study using OH PLIF. Third: perform a UCC performance comparison of synthetic vs. traditional fuels and straight vs. curved sections using species concentrations, flame temperatures, emissions and other characteristics.

II. Theory and Previous Research

II.1 Standard Gas Turbine Engine Combustor

A typical gas turbine engine consists of an inlet, compressor, combustor, turbine, and nozzle. The compressor, combustor and turbine are referred to as the gas generator of the engine and are common to the turbojet, turboprop, turbofan, and turboshaft engines. The combustion section makes up a significant portion of the engine as shown in Fig. 1. Its optimal performance is very important to efficient engine operation. The primary goal is to supply high-temperature and high-energy gas to the turbine. The following properties of a gas turbine engine combustor are preferred[6]: total combustion, pressure losses held to a minimum, combustion stability, uniform temperature distribution, short length, small cross section, reduced chance of flameout, relight ability, and operation over a broad range of mass flow rates, pressures, and temperatures.

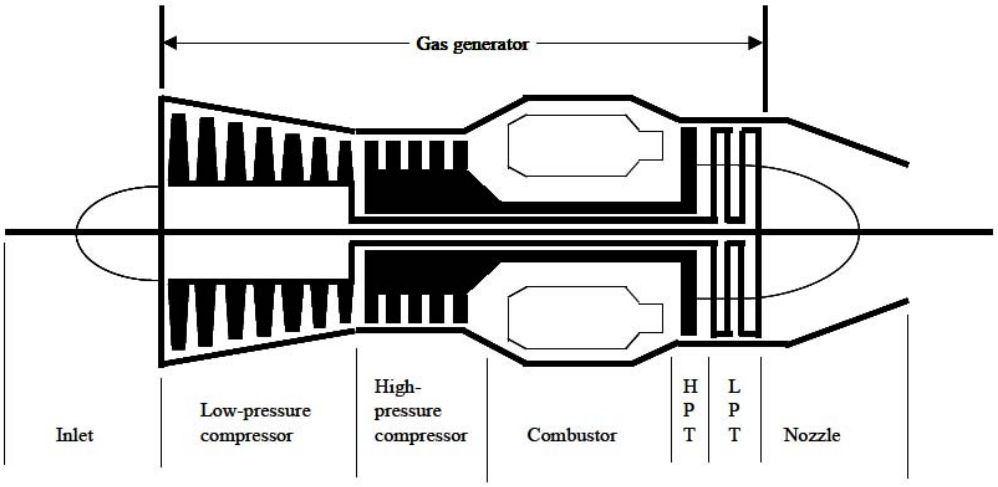

Figure 1. Schematic of a turbojet with dual axial compressor and turbine[6]

A standard combustor contains primary and secondary air mixed with vaporized fuel injected in the axial direction as depicted in Fig. 2.

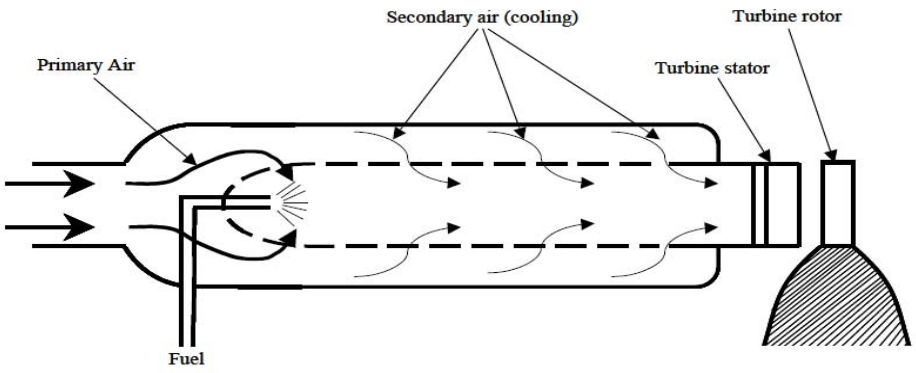

Figure 2. Flow through standard combustor[6]

It is desired for the mixture to burn at a uniform temperature. Combustors designed to operate in this configuration are of the can, annular, or can-annular type. Inside these type chambers, combustion occurs in two zones. In the primary zone, high-temperature, high-pressure air enters from the compressor and flows around fuel injectors spraying atomized liquid-droplet fuel and the combustion process begins.[6] As air circulates around fuel injectors, flame stability is accomplished. The primary zone fuel-air mixture is slightly fuel-rich resulting in higher temperatures and increased emissions such as unburned hydrocarbons, carbon monoxide and nitrous oxides. The addition of air creates a fuel-lean mixture in the secondary or dilution zone, providing cooling so the allowable structural temperature limit of the turbine is not exceeded.[6] Since the process occurs in the axial direction, all of the fuel does not have time to totally combust.

Therefore, losses occur in standard combustors resulting in decreased efficiencies and increased emissions.

Combustors create heat and entropy (*S*) in the flow through chemical reactions, adding energy used by the turbines. This energy drives the compressor as well as any powered systems aboard the aircraft. Figure 3 shows a T-S diagram from the inlet to the exit of a conventionally designed gas-turbine engine. The line from the inlet to point 03 corresponds to the compression section, where in an ideal engine temperature increases but entropy remains constant.

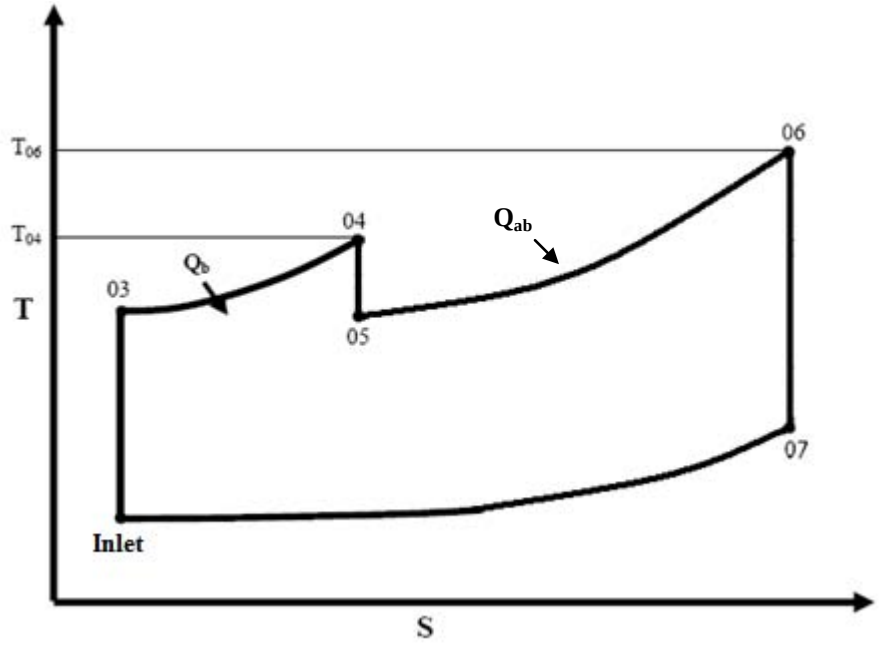

Figure 3. Engine cycle for a typical gas-turbine combustor[7]

In the diagram, Q_b represents the heat added by a traditional in-line combustor. Both the temperature and entropy increase during the process. Between points 04 and 05, the turbines draw power from the flow and the temperature decreases. Point 06 represents the condition of the mixture when an afterburner is used to reheat it and provide more thrust.

A major limiting factor for the performance of combustors occurs at point 04, where the temperature after combustion cannot exceed the maximum threshold for the turbine blades.

II.2 Ultra-Compact Combustor Concept

The UCC was developed by the US Air Force Research Laboratory (AFRL) Propulsion Directorate at Wright-Patterson Air Force Base in Dayton, Ohio. The concept of the UCC was inspired by the idea of a constant temperature (CT) cycle gas turbine engine proposed by Sirignano and Liu.[7] The proposed CT cycle is represented by a solid line in Fig. 4 while a dashed line represents a typical engine cycle for a gas turbine engine discussed earlier.

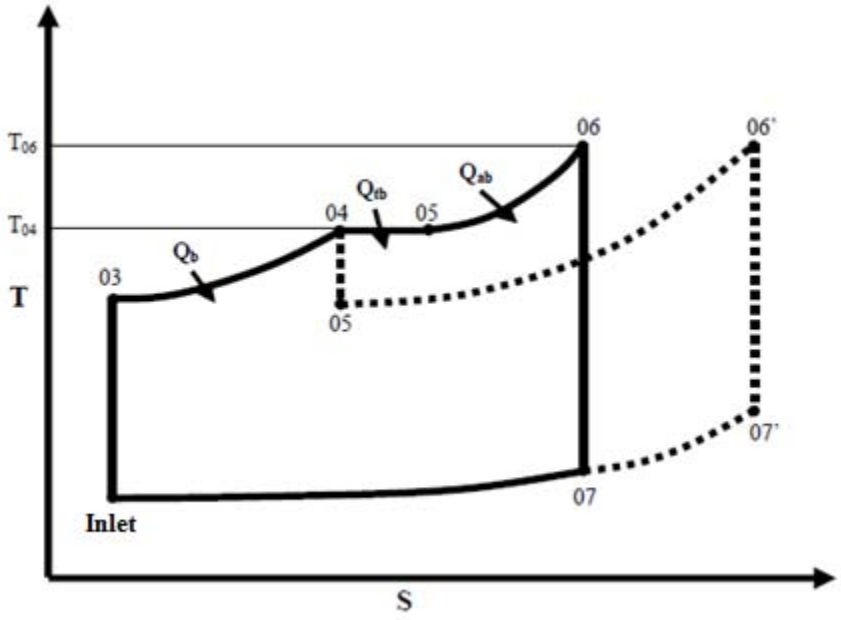

Figure 4. Typical engine cycle (dashed line) and a CT engine cycle (solid line)[7]

Using a CT model, Sirignano and Liu[7] predicted an improvement in specific thrust (ST) of over 50% with little impact on thrust specific fuel consumption (TSFC). The problem

with implementation is that a true CT cycle is virtually impossible because it requires burning inside the rotor. The most practical alternative to achieving a similar effect is an ITB. Since traditional combustors are much too large to fit between turbine stages, the concept of the UCC was created.

The UCC operates like a standard combustor only on a smaller scale. Combustion in the UCC occurs in a cavity that wraps around the circumference of the engine as shown in Fig. 5. The primary zone is the circumferential cavity, and the secondary zone is made up of each of the radial vane cavities.[8] This particular configuration provides for increased residence time for fuel to more completely combust resulting in a decreased amount of unburned hydrocarbons and lowering of the amount of harmful emissions produced. Conventional combustor designs are limited by the fact that combustion reactions require a finite amount of time for completion and the flow through these devices is moving at a finite velocity. By necessity, traditional combustors are long and comprise a significant portion of a gas-turbine engine's volume. The UCC was designed to allow a long residence time of the flame by lengthening its flow path while still significantly reducing the length of the combustion section. The overall goal of the UCC is a reduction in the size of traditional gas turbine combustion devices.

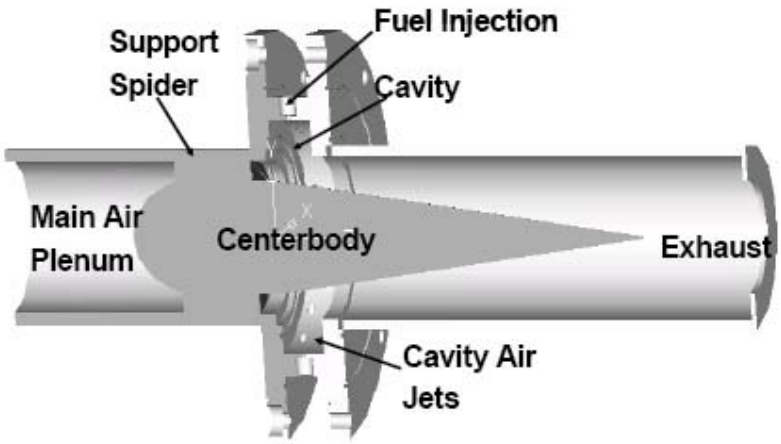

Figure 5. UCC cross section – radial vane cavities not shown[9]

The UCC concept can be seen in Fig. 5. Air is injected into the cavity through angled inlets to create a highly swirled flow while fuel is injected into the cavity through recessed ports. Flame stability is achieved through trapped vortex combustion (TVC).[4] The swirling fuel and air inside the cavity create a high g-load on the mixture increasing the mixing thus reducing the time required for combustion.[10] The cavity is open to the main axial flow. Airfoils on the centerbody in Fig. 5 simulate inlet guide vanes (IGV) or stator blades. In each airfoil, there is a radial vane cavity (RVC) establishing an intermediate combustion zone helping draw the mass from the cavity into the main flow by creating a pressure gradient. The guide vanes and RVCs can be seen in Fig. 6.

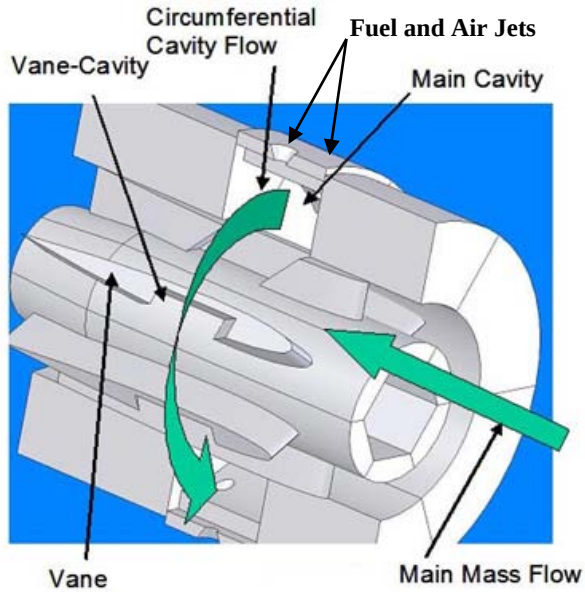

Figure 6. Detail of the UCC

The AFRL Propulsion Directorate has built a research model of the UCC design shown in Fig. 6; this model is found in their Atmospheric-Combustion Research Facility, shown in Fig. 7.

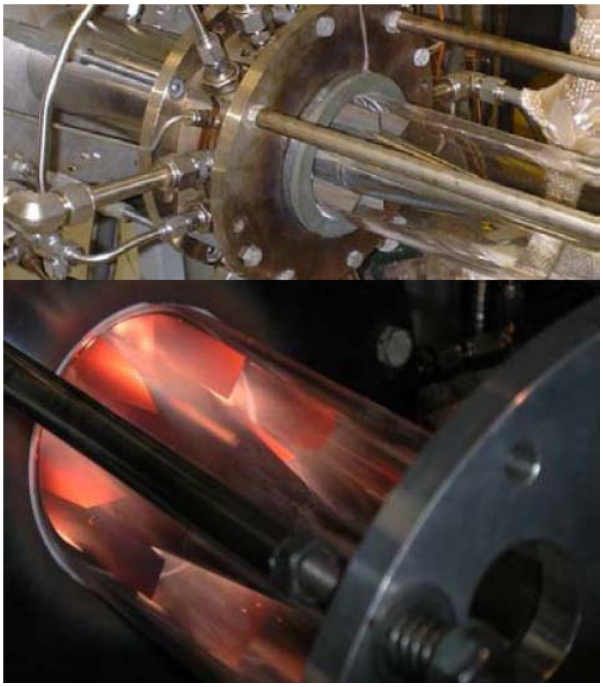

Figure 7. AFRL UCC[11]

A small-scale sectional model of a UCC made of stainless steel has been designed and built for combustion research in the COAL lab at AFIT. The sectional rig has been designed to allow greater optical access to study the flow fields and combustion within the UCC eliminating the geometry constraints of AFRL's full-scale UCC rig. The supporting equipment of the COAL lab for the small-scale model includes main and secondary airflow. They both can be heated to temperatures of up to 500 Kelvin (K) to better simulate conditions inside the engine. The main airflow has delivery rates up to 7 kg/min; secondary airflow has delivery rates up to 2 kg/min.[13] The small-scale model UCC was made $1/6^{th}$ scale based on these airflow rates.[14] The AFIT UCC uses both gaseous and liquid fuels. Up to 5.67 ml/s of JP-8 or other liquid fuel can be delivered to the combustor using a dual syringe pump with nanoliter precision. High precision mass flow controllers meter hydrogen (H_2) or other gaseous fuel. The mass flow controllers also meter ethylene (C_2H_4) used in the spark ignition system for lighting the combustor.

The UCC model can be fitted with either a straight cavity section representing an infinite radius of curvature, or a curved section. The two curvatures change the amount of centrifugal force, or g-load on the flow. Figure 8 shows the UCC assembled using the straight section, and Fig. 9 shows the UCC assembled using the curved section.

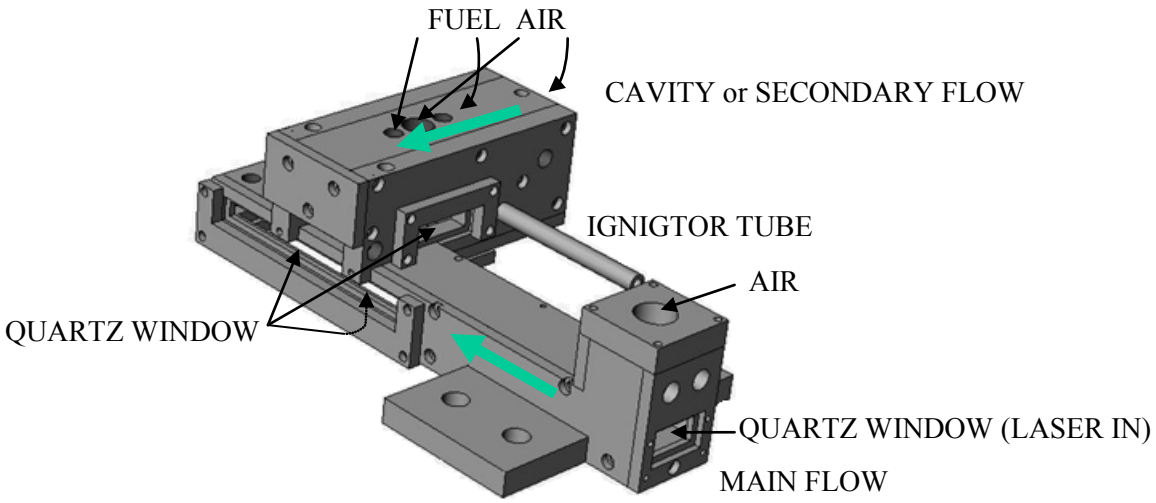

Figure 8. UCC fitted with straight section

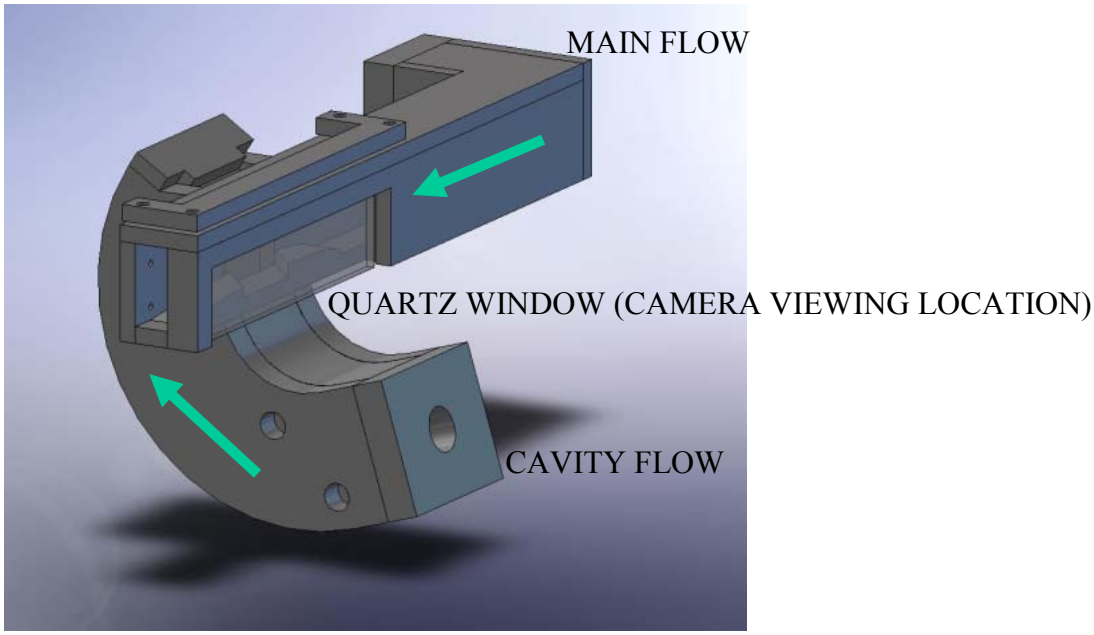

Figure 9. UCC fitted with curved section

To take advantage of the laser diagnostic capabilities of the COAL lab, optically clear quartz windows were added to the UCC model. These windows allow measurements taken of interactions inside the UCC to quantify flame speeds, mixing, and vorticity thus validating combustion efficiency measurements.

II.3 UCC Operating Terms

The UCC is advantageous to a traditional combustor due to three concepts: inter-stage turbine burning, trapped vortex combustion and centrifugally enhanced combustion.

II.3.1 Inter-Stage Turbine Burning

Ideally, gas turbine engines would operate on a CT cycle.[15] However, as mentioned previously, a true CT cycle would require burning in the turbine rotor, a method too technically complex and expensive. An alternative is an ITB acting as a reheat cycle located between high pressure turbine (HPT) and low pressure turbine (LPT) stages. Sirignano and Liu[16] have verified promising results of increased ST with little gain in TSFC in the use of a reheat cycle over the conventional non-reheat Brayton cycle.

An ITB consists of a fueled-cavity type flame holder combined with an injection of air in an angled manner from the outer casing in a turbine vane and it is located between the HPT and LPT.[17] The goal is to promote additional thrust without significantly increasing engine size and weight. As seen in Fig. 10, a circumferential cavity is aligned with radial vane cavities for each turbine vane.[18]

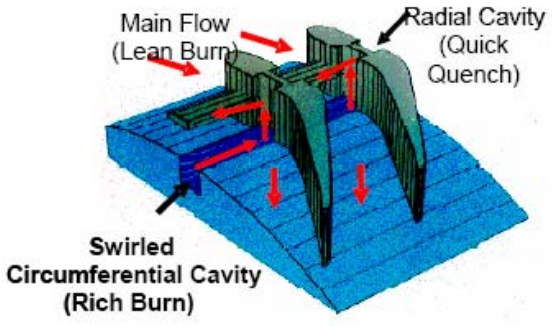

Figure 10. UCC/ITB Concept for Advance Combustion System[18]

Fuel burns rich in the circumferential cavity and has more residence time to burn as it circulates, thus more power is extracted from increased burning of the fuel. This method is superior to conventional combustors burning fuel in the axial direction. Flame stability is also created, hence the name flame holder, allowing combustion products to burn more completely. The complete combustion increases combustion efficiency and produces less harmful emissions. Numerous CFD studies have been done to optimize the design of the ITB. Overall, they show the performance of the ITB is inherently dependent on the shape of the RVC. The small-scale UCC in the AFIT COAL lab has an angled RVC. Since a conventional combustor is too large to fit between turbine stages, a UCC is needed to implement the ITB concept.

II.3.2 Trapped Vortex Combustion

The purpose of TVC is to provide flame stability inside the cavity of the UCC. Essentially, the injecting fuel and air create a vortex in a way to promote a swirling motion like a vortex in the cavity as seen in Fig. 11.

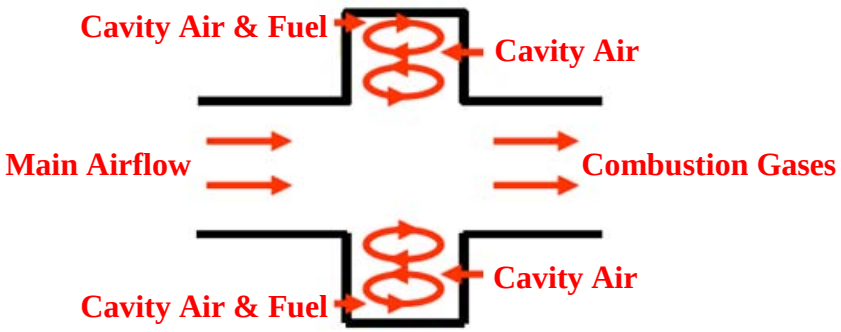

Figure 11. Trapped Vortex Combustion

Air also travels along the axial direction. When these two flows meet, the vortex is enhanced creating increased mixing. Increased mixing produces a stable flame region in the combustion zone for increased burning. As a result, very low overall lean-blow-out equivalence ratios are obtained along with an enhanced combustion efficiency of about 99%.[19] Compared to traditional swirl stabilized combustors, TVC has been shown to give a wider operating range, improved altitude relight, and decreased nitrous-oxide (NO_X) emissions.[20] The UCC will utilize the TVC concept to improve mixing of the fuel and prolong flame stabilization. Future work will involve the continued use of laser diagnostic techniques to determine the location and strength of trapped vortices inside a small-scale UCC while using different geometries.

II.3.3 Centrifugally Enhanced Combustion

Greater residence time is achieved as fuel and air travel circumferentially around the engine. By spinning a flow at high velocities, centrifugal force can be imparted on the components of the flow. This force, also known as a "G-load," has positive effects on combustion by enhancing component mixing and increases the flame propagation rate. Centrifugal acceleration further enhances the effect. Also known as centrifugally loaded combustion, flame speed is increased as it accelerates due to the increased mixing. As a result, buoyancy forces act on the flow field and the flame travels into less dense regions maximizing the burning process.

Lewis[21] found flame speeds from buoyant forces are greater than laminar or turbulent flame speeds. As the flow is centrifugally loaded, centripetal acceleration increases causing buoyant flame speeds to become very large. Lewis also determined for

a g-loading of up to 800, buoyant flame speed increases with increasing acceleration. Buoyant flame speed (S_B) can be found using the relation below:

$$S_B \propto 1.25\sqrt{g} \quad (1)$$

Above a g-loading of 800, speed immediately decreases causing flame extinction. Yonezawa et al.[22] incorporated this idea of high g-loading into a jet-swirled combustor where a ring of inclined combustor air inlets brings air in creating swirling vortexes. They determined increased combustion efficiency could be achieved with this combination.

The UCC will operate with both trapped vortex and centrifugally enhanced combustion to promote flame stability and increased flame speeds. The UCC combines this capability with the performance capabilities of the ITB. The result is more efficient burning of fuel in a shorter axial length therefore reducing engine size and improving cycle efficiency. These concepts enable the UCC to remain small without negatively affecting performance.

II.4 Past and Present Research on the UCC

II.4.1 Previous work on the UCC

AFRL began experiments on the UCC in 2001. Anthenien et al.[4] performed the first studies on a UCC by varying equivalence ratios of air and JP-8 over a wide range of operating conditions at atmospheric pressure. The results of the experiment were promising. Much shorter acoustic wavelengths were observed as compared to a swirl-stabilized combustor, lean blowout was near an equivalence ratio of $\varphi = 0.5$, and efficiencies of greater than 99% were achieved up to an equivalence ratio of $\varphi = 2.0$. [4]

In 2003, Zelina et al.[9] found the angle and type of fuel injector used in the UCC had a large impact on combustion efficiency. For low centrifugal loadings, they found the flame was injector-stabilized and at high centrifugal loadings, the flame was bulk-flow stabilized. They also found the combustion chamber had a small pressure drop of 2% and a high g loading created high radial turbulence in the cavity that increased combustion efficiency. [9]

Also in 2003, UCC experiments using a Laser Doppler Velocimeter (LDV) found circumferential velocities of 20-45 m/s with accelerations of 1000 to 4000 g within the cavity.[22] The results by Quaale et al.[23] also showed the cavity velocities were relatively insensitive to main flow velocity. These researchers confirmed an increase in g-loading means an increase in combustion efficiency.

More recently, the UCC has been tested in a high-pressure environment. The high-pressure tests show the UCC operating at 97 to 99% combustion efficiency over a wide range of operating conditions.[11] The major tests still ongoing for the UCC at AFRL include increasing efficiency, reducing lean blowout, and reducing emissions in all pertinent environments.

Currently, the experimental results for the UCC are promising. However, there are still questions about the physics of the flow inside the cavity and how the cavity flow interacts with the guide vanes and RCV. This has not been studied by AFRL primarily due to the geometry constraints of the full-scale UCC rig. In response, the 2-D sectional rig has been designed to allow greater optical access to study the flow fields and combustion within the UCC and is currently being used in the COAL lab.

To help design the rig, a computational fluid dynamic (CFD) model was created by Moenter.[24] CFD is a valuable tool for theoretically determining the physical interactions inside the UCC. Researchers at AFRL and previous students at AFIT have done much work. Anderson's thesis provides a comprehensive list and description of this previous CFD research.[25] In several studies, combustion and mixing qualities have been predicted and compared with experimental results. Moenter's CFD code, a follow on from the codes of Anisko[10] and Greenwood[26], predicted certain operational conditions for a planar and curved 60-degree sector rig. The main goal was to better understand cavity-vane interactions of the UCC. An emphasis was placed on the axial aerodynamic vane and effect of the RVC in pulling flow from the cavity. This CFD research by Moenter[24] was done to help design a planar and curved sectional small-scale model of the UCC in 2006. Anderson completed the small-scale model with a straight, or infinite, radius of curvature cavity.[25]

In addition to the work on the sectional model, Anderson completed most of the setup of the COAL lab started by Dittman.[14] Koether[13] was the first to take measurements from the UCC model in the COAL lab and started the first laser induced fluorescence (LIF) experiments using the Hencken burner. Hankins[27] was first to burn liquid fuel in the UCC model and compared experimental data from initial operation of this model to predictions from Moenter's code. Lakusta[28] continued Hankins' work with improvements to the igniter system and LIF temperature measurement methods.

II.5 Combustor Operating Parameters / Terms

Numerous operational parameters are used to measure the performance of combustors. Those pertinent to this research are presented in the following section and will be used to characterize the operation of a small-scale UCC.

II.5.1 Thrust Specific Fuel Consumption and Specific Thrust

Specific thrust and thrust specific fuel consumption are frequently used as metrics to describe improvements in whole-engine performance when discussing the addition of the ultra-compact combustor. The relationships defining these terms are shown below.[29]

$$ST = \frac{T}{\dot{m}_{air}} \tag{2}$$

$$TSFC = \frac{\dot{m}_f}{T} \tag{3}$$

Here, T represents thrust in units of Newtons, $\dot{m}_{air}$ is mass flow rate of air in units of kg/s, and $\dot{m}_f$ is mass flow rate of fuel in units of kg/hr.

II.5.2 Stoichiometric Air-Fuel Ratio

A stoichiometric amount of oxidizer means there is just enough oxidizer or air mixed with fuel to completely burn all of the fuel. If there is more than a stoichiometric amount the mixture is fuel-rich and if there is less the mixture is fuel-lean. The stoichiometric air-fuel ratio can be determined from balancing a simple chemical equation under the assumption of complete combustion. The following stoichiometric relation represents the chemical equation for a hydrocarbon fuel such as C_xH_y:

$$C_xH_y + a(O_2 + 3.76N_2) \rightarrow xCO_2 + (y/2)H_2O + 3.76N_2 \tag{4}$$

where a = x + y/4. Using this formula, the stoichiometric air-fuel ratio can be found by using the following equation:

$$(A/F)_{STOIC} = \frac{4.76a}{1}\frac{MW_{air}}{MW_{fuel}} \quad (5)$$

where MW_{air} and MW_{fuel} are the molecular weights of the air and fuel respectively in units of kg/kmol.

II.5.3 Equivalence Ratio

The equivalence ratio (φ) is used to describe the fuel-air mixture and is given by the following equation:

$$\varphi = \frac{(\frac{A}{F})_{STOIC}}{(\frac{A}{F})_{ACTUAL}} \quad (6)$$

where φ > 1 denotes a fuel-rich mixture and φ < 1 denotes a fuel-lean mixture. When φ = 1 the mixture is stoichiometric.

II.5.4 Emissions Index

The emissions index (EI) is a dimensionless number used to represent the amount of pollutants emitted per quantity of fuel used for a particular engine. The method used to calculate EI listed here is an aerospace recommended practice from the Society of Automotive Engineers (SAE).[30] For a hydrocarbon fuel, the emission index is determined using the following equation:

$$EI_Z = \left(\frac{moles\ of\ Z}{moles\ of\ fuel}\right)\left(\frac{molecular\ wt.of\ Z}{molecular\ wt.of\ fuel}\right)(1000) \quad (7)$$

where Z is the species of interest.

II.5.5 Combustion Efficiency

Combustion efficiency (η_b) is a measure of how close a combustor comes to operating at an ideal condition, i.e., extracting the most amount of power available from

an amount of fuel consumed and is given in terms of a percentage. Emissions representing incomplete combustion such as unburned hydrocarbons and carbon monoxide are taken into account. The method used to calculate combustion efficiency listed here is also an SAE aerospace recommended practice.[30] The equation listed below is used for combustion efficiency calculations based on emissions data from the main flow exhaust of the UCC in this thesis.

$$\eta_b = 100[1.00 - 10109\frac{EI_{CO}}{H_C} - \frac{EI_{CxHy}}{1000}] \quad (8)$$

H_C is lower heating value (LHV) of the fuel in units of J/kg. For calculations in Chapter 4.4.1, a value of 4.4467x10^7 J/kg was used for n-dodecane ($C_{12}H_{26}$), a JP-8 equivalent.[31]

II.6 Alternative Fuels

The U.S. Air Force has been looking for alternative sources of jet fuel to JP-8 for the past several years. These alternative fuels are made using the Fischer–Tropsch process (or Fischer–Tropsch Synthesis), a catalyzed chemical reaction in which synthesis gas, a mixture of carbon monoxide and hydrogen, is converted into liquid hydrocarbons of various forms. The most common catalysts are based on iron and cobalt, although nickel and ruthenium have also been used. The principal purpose of the process is to produce a synthetic petroleum substitute, typically from coal, natural gas or biomass, for use as synthetic lubrication oil or as synthetic fuel. One form of the fuel, a 50/50 blend of synthetic and petroleum fuel, is being tested as part of an ongoing Air Force program to help the environment and to use a fuel produced domestically. Air Force officials are in the process of evaluating and certifying this alternative fuel derived from natural gas for use in all Air Force aircraft. The goal is to have every aircraft using synthetic fuel blends

by 2011 with at least 50% of this fuel produced domestically by 2016.[32] There have been several recent milestones as the Air Force tries to certify its fleet for the use of FT fuels. The first B-52 flight using FT fuel occurred Sept. 2006 when a B-52 successfully flew with two-engines using the synfuel-blend at Edwards AFB, CA. In Dec. 2006, A B-52 took off on a flight-test mission using a synfuel-blend as the only fuel on board. In March 2008, B-1B became the first Air Force aircraft to fly at supersonic speed using an alternate fuel. In Sept. 2008, an Edwards F-22 performed aerial refueling using a synthetic fuel, the first time an Air Force aircraft refueled mid-air using an alternative jet engine fuel.

The FT process gives the Air Force a cleaner, more cost-efficient fuel source. Synthetic fuel created using the FT process costs an estimated $30 to $50 less per barrel than its petroleum counterpart does.[33] Each time the price of oil goes up $10 per barrel, it costs the Air Force an additional $600 million for fuel[33] and increases Defense Department costs by $1.3 billion per year.[34] The domestically produced fuel will also help alleviate the dependence on foreign energy sources. Alternative fuels can be produced from domestically available hydrocarbon products like natural gas, coal and shale. The domestic sources can be gasified and converted into any number of liquid fuel products. These fuels are also proven to burn cleaner, reducing combustion-related emissions and particulates in the air all without compromising performance. The fuels branch of AFRL has tested several types of synthetic fuels such as Syntroleum® S-8, the same used in this research. To remain a viable combustor of the future, the UCC must be compatible with these new fuel sources.

II.7 Laser Diagnostic System and Techniques

Laser diagnostic techniques receive much attention in the combustion field because of their non-intrusive nature. Traditionally, combustion diagnostics is performed in two ways. The most common method is sampling. In this method, a sample of the combustible gas is gathered followed by some sort of analysis on the sample. Time accurate results are difficult with sampling since the combustion process occurs through a series of chemical reactions and the molecules in the sample will not stop reacting with one another as the sample is taken out of the process. Another commonly used method is probing. Probing involves putting some solid object or probe into the flame such as a thermocouple or some other temperature measuring device. The problem is a probe is intrusive to the flame; it disrupts the flame and changes the dynamics of combustion resulting in less than accurate data about the true nature of the flame. When high temperatures threaten to melt or disable traditional thermocouple or probe devices, or the dynamics of interest may be disturbed by the methods used for analysis, optical analysis can be used. Accurate combustion diagnostics are possible with the use of laser spectroscopic methods. Laser spectroscopic techniques give instant, real time information about the flame and combustion proces.[35] They are non-intrusive, do not disrupt the flame, are accurate and can provide high resolution. [35] There are many varieties of optical and laser diagnostic techniques, but this research focused on PLIF.

II.7.1 Planar Laser-Induced Fluorescence

One particular laser spectroscopic method is Laser- Induced Fluorescence (LIF) or Planar Laser- Induced Fluorescence (PLIF). PLIF is a 2-D diagnostic technique widely used in combustion diagnostics introducing a plane of light created by a laser passing

through a region of interest (ROI). This technique makes use of the molecular absorption and emission of energy in the form of light at high energy levels. In a general sense, a molecule absorbs a photon, which excites the electrons of that molecule to a higher energy state. Following this excitation, the molecule naturally tends to relax back to a balanced electron configuration, releasing energy, again in the form of photons, in the process. This photon release is called fluorescence. Fluorescent absorption refers to wavelengths of light which, when introduced upon a molecule, result in fluorescence at a different wavelength. From a combustion standpoint, LIF is most commonly used to calculate the concentrations of different species and the temperature within a flame.

II.7.2 Mechanics of LIF

The concept of fluorescence is relatively simple and follows the law of conservation of energy. Fluorescence is an energy absorption followed by a light emission.[36] In the case of LIF, a photon generated by a laser excites a molecule to a higher energy state, but the molecule does not like to stay at that excited state. In order for the molecule to return to a lower energy state, it emits energy in the form of light. The light emitted by the molecule makes up the fluorescent signal and can be generally detected by a camera to produce an image. The fluorescence signal or intensity directly correlates with the concentration of the emitting species.[36] The stronger the fluorescent signal, the higher the concentration of the species. The fluorescence phenomenon is depicted in Fig. 12a by an arrow going up representing the photon being absorbed and moving to a higher energy state, and then an arrow going back down representing a photon release and return to a lower energy level. For LIF, the absorption occurs at a

precise wavelength and the emission occurs over a span of different wavelengths as depicted in Fig. 12b.

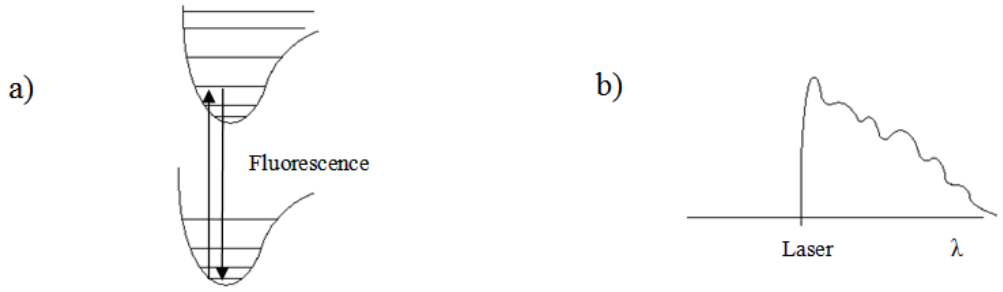

Figure 12. a) Depiction of fluorescent absorption and emission. B) Emission spectra[36]

LIF can be used to detect the concentration of several different molecules in a combustion environment. Most electronic transition occurs within the visible light spectrum and almost all important molecules in a combustion environment containing H, O, C, N, and S have been detected by LIF.[36] However, every molecule has its own discrete region of spectral absorption. The unique spectral absorption bands means each molecule will only absorb a photon at very specific wavelength. Table 1 shows a list of common species detected using LIF methods and the known range of electronic transitions for that molecule. In general, the fluorescence wavelength is different from that of the incident excitation and primarily occurs at longer wavelengths.[35]

Table 1. Range of electronic transition for selected molecules[36]

Molecule	Electronic Transition (nm)
C_2	400-600
	230-330
CH radical	500-430
	450-360
CO	200-250
	150-240
N_2	100-500
	Vac u.v.
NO	195-340
	200-500
O_2	500-900
	170-220
OH radical	240-400
CH_4	145.5-500
C_2H_2	237-210
CO_2	140-170
H_2O	145-186

Electronic transition does not occur over the entire range listed in Table 1, but rather at a few discrete wavelengths within that range. Therefore, a prerequisite of any LIF experiment is a database of known absorption spectra for the molecule of interest. This research relied on LIFBASE, a freely available database system used for the simulation of electronic transition behavior for diatomic molecules. It has the capability to simulate both absorption and emission, including the calculation of the collisional and Doppler broadening correction factors.[27] The collisional correction factor is necessary to account for deviations from the theoretically expected fluorescence due to pressure effects. The Doppler broadening is due to a shift in the expected wavelength due to temperature effects.

II.7.3 Detection of the OH Radical

The most common molecule detected by LIF methods in combustion research is the hydroxyl (OH) radical. The OH molecule is good for combustion diagnostics because

it is a radical produced in the intermediate reactions of combustion and then destroyed by the end of the combustion process. The OH radical is very abundant in most flames and its spectroscopy is well known.[36] The OH molecule is a great indicator of the behavior of the flame and can provide information on flame mixing, propagation, ignition, structure, and local extinction.[35] OH PLIF has a range of uses, including acting as a flame marker for flame location studies, temperature measurement, and determining OH species concentration.[27]

OH is also a good source for calculating the temperature of the flame. The fluorescent intensity of a species' photon emissions is approximately linearly related to its concentration in the ROI. In general, a higher concentration of OH will lead to a higher temperature. The intensity of the light emitted can be measured using specially designed and tuned cameras. The abundance of the OH molecule in high temperature combustion processes and its associated long fluorescence time - between 10^{-10} and 10^{-5} seconds - make it a prime candidate for PLIF studies in combustive environments.[36]

II.7.4 OH PLIF Thermometry

Planar laser thermometry studies play an important role in the evaluation of combustion dynamics, offering insight into regions where unburned pockets of gas may exist and indicating the temperature distribution across a region of interest.[37] OH PLIF provides these benefits by making use of the OH (A-X) electronic transition system. This term designates the energy states being manipulated by the incident laser sheet, as shown in Fig. 13.

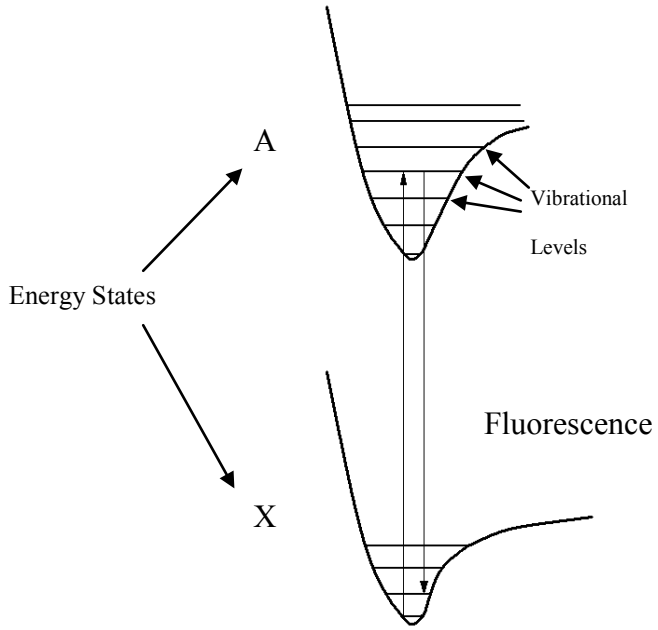

Figure 13. The X and A energy states - sub vibrational levels shown, rotational levels not shown. Vertical arrows designate increasing and decreasing energy. [35]

The figure shows the X energy state as the ground state for electrons in the OH molecule, and the upward arrow designates their excitation to the higher A energy state. The horizontal lines represent the vibrational levels within each energy state. These levels are written after the (A-X) designation in common notation, as OH (A-X) (1-0) or (1,0), with different numbers representing different levels. Not shown in Fig. 13 are the rotational states within each vibrational level.[35] These states further quantize the description of an electron's condition, and are the level at which PLIF excites subject molecules. As shown in Fig. 14, there are many rotational states within each vibrational level, with multiple variations on the rotation.

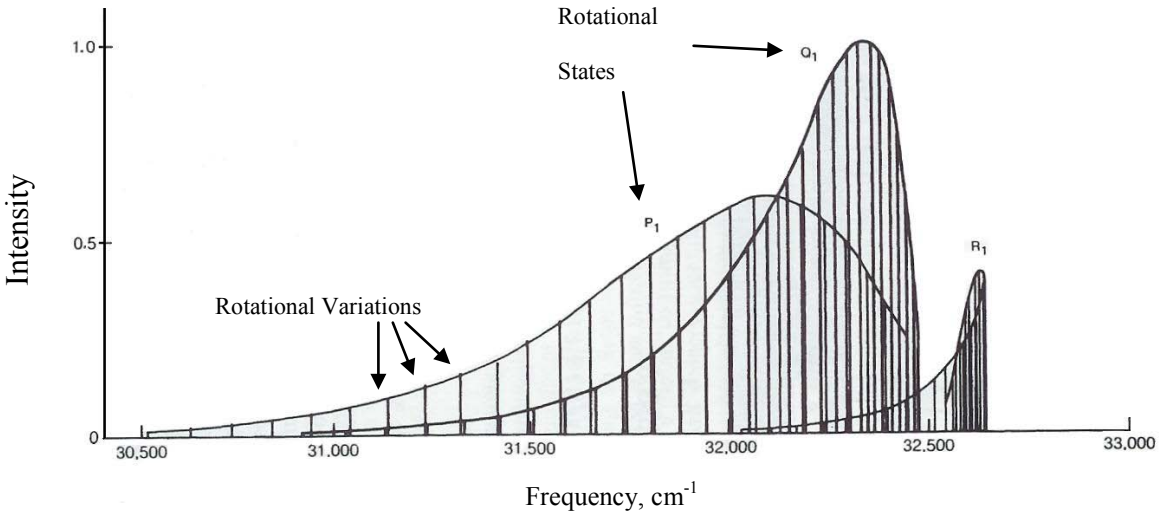

Figure 14. An example of the rotational structure of a vibrational level[35]

Rotational states are designated by letter and number combination followed by the specific variation in parenthesis, as $Q_1(5)$.[35] These states are excited by specific wavelengths of incident light, and are generally referred to as "lines."

Two methods of PLIF thermometry are often used. The first examines the ratio of fluorescent intensities produced by two different wavelengths of light. These two wavelengths are known as line pairs, and are selected for their sensitivity to temperature and wavelength proximities. By choosing one line insensitive to temperature and another with an intensity varying greatly with temperature, the fluorescent intensity ratio of these two lines can be correlated with theoretical data generated by LIFBASE in order to determine temperature.[27] Past researchers have examined several line pairs in the OH (A-X) (1-0) vibrational level to find line pairs suitable for intensity-ratio OH PLIF thermometry. A study conducted by Seitzman, Hanson, and others[37] used three line pairs to observe a hydrogen-air flame with a temperature range of 1000-3000 K. The line pairs used were: $Q_2(11)/R_2(5)$, $Q_2(11)/P_1(7)$, and $Q_2(11)/R_2(8)$. The wavelengths for these lines

were: $Q_2(11)$ – 285.16 nm, $P_1(7)$ – 285.09 nm, and $R_2(8)$ – 281.72 nm. Using the $Q_2(11)/P_1(7)$ pair, temperatures were measured with as low as 7% error, a level of accuracy valuable for engine research.[27] Hankins' research examined five line pairs: $R_2(8)/Q_2(11)$, $Q_1(14)/Q_1(5)$, $R_2(13)/P_1(2)$, $P_1(7)/Q_2(11)$, $R_2(5)/Q_2(11)$.[27] The wavelengths for these lines were: $R_2(8)$ – 281.725 nm, $Q_2(11)$ – 285.16 nm, $Q_1(14)$ – 286.455 nm, $Q_1(5)$ – 282.75 nm, $R_2(13)$ – 282.64 nm, $P_1(2)$ – 282.665 nm, $P_1(7)$ – 285.09 nm, $R_2(5)$ – 281.74 nm. Lakusta[28] followed on to Hankins and further refined the work recommending $R_2(13)/P_1(2)$ and $Q_1(14)/Q_1(5)$ for future research in the COAL lab and giving a fifth order polynomial equation that can be used to find temperature based on the ratio of the intensities of the two lines. Both Hankins and Lakusta found the $Q_1(14)/Q_1(5)$ line pair produced the most accurate temperature measurements. This work will use the $Q_1(14)/Q_1(5)$ ratio with the recommended equation used to find temperature based on a ratio of intensity from the line pair:[28]

$$T = (62819)R^5 - (116871)R^4 + (84375)R^3 - (29553)R^2 + (8258.5)R + 821.03 \qquad (9)$$

where T is temperature in degrees Kelvin and R is the corrected intensity ratio.

Another method of PLIF thermometry is called an excitation scan. After selecting a line of interest from LIFBASE, the incident laser is tuned in small increments through a range of wavelengths just below and above the peak.[27] The recorded fluorescent intensities, when plotted versus wavelength, show the "shape" of the line. The line shape also depends on temperature, and thus can be correlated again with LIFBASE data in order to determine flame temperature.[27] It requires several correction factors for accurate readings, however.

The first of these corrections accounts for laser, or line broadening. Although the lab laser may be tuned to a specific wavelength, it is actually emitting a very small range of wavelengths termed the "line-width".[35] This property limits the resolution, and thus accuracy, with which the OH line's shape can be determined.

The second correction factor accounts for Doppler broadening, which is a function of temperature. This type of broadening is a result of the small-scale motion of the radiating molecules. Based on the Doppler principles, particles moving toward the collection device will appear to emit at a higher frequency, while those moving away will produce an apparent lower frequency.[35] Thus, a range of frequencies wider than those actually emitted is recorded.

The third source of error is called collisional, or pressure broadening. Collisional broadening is a factor of molecules colliding with each other as they interact with radiation, interrupting the absorption or emission process.[35] Line-width can be experimentally measured, and Doppler broadening can be calculated by LIFBASE based on the anticipated temperature predicted by an equilibrium kinetics code such as STANJAN. Therefore, collisional broadening can be empirically determined. The technique employed allows all three correction factors to be applied to recorded data.

Since line shape is the quantity of interest for the excitation scan, a method of quantitatively analyzing these shapes must be used. The technique used in the past studies evaluated the full-width, half-maximum (FWHM) values of recorded line shapes. Figure 15 shows an illustration of this method using LIFBASE.

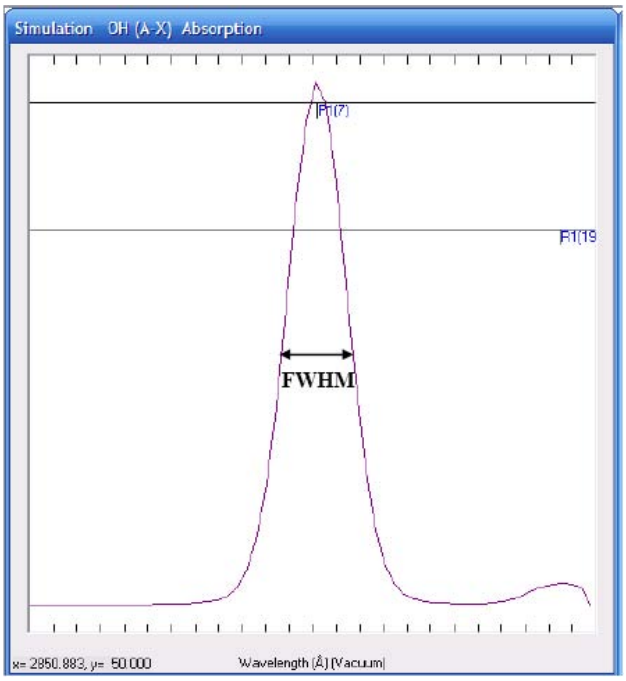

Figure 15. Illustration of the full-width, half-maximum method for excitation scan analysis. Image generated by LIFBASE.[27]

This method is accomplished by determining the width of the line in wavelength at half of its peak intensity. The FWHM value provides a repeatable technique to characterize the line width. This value is a function of temperature, and when correlated with LIFBASE data provides a useful technique measuring temperature.[27]

Both the ratio of intensity, or line center technique, and line scan OH PLIF thermometry methods have been used in the COAL lab. The ratio of intensity method requires two lasers systems to do simultaneous measurements or is limited to steady flames. Since previous researchers had only one laser system available, a ratio of intensity PLIF measurements were performed on the steady, laminar Hencken burner only using non- simultaneous measurements. The line scan temperature measurement method can be performed with one laser system, but requires more correction factors to

obtain accurate results and is not an instantaneous measurement. This research focuses on the intensity ratio method using two-line PLIF with the newly installed second laser system.

II.7.5 Quenching

The fluorescent quantum yield is the most important quantity when trying to determine concentration and temperature from fluorescent signal.[36] The fluorescent signal strength is adversely affected by quenching. Quenching is the depopulation of the excited energy state without releasing a fluorescent signal. Quenching is the general term describing three possible occurrences that prevent the emission of fluorescent spectra by molecules excited to a higher energy state. These occurrences include dissociation, energy transfer to another molecule or internal energy state, and general chemical reactions.[27] Quenching depends mostly on the cross section and quantity of the other molecules in the mixture. The cross sections of the species in the mixture are dependent on the temperature of the flame.[38] Analytical models, such as the one published by Tamura et. al,[38] must be used to adjust the LIF signal for quenching effects.

First, species concentration, temperature, and pressure data must be calculated for an equilibrium condition using equilibrium combustion software.[13] Several tabulated constants were also needed. The OH spontaneous emission coefficient (A) is given in LIFBASE for each line and the Boltzman's constant (k) is 1.38065 x 10^{-23} $\frac{m^2 kg}{s^2 K}$. Table 2 shows empirically determined values published by Tamura.[27]

Table 2. Empirical values for quenching correction factor calculations[38]

Colliding Species	$\sigma_{Q(INF)}$ (Angstroms)^2	ε/κ (K)	Quenching Rate Coefficient
CH_4	11	320	$(5.07 \times 10^{-19})(\sigma_Q)(T^{0.5})$
H	14.5	84	$(15.0 \times 10^{-19})(\sigma_Q)(T^{0.5})$
O	0	0	$(0 \times 10^{-19})(\sigma_Q)(T^{0.5})$
N	0	0	$(0 \times 10^{-19})(\sigma_Q)(T^{0.5})$
H_2	4.5	224	$(10.88 \times 10^{-19})(\sigma_Q)(T^{0.5})$
OH	20	384	$(4.99 \times 10^{-19})(\sigma_Q)(T^{0.5})$
CO	12	397	$(4.97 \times 10^{-19})(\sigma_Q)(T^{0.5})$
NO	0	0	$(0 \times 10^{-19})(\sigma_Q)(T^{0.5})$
O_2	8	243	$(4.37 \times 10^{-19})(\sigma_Q)(T^{0.5})$
H_2O	20	434	$(4.92 \times 10^{-19})(\sigma_Q)(T^{0.5})$
CO_2	11	488	$(4.16 \times 10^{-19})(\sigma_Q)(T^{0.5})$
N_2	0.4	624	$(4.47 \times 10^{-19})(\sigma_Q)(T^{0.5})$

Correction for quenching was accomplished by calculating LIF Efficiency through the following multi-step process. Since temperature is required to determine the quenching rate, an iterative procedure was used with the equilibrium temperature as the initial guess.[39] Equation 10 is used to determine the temperature dependence of each molecule's cross-section:

$$\sigma_Q = \sigma_{Q_{INF}} e^{\left(\frac{\varepsilon}{kT}\right)} \tag{10}$$

The number density for each species must also be known, and is found using eq. 11.

$$Species\ Number\ Density = \left(mole\ \ fraction\ of\ the\ species\right)\left(\frac{P}{kT}\right) \tag{11}$$

Using this quantity and Table 2, the quenching rate for each species was calculated according to eq. 12:

$$Q_{species} = \left(Species\ \ Number\ Density\right)\left(Quenching\ \ Rate\ Coefficient\right) \tag{12}$$

Total quenching rate is the sum of each of the species' rates:

$$Q_{Total} = \sum Q_{species} \tag{13}$$

Finally, LIF Efficiency is calculated using eq. 14.

$$LIF\ Efficiency = \frac{A}{A + Q_{Total}} \tag{14}$$

By dividing the measured intensity by the LIF Efficiency calculated, the corrected intensity was found.

III. Test Setup and Apparatus

III.1 Laser diagnostic system

The laser diagnostic system makes the COAL lab a state-of-the-art combustion diagnostics facility. The overall arrangement consists of lasers, various optics to include visible light and ultra-violet (UV) filters, lenses, rails and electronically controlled traverse systems for accurate location of optics and cameras for image collection. The system is mounted on several mobile optics tables located around the UCC in the AFIT COAL laboratory.

The heart of the PLIF laser system is a Quanta-Ray PIV-Series dual pulsed neodymium-doped yttrium aluminum garnet (Nd:YAG) made by Spectra-Physics, see Fig. 16.

Figure 16. Quanta-Ray PIV-Series dual pulsed Nd:YAG laser

The YAG pump laser provides an initial infrared beam to the rest of the laser system. Using two flash lamps, the system excites triply ionized neodymium, which emits photons at 1064 nm. It produces 200 to 400 mJ of pulsed energy with pulse separation times ranging from 100 ns to 100 ms.

The infrared beam from the YAG is then passed through a series of frequency-doubling units, one is internal to the YAG and one external. Frequency-doublers placed in the beam path emit light at double the incident frequency, cutting the beam's wavelength in half. After frequency doubling, the laser pulses enter the two tunable dye lasers which also have frequency doublers. The beams pumped two Continuum ND6000 narrowband dye lasers, see Fig. 17, assembled by Innovative Scientific Solutions, Inc. (ISSI). One of these dye laser systems is a new addition to the COAL lab making simultaneous two-line PLIF possible. By altering the concentration of a methanol and Rhodamine 590 dye solution pumped into cells placed in the beam path, the dye system allowed the output frequency of the entire system to be adjusted at very small intervals. Figure 17 also shows the dye solution pumps used by the Continuum dye lasers. The doubling crystals were electronically controlled by ND6000 software with 0.001 nm adjustments available providing the precision necessary when conducting combustion laser diagnostics. More specific details on the use of the COAL lab laser system are found in App. A.

Figure 17. ND6000 narrowband dye laser with frequency doublers

The generated dye-laser beam was passed through another doubling crystal located within a UVT-1 automatic tracking unit, through which both the residual dye beam and the generated UV beam exited. The beams were separated via a prism located within the exit of the auto-tracking unit. Since not needed for the experiment, the residual dye-laser beam was used to track the wavelength. To check the wavelength, the beam was transmitted through a single-mode optical fiber to a High Finesse WS-7 wavemeter, providing measurement of the wavelength with an absolute accuracy of 0.2 pm for the wavelengths used. When using the wavemeter, a series of neutral density filters were used before the collimating lens and the dye laser was operated without amplification to protect the optical fiber and wavemeter. Units are important when checking the wavelength. Transition lines are often reported in the literature using vacuum

wavelength, such as the $Q_1(14)$ 286.456 nm line, but the ND6000 software uses nm in air to adjust the doubling crystal and the High Finesse wavemeter software outputs its results in nm air. LIFBASE can show line transitions in Angstroms of air or vac. Since there are several transitions in the A-X system, it is important to be at the right transition and at the line's peak. As a final verification the dye lasers were producing the peak wavelength for these transitions, OH signal was collected from the Hencken flame while making very small changes to the wavelength using the doubling crystal.

Figure 18. Checking wavelength using wavemeter

III.2 PLIF Camera System

The camera used to detect the LIF signal is an intensifying charged-coupled device (ICCD) camera made by Princeton Instruments (PI-Max, 512 x 512 pixels) with a Nikon PK-11A and PK-12 lens and one CVI camera filter allowing the camera to record fluorescence without gathering the laser beam, see Fig. 19. One of these cameras is also a new addition to the COAL lab along with the associated computer system and software to support its operation.

Figure 19. Princeton Instruments ICCD cameras

Win-View 32® software performed image collection. The image math feature of Win-View® could have been used to determine intensities in the ROI for various PLIF images. However, during this research a MATLAB® program was developed to give the average image intensity and standard deviation for a series of images at the desired size and location of ROI. MATLAB® is a programming language developed by The MathWorks, Inc. This program analyzes the images much faster than Win-View since stacks of images for a test run were analyzed at the same time. App. B lists the code for use by future students. To ensure the collected image is recording fluorescence of OH only, a background image obtained under the same conditions but without a flame or laser was subtracted from the LIF images. Even though a WG-295-205 filter is reducing the signal from the laser by 99%,[13] an image with the laser only should be taken of the ROI and it was also subtracted. Finally, the flame itself produced signal, especially at higher φ. Eq. 15 lists the image math for reducing an image to the fluorescent event only used in this research.

$$Image\ intensity = TS - (Laser\ only - background) - (flame\ background - background) - background \quad (15)$$

where TS is the total signal in the ROI recorded by the camera for a set φ. An example of the use of eq. 15 using actual images is shown in Fig. 20.

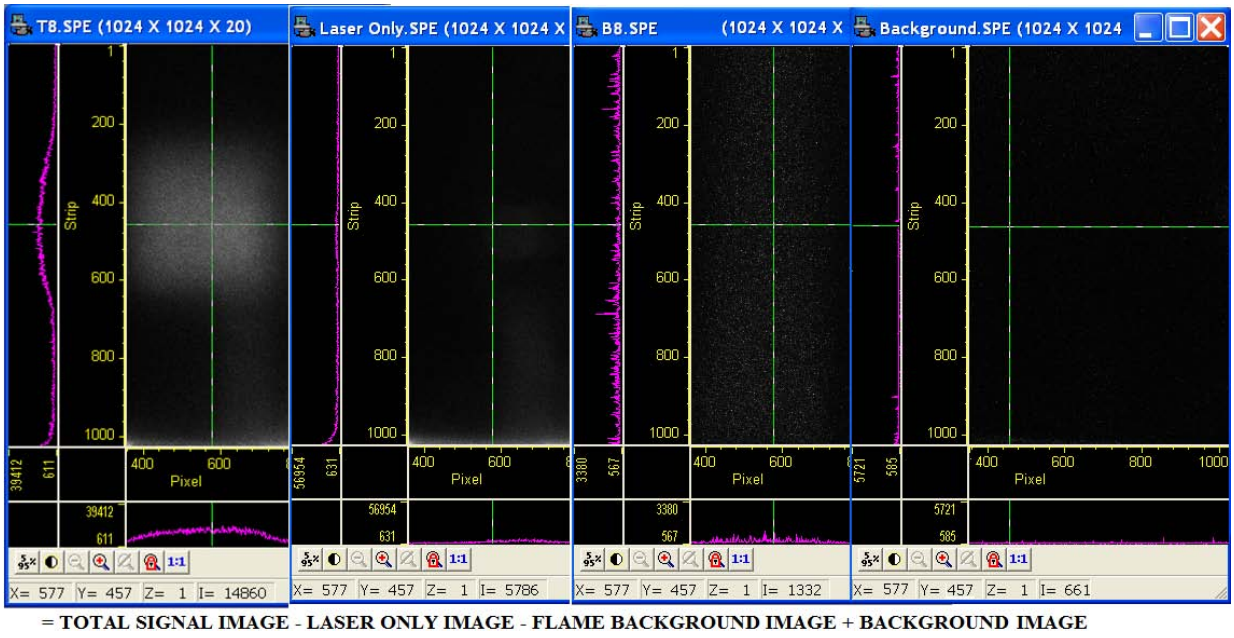

Figure 20. Reducing images to fluorescent event only using image math

An optical train with a series of optics, lens and mounts were needed to get the two laser beams from the YAG source, through the frequency doublers, into the dye laser, formed into a sheet and to the test sections. Specific details on the setup of the optical train used in this experiment is found in App. C. An f = -250 mm cylindrical lens coupled to an f = 1000 mm spherical lens created a focused ~ 1mm sheet shown in Fig. 20. The sheet then passed through the flame of the Hencken burner or the UCC depending on the area of interest. To move the sheet within the flame, the last mirror in the optical train was placed on a Newport ESP300 motion controller to allow for precise movements as shown in Fig. 21. To keep the ROI in focus, the cameras also needed moved in the same direction and

amount as the sheet. A Newport ESP300 controlled their movements as well as shown in Fig. 19.

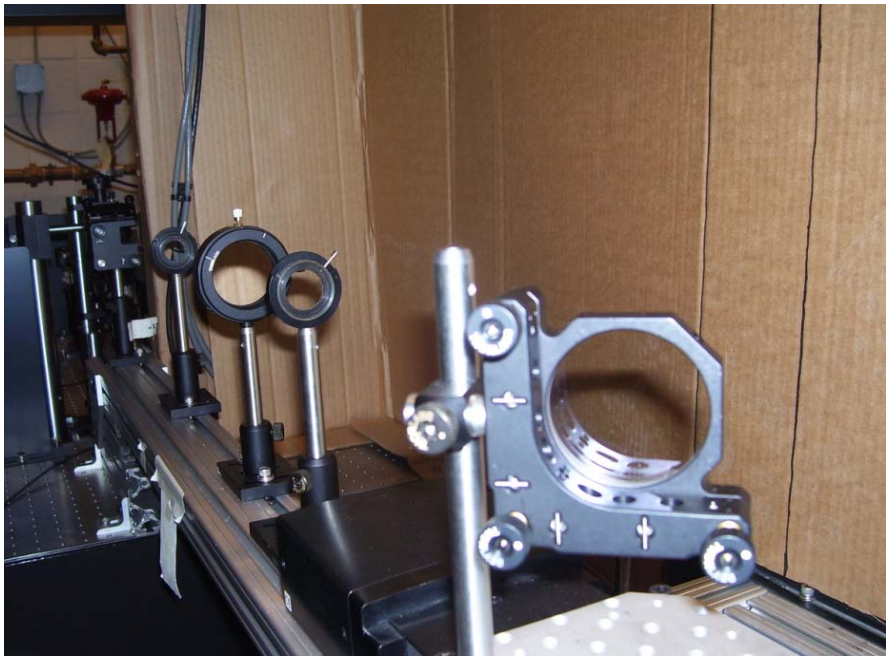

Figure 21. Sheet forming optics with motion controller

The entire optical setup is detailed in Fig. 22. The specific optics used were included to ease repeatability with future researchers.

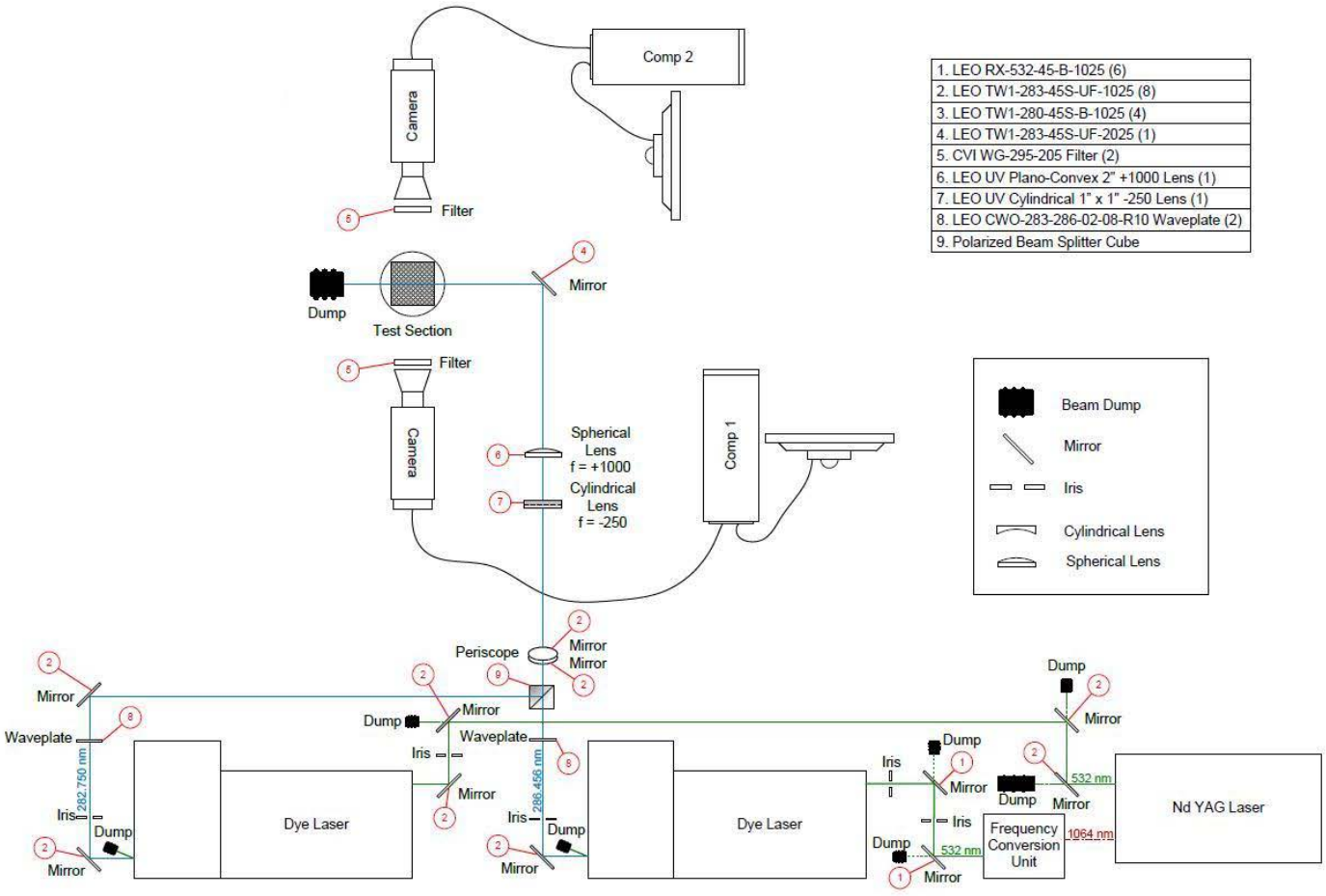

Figure 22. Two-line PLIF setup with Hencken burner

In addition to PLIF, the Quanta-Ray PIV-Series dual pulsed Nd:YAG laser and surrounding components can also be used for Coherent Anti-Stokes Raman Scattering (CARS), Instantaneous Raman Scattering, Raman Spectroscopy, Laser Induced Incandescence (LII), Particle Image Velocimetry (PIV), and Tunable Diode-Laser-Based Absorption Spectroscopy (TDLAS). This laser diagnostic capability distinguishes the AFIT COAL laboratory as a highly advanced combustion diagnostics facility. During this period of research, a team of researchers was able to develop a laboratory setup that allowed for conducting PLIF, PIV, and LII on the same test item with a minimum amount of time and adjustment between setups. All three setups used the same sheet forming

optics of Fig. 21 to keep the same ROI. Figure 23 shows the PIV setup, Fig. 24 the LII setup and Fig. 25 showing all three setups with arrows indicating the changes between techniques.

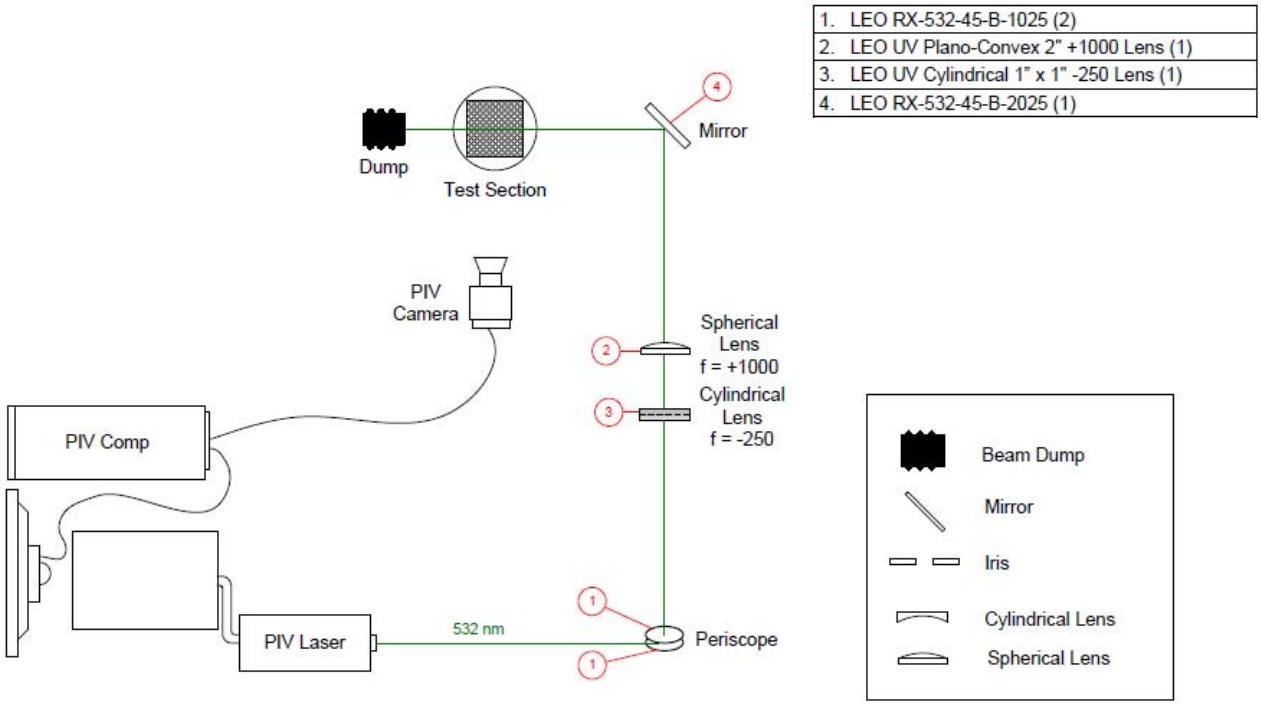

Figure 23. PIV setup

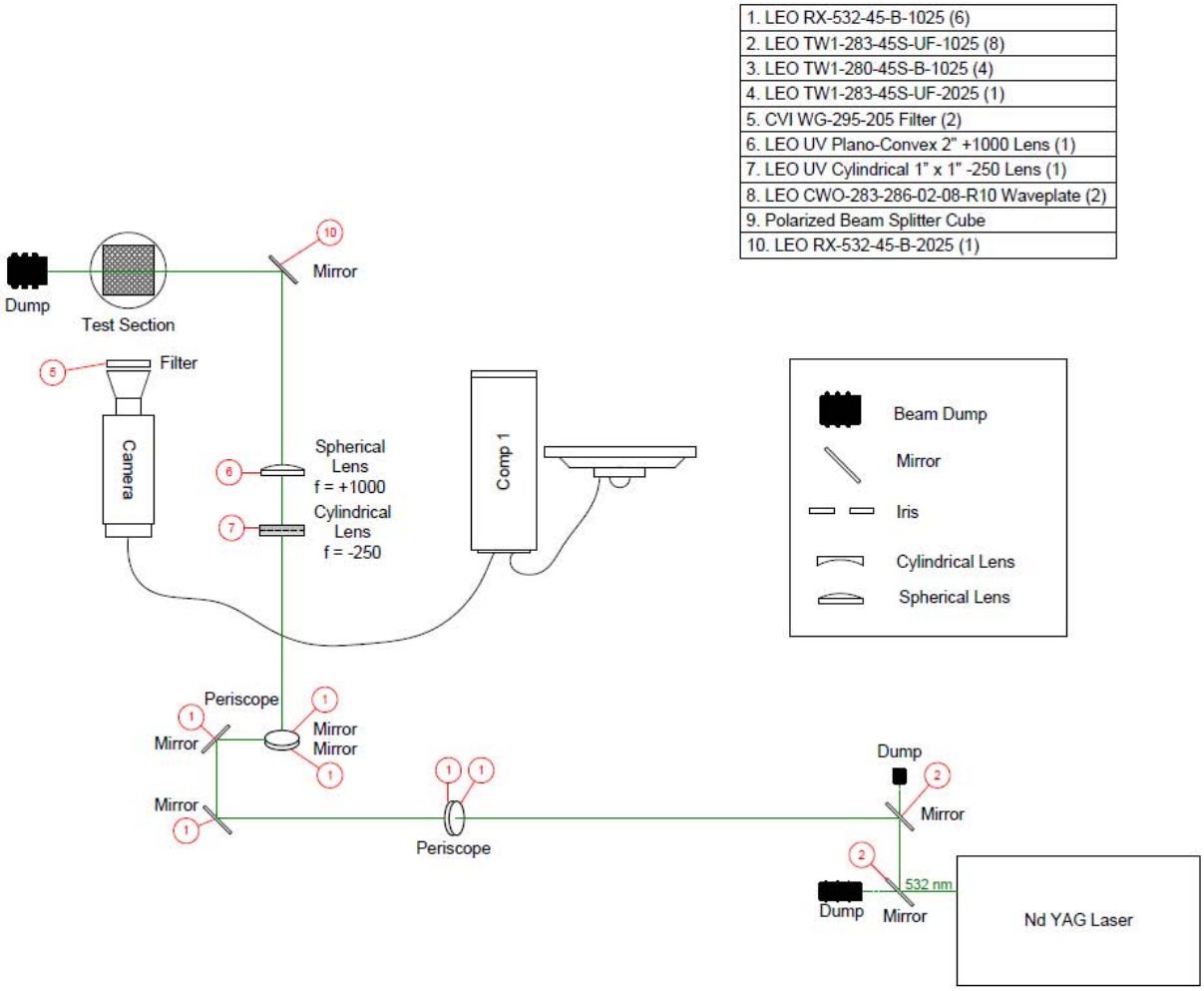

Figure 24. LII experimental setup

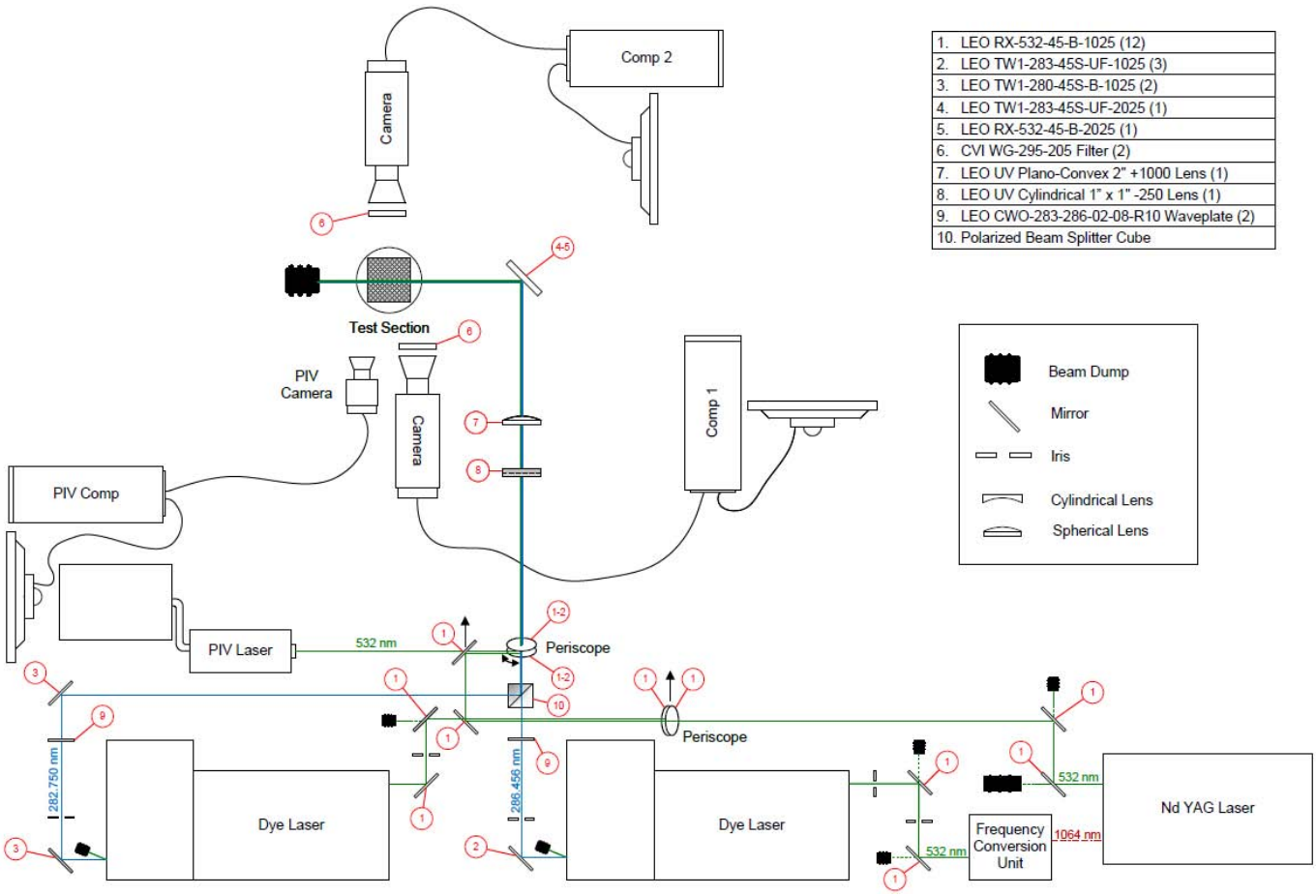

Figure 25. PLIF, PIV and LII experimental setup

Flip down optics eased the transition time between setups allowing movement of an optic not needed for one of the setups while still keeping it aligned.

III.3 Control of gasses and data collection

National Instruments' Lab-View program provides the basis for the COAL lab's control and data acquisition capabilities. The virtual instrument (VI) interface designed by Anderson[25] and shown in Fig. 26 controls all air and fuel delivery to the test stand,

most associated adjustments to the state of these flows, and is the hub for much of the data acquired directly from the UCC system.

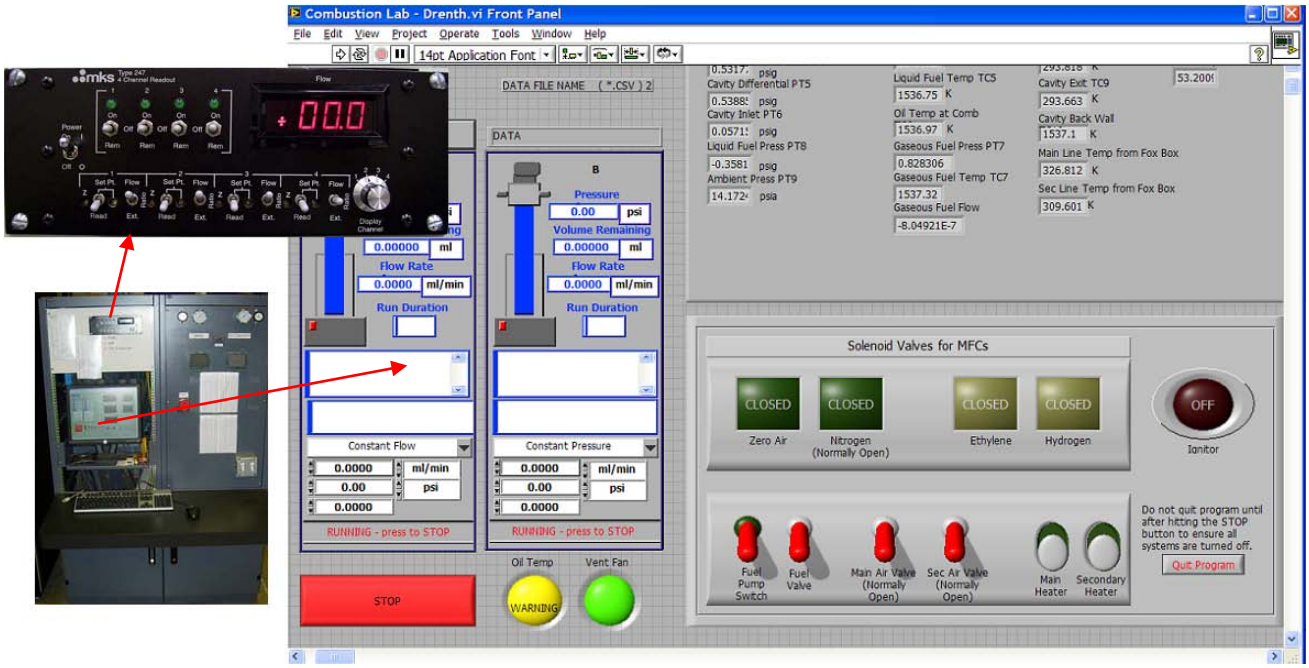

Figure 26. VI Interface

During this research, the VI front panel was modified and updated so each switch was properly labeled as well as labels indicating which valves/solenoids are normally open when the program is started. These changes were saved in “Combustion Lab – Drenth. Vi front panel”. The COAL lab is limited to controlling four mass flow controllers with its MKS four channel readout. During this research, a second MKS control panel was ordered along with four additional 50’ cables to interface with the mass flow controllers. When installed, this additional capability will allow the performance of more complex experimental setups in the lab or multiple students to perform experiments without changing between setups. The arrangement of filters, solenoids and mass flow controllers was also updated. The new arrangement is more organized and centrally located; Fig. 27 contrasts the new and old arrangements. Future students should be aware that the mass

flow controllers are susceptible to damage when moved. To switch the size of the mass flow controller that is controlling a gas line, move the line going into the test stand versus moving the mass flow controller.

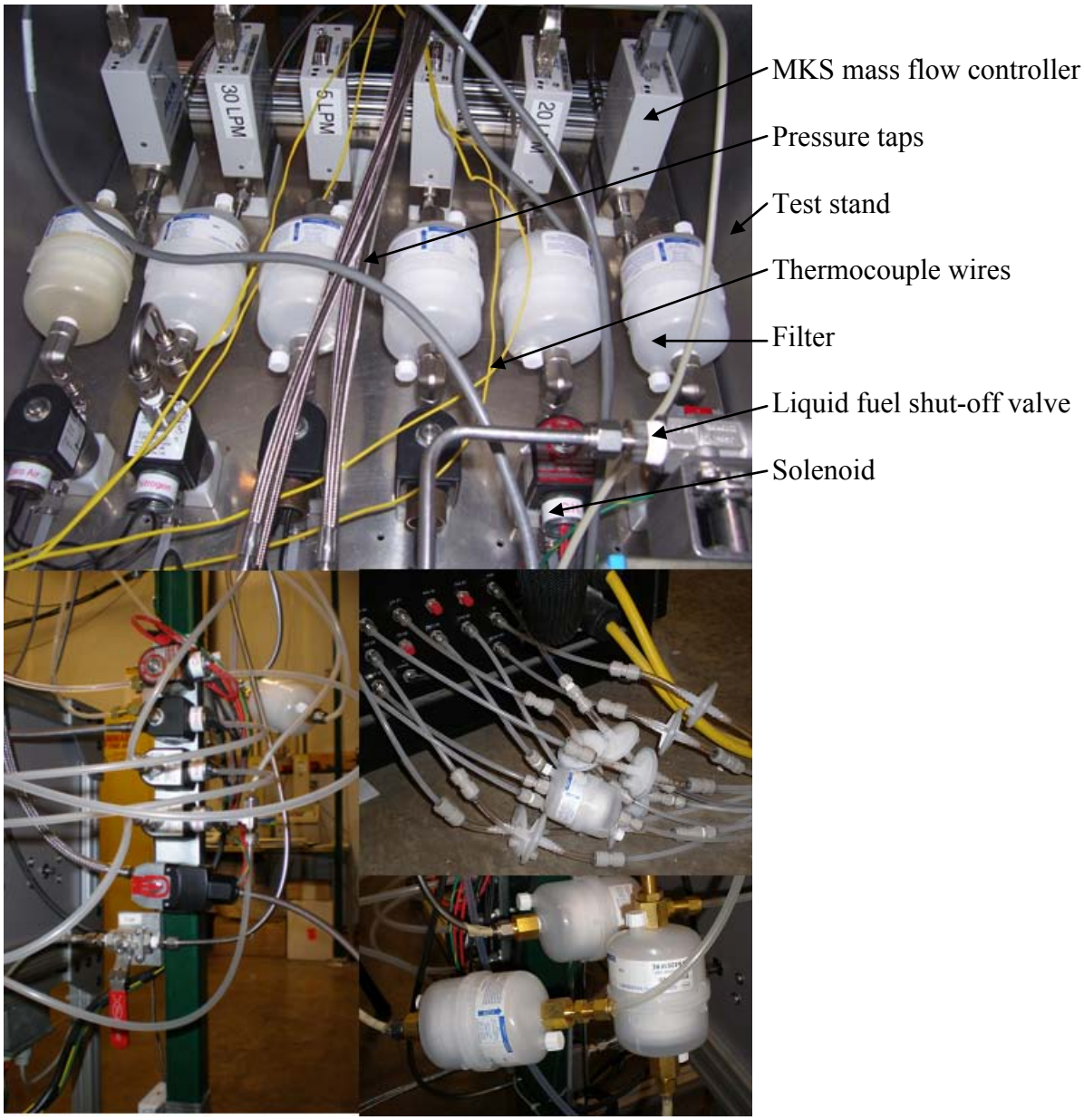

Figure 27. New (top) versus old arrangement of solenoids, filters and MFCs

III.4 Hencken Burner Operations

The calibration of the PLIF setup was made using a Hencken burner, which produces a near-adiabatic, laminar flame as shown in Fig. 28. The burner consists of a 24-mm-square, Hastalloy honeycomb supporting hypodermic needles within a quarter of its cells.[39] Hydrogen flows through the hypodermic needles, and air passes through the remaining cells. At the exit of the burner, the gas streams mix and create a flat flame just above the burner surface. The inner Hastalloy honeycomb is surrounded by a 6-mm-wide nitrogen co-flow, separated from the main flow by a 0.73-mm wall. The nitrogen co-flow improves flame stability in the center of the burner while also reducing the effects of room air on the flame itself.

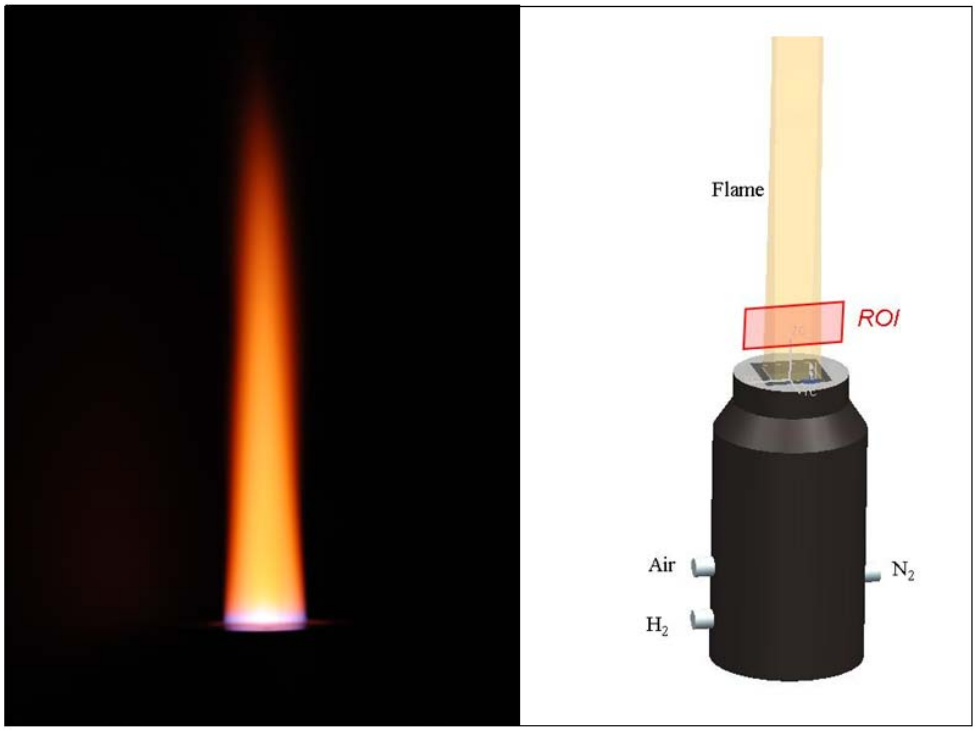

Figure 28. Laminar Hencken flame and sketch of Hencken burner[39]

Three MKS Alta-series mass flow controllers set the gas flow rates. Following the recommendations of past researchers[27,28] higher flow rates than previous experiments allowed the flame to stabilize at a sufficient height from the burner surface to ensure heat losses to the surface would be minimized during combustion. For the experiments of this portion of the research, the airflow rate was maintained at 50 SLPM. The hydrogen flow rate was changed from ~ 8 to 30 SLPM to produce equivalence ratios ranging from 0.4 to 1.4 creating a large region of uniform flame from 1.0 to 6.0 cm above the burner surface. The ~ 4 x 4 mm ROI used for calibration was a region of uniform intensity located 2 cm from the surface in the middle of the flame. Nitrogen flow maintained at 30 SLPM provided flame stability and isolation from the surrounding air. A Bios International Definer 220H flow meter calibrated all flows as shown in Fig. 29.

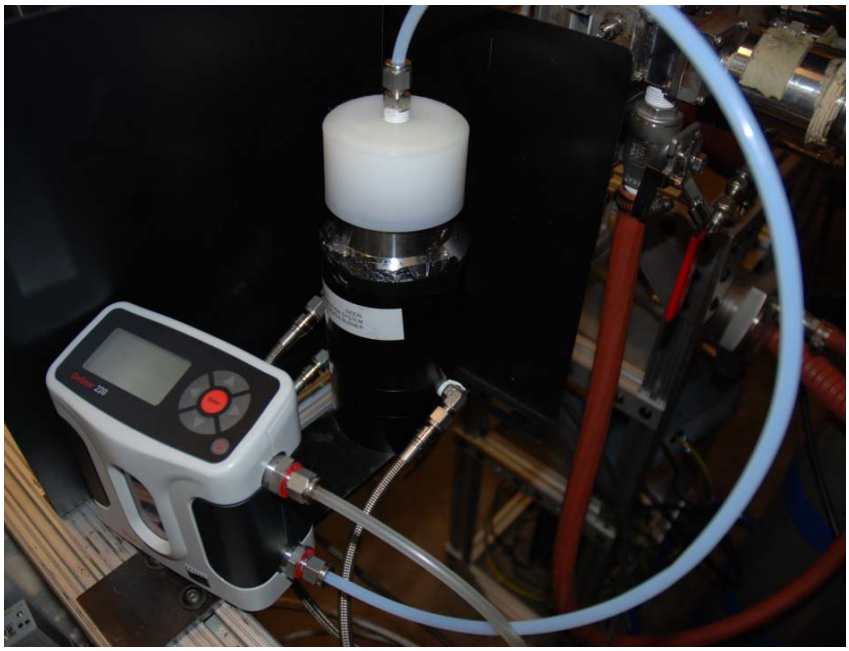

Figure 29. BIOS Definer 220 calibrating the Hencken burner

The actual flow rates were calculated using eq. 4. For hydrogen, the balanced chemical reaction is written as:

$$H_2 + 0.5(O_2 + 3.76N_2) \rightarrow H_2O + 1.88N_2 \quad (16)$$

The volumetric air-to-fuel ratio at $\phi = 1$ is:

$$\left(A/F\right)_{ST} = 4.76(0.5) = 2.38 \quad (17)$$

For air held constant at 50 SLPM, eq. 6 shows fuel flow rate varies with equivalence ratio according to the following relationship:

$$F = \frac{50\phi}{2.38} \quad (18)$$

Hydrogen flow rates calculated using this method and used in Hencken burner operations are tabulated in Table 3.

Table 3. Hencken burner setpoints

Hencken Burner Setpoints	
φ	Hydrogen (SLPM)
0.4	8.40
0.5	10.50
0.6	12.60
0.7	14.70
0.8	16.80
0.9	18.90
0.95	19.95
1	21.00
1.05	22.05
1.1	23.10
1.2	25.20
1.3	27.30
1.4	29.40
Notes: Air constant at 50 SLPM Air composition: 21.0% O_2, 79% N_2 Coflow (N_2) constant at 30 SLPM	

The exercise of using two-line PLIF simultaneously requires two separate cameras to capture the light intensity emitted from the two different excitations that

occur. The intensities of light emitted from the two different excitation wavelengths were compared to each other to approximate a temperature at a particular air to fuel ratio. Triggered by a 10-Hz pulse generated by an external timing unit, a Princeton Instruments programmable timing generator (PTG) controlled the intensifier pulse and delay time.[40] A photo-diode captured residual light from the last turning mirror. An oscilloscope tracked this signal was for each laser pulse as in Fig. 30. The oscilloscope also tracked the shutter from the camera. Adjustments to the timing ensured the fluorescence was captured for its line but for its line only. The timing is shown in Fig. 31.

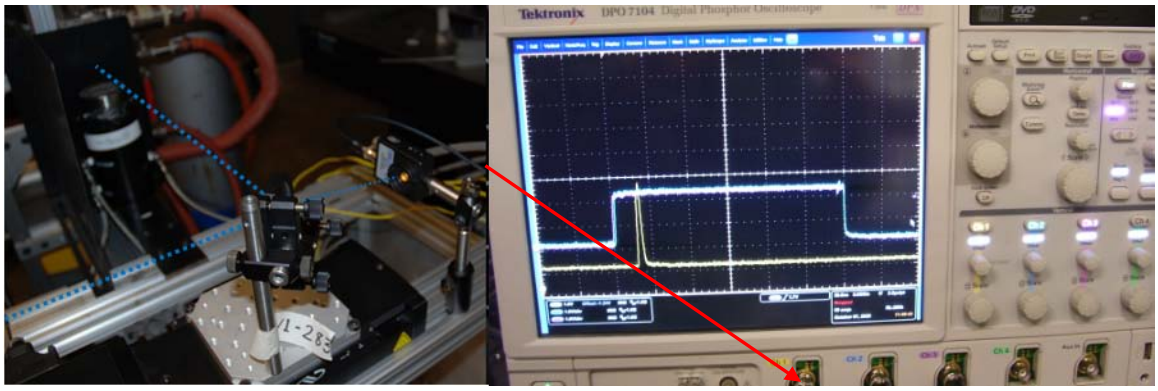

Figure 30. Timing the cameras

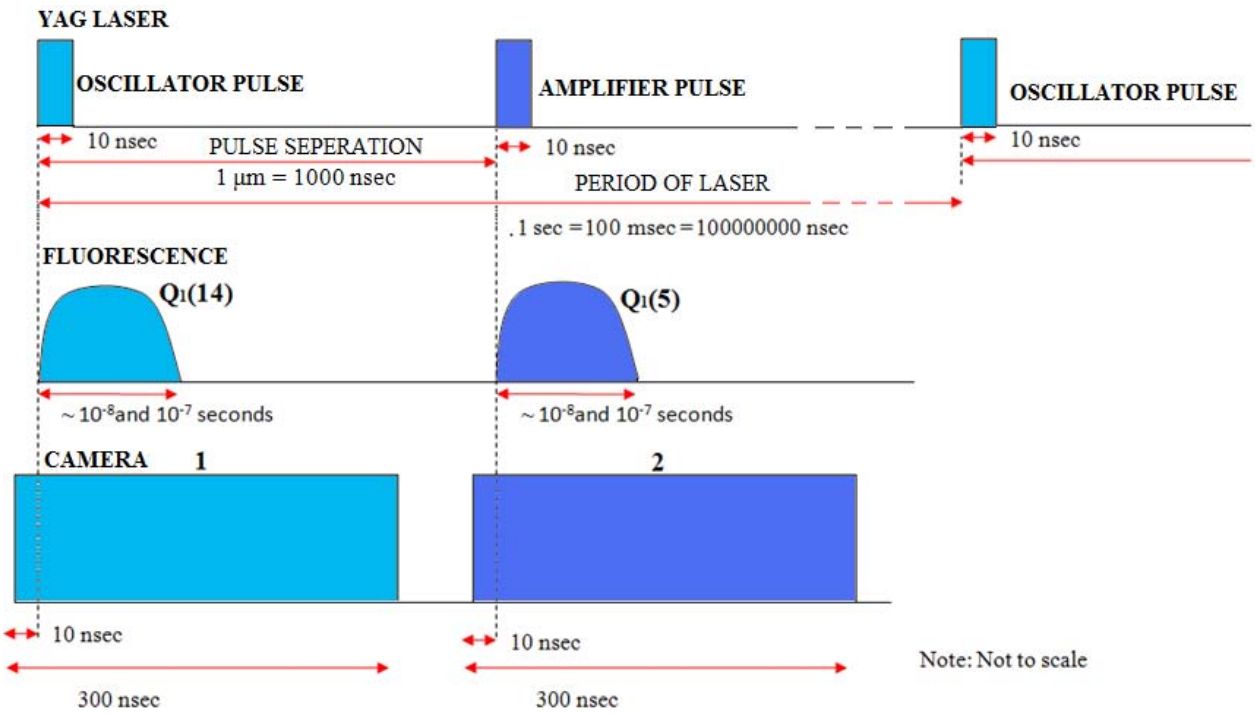

Figure 31. Timing of experimental setup

III.5 UCC Experimental Setup

The experimental setup for the UCC was very similar to the Hencken burner PLIF setup. One of the cameras in Fig. 22 was moved so both could look into the quartz window of the UCC. This research utilized both the straight infinite radius cavity and the curved cavity. Previous researchers had designed and ordered parts for the UCC curved section, although it was never completely assembled or fuel burned. Several fittings were needed to adapt it to the COAL lab main and secondary air delivery system, fuel system, and pressure and temperature taps. The curved section is now completely operational and has been assembled in a manner to quickly and easily allow switching between the straight and curved sections.

Four regions in the UCC were selected for investigation using PLIF thermometry. Two regions were the main vane exit for the straight and curved section, after the RVC as

shown in Fig. 32. In an actual engine, this temperature would represent the temperature going to the rotor of the turbine. The other two ROIs were for the cavity exit for both straight and curved section. This region would represent the temperature of combustion products in the cavity flow swirling around the engine also shown in Fig. 33.

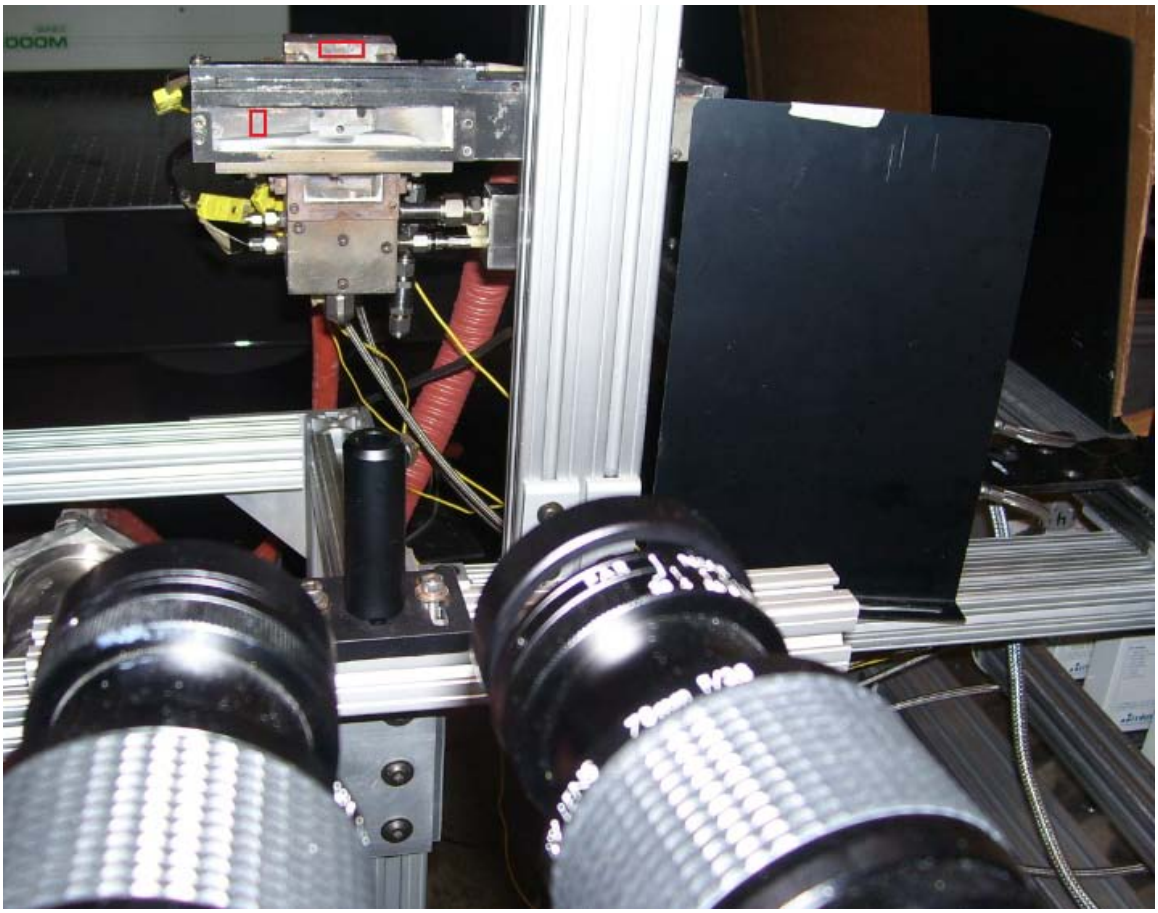

Figure 32. PLIF thermometry areas of investigation (straight section side view)

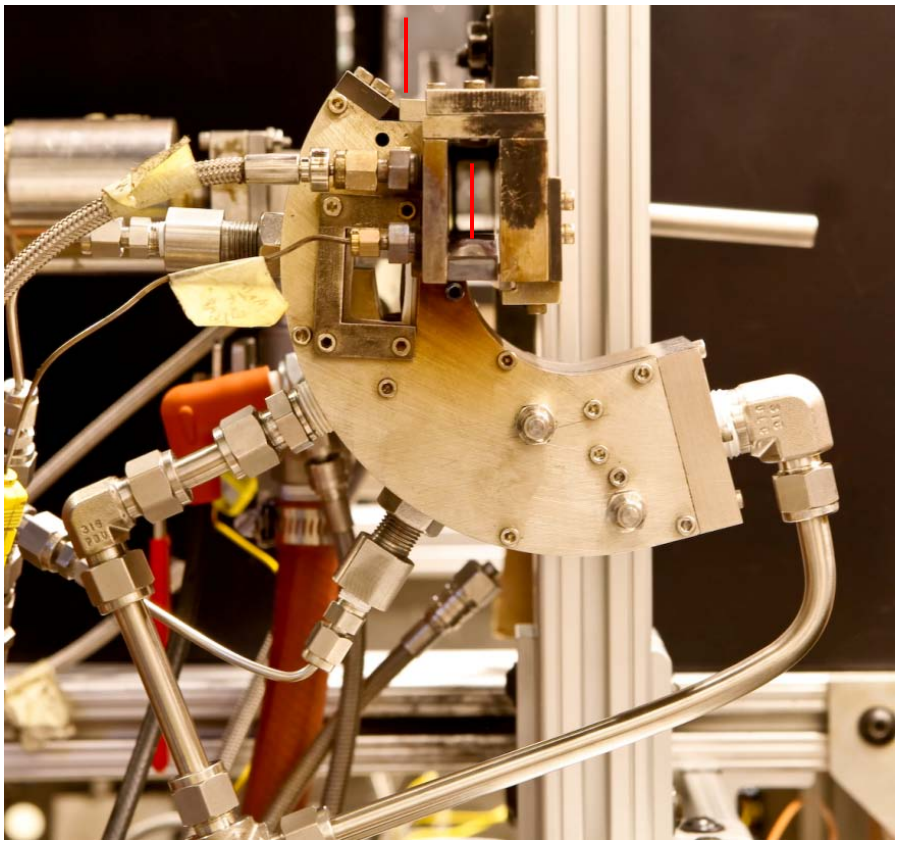

Figure 33. PLIF thermometry areas of investigation (curved section back view)

Calculating the mass flow rates for hydrogen in the UCC is similar as described with the Hencken burner. Ethylene was used in the torch ignition system of the UCC. Eq. 19 shows the balanced chemical reaction:

$$C_2H_4 + 3(O_2 + 3.76N_2) \rightarrow 2CO_2 + 2H_2O + 11.28N_2 \tag{19}$$

Using eq. 4 results in:

$$\left(A/F\right)_{ST} = \frac{4.76(3)}{1} = 14.28 \tag{20}$$

Holding airflow rate constant at 5 SLPM, rearranging eq. 5 results in:

$$F = \frac{5\phi}{14.28} \tag{21}$$

Calculating the equivalence ratio for JP-8 and air was done the same way. The equation for perfect combustion of JP-8, a kerosene ($C_{12}H_{23}$) based fuel, and air flame representing an equivalence ratio of one is given by the following:

$$C_{12}H_{23} + 17.75\left(O_2 + 3.76N_2\right) \rightarrow 12CO_2 + 11.5H_2O + 3.76N_2 \tag{22}$$

Using eq. 5 results in:

$$\left(A/F\right)_{ST} = \frac{4.76(17.75)}{1}\frac{(28.89)}{167} = 14.616 \tag{23}$$

Fuel was held constant at 25.0 ml/min, which is 0.0187 kg/min. This conversion was made using 749 kg/m^3, the density of n-dodecane, a JP-8 simulant. Equation 6 was used to solve for different amounts of airflow in the cavity while varying the equivalence ratio as follows:

$$\phi = \frac{14.616}{\left(\frac{A}{25.0}\right)} \tag{24}$$

A 10 to 1 main to cavity flow rate ratio was used for most of the test runs since previous studies have shown the most favorable conditions for trapping a vortex in a cavity were when cavity flow rates were roughly 10-20% of the flow rate in the main channel.[19]

Propane (C_3H_8) was also used in the UCC for emissions testing. Calculating its equivalence ratio was in a similar manner to JP-8 described above. Data calculated in this way is found in Table 4. These equivalence ratios were calculated for airflow in the cavity.

Table 4. UCC setpoints

UCC Setpoints										
Gaseous fuel							Liquid fuel			
Hydrogen (PLIF)				Propane (EMISSIONS)			JP-8 & S-8 (EMISSIONS)			
Cavity φ	Cavity Air	Main Air (kg/min)	Fuel (SLPM)	Cavity Air (kg/min)	Main Air (kg/min)	Fuel (SLPM)	Cavity φ	Cavity Air (kg/min)	Main Air	JP-8 & S-8 (ml/min)
0.5	0.1	1.0	16.32				0.5	0.55	5.47	25.0
0.6	0.1	1.0	19.58				0.6	0.46	4.56	25.0
0.7	0.1	1.0	22.84				0.7	0.39	3.91	25.0
0.8	0.1	1.0	26.10	0.1313426	0.875617	3.46	0.8	0.34	3.42	25.0
0.9	0.1	1.0	29.37				0.9	0.30	3.04	25.0
0.95	0.1	1.0	31.00				0.95	0.29	2.88	25.0
1.0	0.1	1.0	32.63	0.0919398	0.612932	3.03	1.0	0.27	2.74	25.0
1.05	0.1	1.0	34.26				1.05	0.26	2.61	25.0
1.1	0.1	1.0	35.89				1.1	0.25	2.49	25.0
1.2	0.1	1.0	39.16	0.0707229	0.471486	2.8	1.2	0.23	2.28	25.0
1.3	0.1	1.0	42.42				1.3	0.21	2.11	25.0
1.4	0.1	1.0	45.68				1.4	0.20	1.95	25.0
1.5	0.1	1.0	48.95	0.0612932	0.408621	2.9	1.5	0.18	1.82	25.0
Ignitor: Air to ignitor set to 5 SLPM, cavity air set to 0.1 kg/min, main air set to 0 kg/min Ethylene set to 2.6 SLPM (φ = 7.43)										

The Bios Definer 220 calibrated the flow of hydrogen and ethylene. FOX Model FT2 flow transmitters controlled the flow of air to the UCC with accuracy of ± 1% of reading. The ISCO 1000 D delivers liquid fuel to the rig with 25.38 nl precision, less than 0.1% of the operating fuel flow.

III.6 Emissions testing

A Testo 350 portable emissions analyzer measured emissions from the UCC. It is capable of measuring numerous emissions parameters. Unburned hydrocarbons (UHC) were measured with an accuracy of less than 400 parts per million (ppm), carbon monoxide (CO) and nitrous oxide (NO_X) with an accuracy of less than five ppm, and carbon dioxide (CO_2) using non-dispersive infrared technology with an accuracy of ± 0.3%. These pollutants were used to calculate an emissions index and combustion efficiency using eqs. 7 and 8. During this research, installment of Testo 350 software

version 3.2, shown in Fig 34, allowed the user to monitor and control the analyzer from a computer. It also allows export of the data to Microsoft Excel, making data analysis much easier.

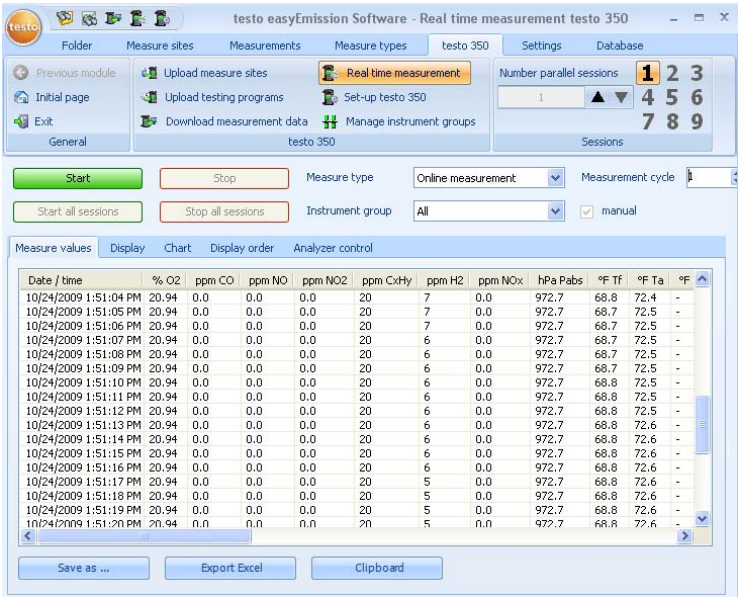

Figure 34. Testo 3.2 software with export capability

The Testo comes equipped with an emissions probe that can withstand temperatures up to 3000 K. Figure 35 shows the UCC in operation with the emissions probe coming in from the left side. The probe measured emissions from the main exhaust, with the probe 1” from the exhaust plane. The results of emissions analysis are discussed in Chapter 4.4.

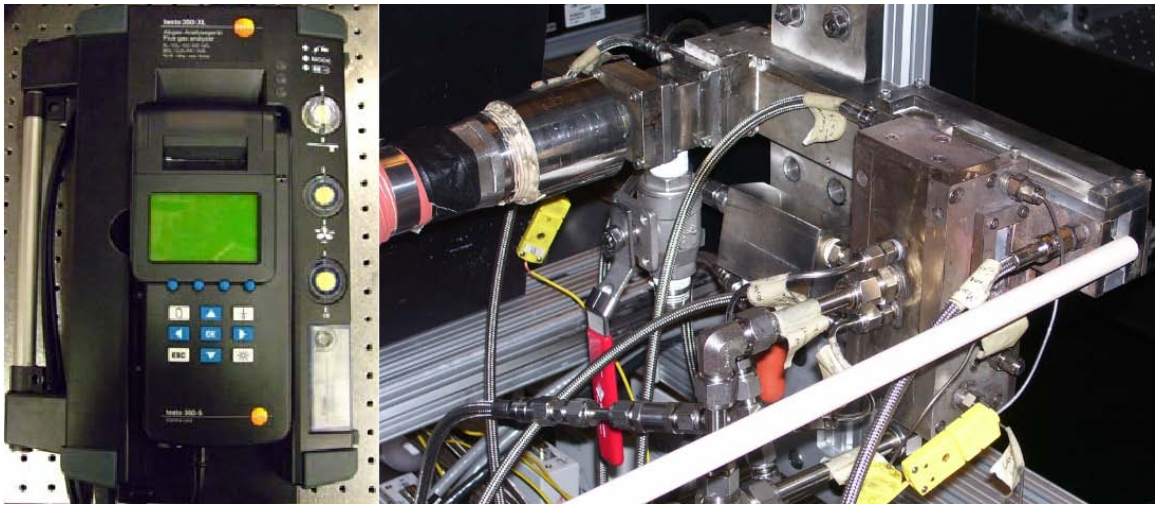

Figure 35. TESTO 350 with high temperature probe

III.7 Error analysis

As with all experiments, one of the underlying axioms is that no measurement can be known to provide an exactly true result. Summarized here are statistical and bias error components of the PLIF thermometry results referenced throughout the following chapter. The main output or response variable of these experiments is temperature. Its measurement was affected by the inputs or experimental variables, controllable factors, and uncontrollable factors.

The main error discussed associated with the inputs include deviations in equivalence ratio due to errors in mass flow rates to the test burner and/or oxygen concentration. Fortunately, the equivalence ratio where peak OH concentration occurs is an experimentally known value. Therefore, shifts in the peak after performing PLIF experiments can tip the experimenter of the error. All air and fuel flow rates used in these experiments were corrected with accuracy of ± 1% or less. Certified zero air has accuracy of ± 1%. If all post-correction input errors were added in a worst-case scenario situation, the φ would still be within 0.3% of setpoint.

One controllable factor that was a potential source of error is a bias between the two cameras. The picture from both cameras should be the same for the same fluorescent event. Finding the bias is discussed in the next chapter and a sensitivity analysis was performed to show the level of measurement error with any bias correction error.

To find the intensity of an image in a certain region, shot-to-shot as well as pixel-to-pixel averaging was performed for many of these temperature measurements. Ten on-chip accumulations produce one image, and 20 images are produced for each φ. Image length and widths were either 100 pixels (~4 mm) for the Hencken flame or 50 pixels (~2 mm) for the UCC. The mean value of the 20 images was used to calculate the temperature. Confidence bounds for the temperature measurement on several plots show the statistical noise or variation due to this image averaging. Shot noise is slightly higher for low temperature images, primarily because of their lower OH concentration.

Fluorescent signal varies with laser intensity in the linear regime so signal is normalized by laser power. Shot-to-shot fluctuations in laser power can results in an incorrect correction. The effect of this error is demonstrated and a sensitivity analysis to the correction is performed.

Several known but uncontrollable factors exist such as the variations in beam intensity or quality within the sheet, run-to-run variations in wavelength, and the effects of absorption as the laser sheets pass through the flame.

Finally, even after correcting for any biases or other known errors, run-to-run variations exist. Several temperature measurements of this research were one time measurements, but confidence bounds were used to show run-to-run variations when multiple runs of the same experiment were performed.

IV. Discussion and Results

IV.1 PLIF thermometry results

The main focus of this research was to add the two-line PLIF capability to the COAL lab. To perform two-line PLIF a second dye laser, dye pump, camera, computer and associated software needed to be installed and work together. After the new camera was installed a calibration exercise was performed to ensure both cameras responded linearly to signal. To calibrate the cameras, a LED flashlight provided a constant intensity light source. The flashlight was installed where the cameras will be focusing in the test section. Rather than varying the brightness of the light source, a set of Spiricon neutral density filters and a Spiricon LBS-100 laser beam sampler kit was used. The filters range in how much light of any wavelength was allowed to pass through, effectively varying the amount of light to the camera by a distinct amount. The laser beam sampler was installed in front of the camera lens, the flashlight is directed towards the camera. Images were taken in Win-View of the flashlight behind different filters. The average intensity of each image captured was obtained from Win-View and plotted on a logarithmic scale against a normal scaled set of values for the optical density of the filter. With a logarithmic scale on the intensity, the plot should be linear. The resulting plot shows both cameras were responding linearly to signal as shown in Fig. 36.

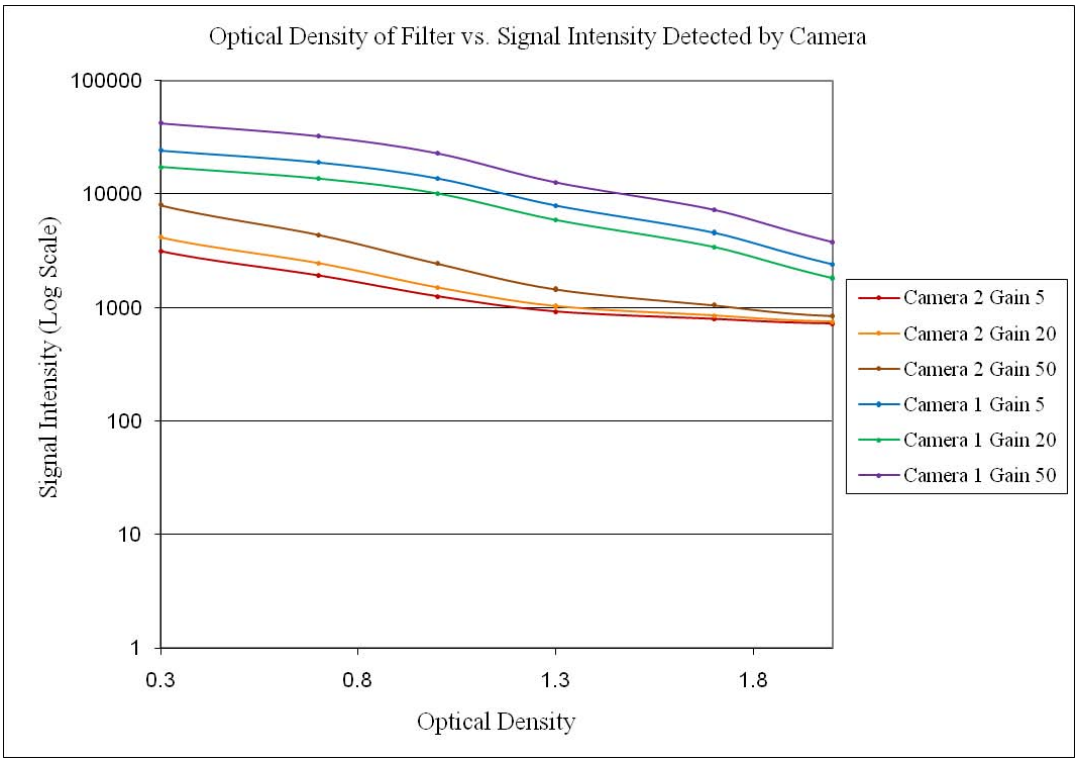

Figure 36. Signal linearity check of ICCD cameras

When performing PLIF thermometry, it is important to know if the experiment will be in the linear or saturated regime. As laser power is increased, the amount of fluorescence by the excited molecule will also increase. However, if too much power is added, the molecule will become saturated and intensity will remain constant. To verify the experiment will be in the linear regime, LIF images of the Hencken burner were recorded over a range of laser powers. The results in Fig. 37 show the signal is linear. With irradiance and power corrections, normalizing the signal is possible.

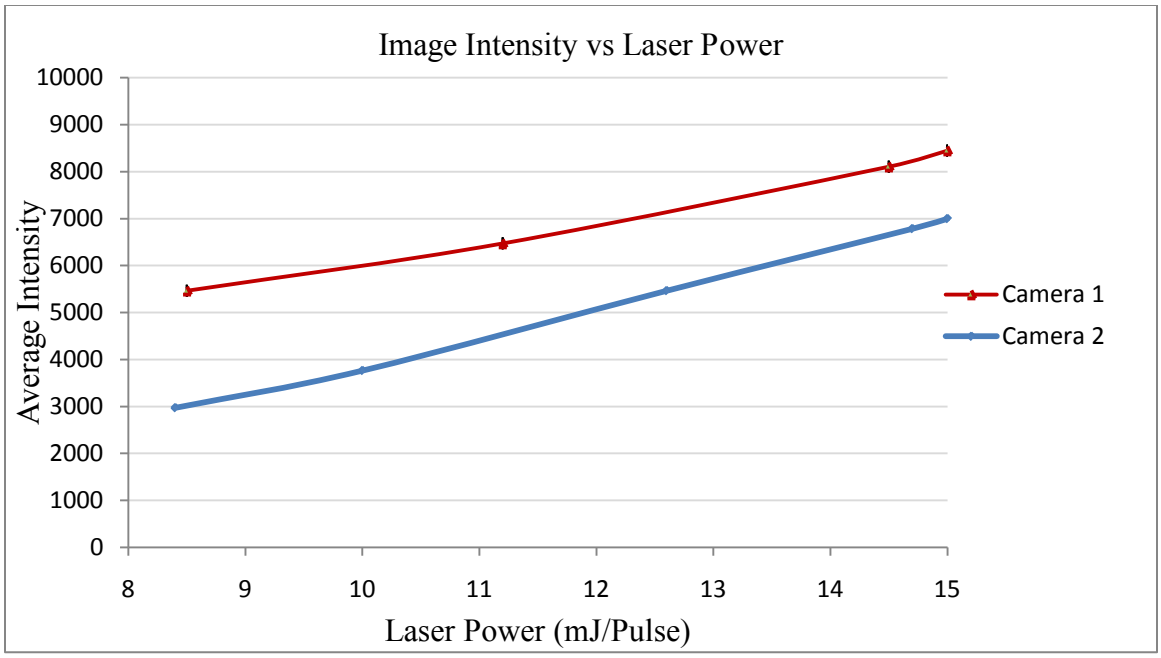

Figure 37. Verifying fluorescence is in linear regime

The next calibration exercise quantified how the new camera performed as compared to the one previously used in the COAL lab. Figures 36 and 37 indicated there is a shift between the two cameras. One of these cameras was new while the other has been in use for over three years. As with any electrical device, no two cameras perform exactly the same even when new. The old camera may also have been damaged over time if the chip was ever oversaturated by an image (65,000 signal counts/image). This can occur if images are taken with full gain with room lights on, for example. When performing a PLIF thermometry experiment, the LIF signal from one transition was divided by the LIF signal from a second line transition. In this case the two transitions are the $Q_1(14)$ and $Q_1(5)$ lines. Since each camera captures fluorescent intensity from one line, if one camera produces a different signal than the other for the same event, the ratio and therefore temperature will not be accurate. This calibration exercise was similar to

the flashlight test; only the fluorescent activity was LIF signal from passing a laser sheet through the Hencken flame, with changes in φ used to vary the signal. After verifying the camera settings were identical such as f-stops settings, the difference in the signal count from the two cameras for the same event was recorded. Each red dot indicates the mean intensity difference for a set of 20 images and the results are shown in Fig. 38.

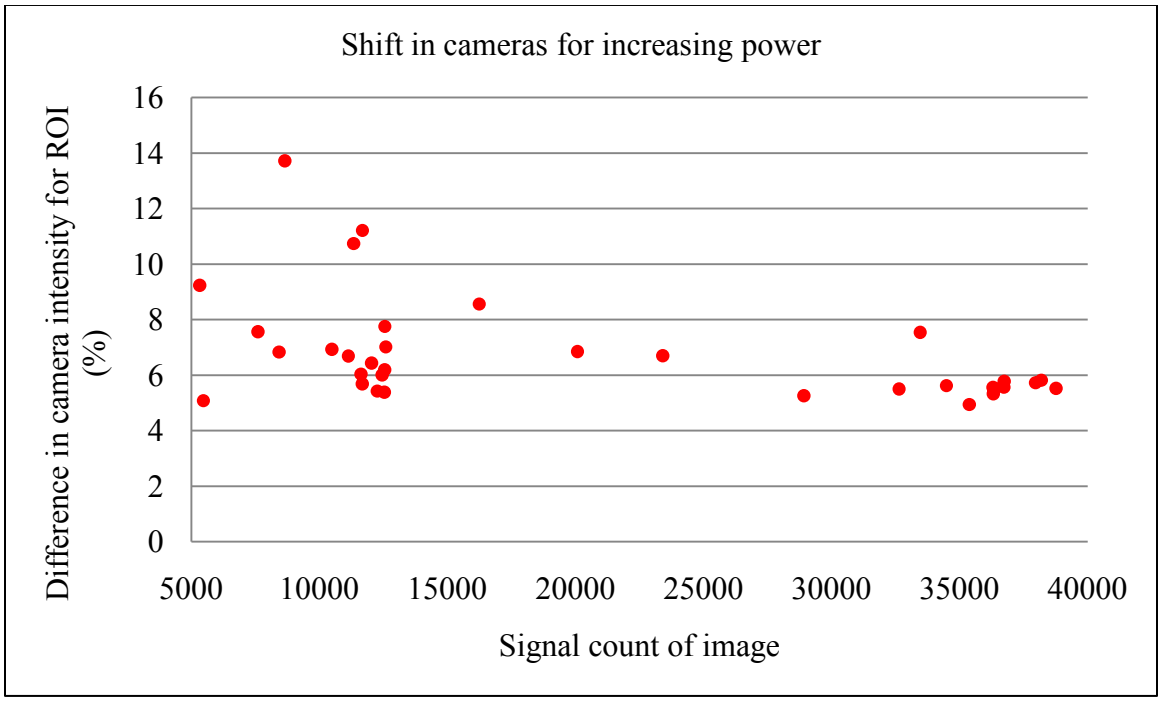

Figure 38. Percentage shift in intensity between cameras for various intensities

This figure revealed several things about the remaining tests. A shift would need to be performed on the output of one of the cameras to make the ratio of intensities give accurate results. The shift needs to be a percentage shift, not a numerical one. Based on this data a 6% shift was performed on the old camera's (1) image intensities when doing PLIF thermometry in the Hencken burner where signal counts were between 15,000 and 35,000. A 7% shift was used on all UCC data, with a reduced signal counts between

5,000 and 15,000 per image. The shift introduced uncertainty into the final temperature measurement. To quantify the amount of uncertainty the difference in cameras introduced if an incorrect correction factor is used, the temperature error for every 1% shift of cameras was plotted as shown in Fig. 39. For the temperature ranges of this research, the temperature error would be ~0.4% for every 1% error in shift of cameras.

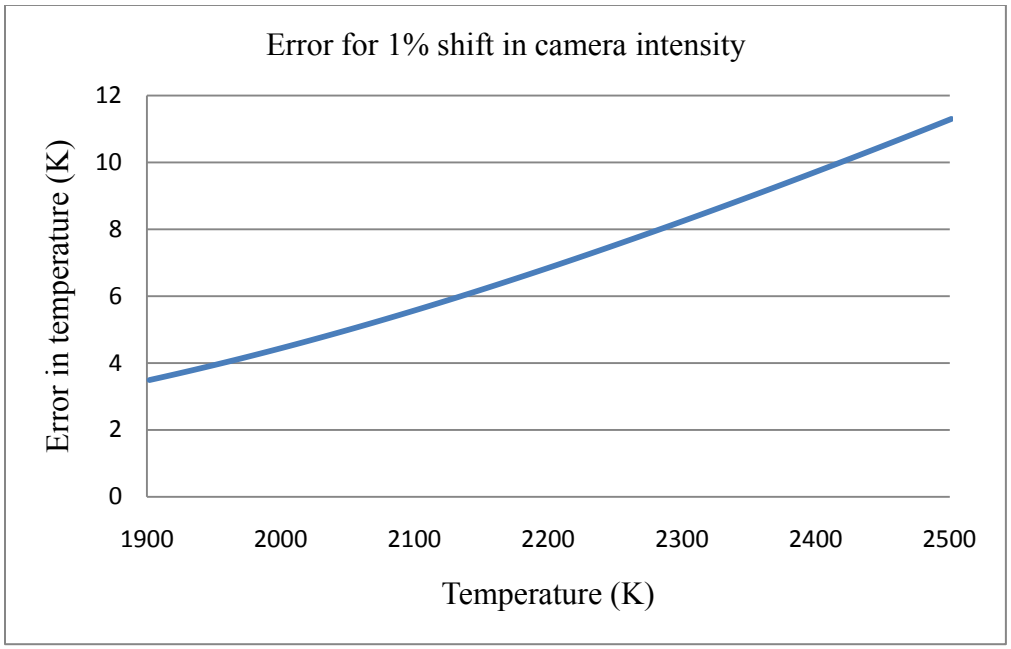

Figure 39. Temperature error for every 1% shift of cameras

IV.1.1 Theoretical Equilibrium Data

Theoretical data was needed as a basis for comparison to data gathered from OH PLIF of a flame produced by a Hencken burner. This data was used to validate the laser system in the COAL lab. A combustion equilibrium solver known as STANJAN[41] was used to calculate theoretical equilibrium data for a hydrogen-air flame. The data is produced from coded adiabatic combustion equilibrium calculations. An equilibrium temperature (adiabatic flame temperature) and OH species concentrations were determined for a range of equivalence ratios at atmospheric pressure and inlet

temperature. To vary the equivalence ratio, moles of hydrogen were varied while moles of air were held constant. Adiabatic flame temperature was found to be the highest for φ = 1.1 and OH concentration was the highest for φ = 0.95 as shown in Figs. 40 and 41 respectively. Both of these conditions assume complete combustion. Experimental data gathered in the lab was compared to this data to determine the accuracy of results.

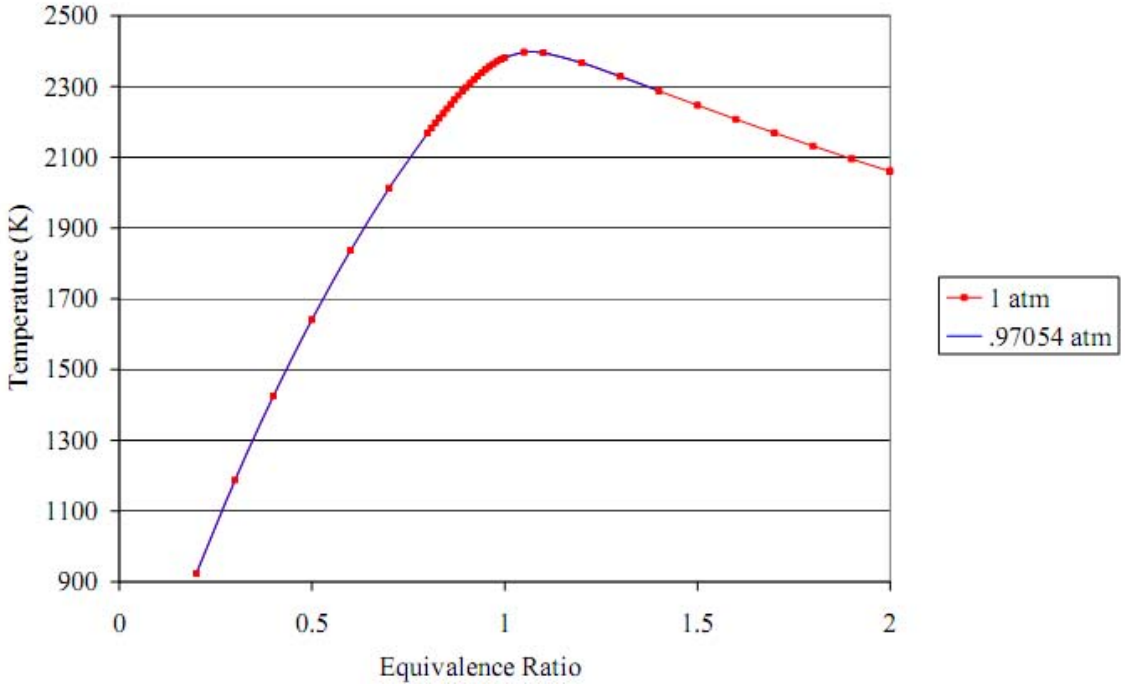

Figure 40. Equilibrium temperature versus equivalence ratio

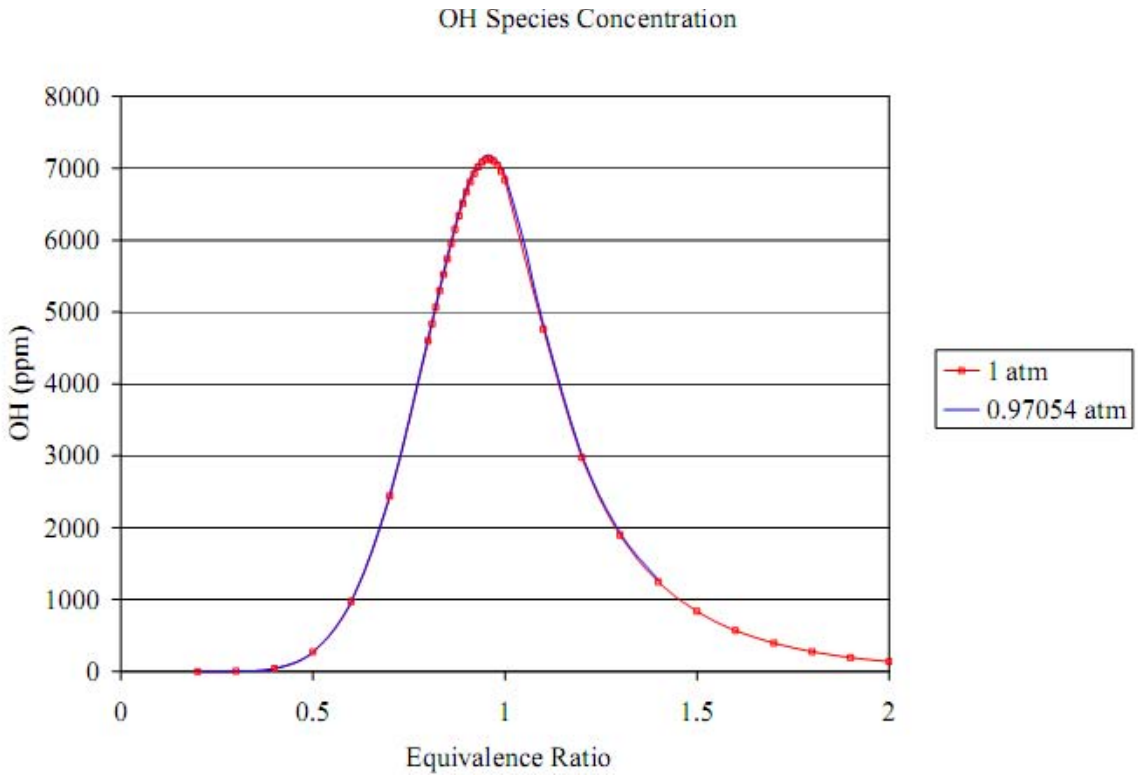

Figure 41. OH concentration versus equivalence ratio

IV.1.2 One-line PLIF thermometry

Once the cameras were quantified, the first experiments were started. The first tests were non-simultaneous PLIF thermometry. Since the Hencken burner will be used to calibrate the thermometry process for use on the UCC, it was important to run each test point at the desired equivalence ratio. The COAL lab uses MKS mass flow controllers to meter the flow of hydrogen, air and nitrogen to the Hencken burner. Previous researchers discovered that when a flow percentage is dialed into the MKS digital readout in Fig. 26, the actual flow delivered by the mass flow controller may be slightly different.[13,27,28] To calibrate the controllers, a BIOS Definer 210 flow meter measures the actual flow for various percentage inputs to produce a calibration curve. However, even after following this process, researchers were experiencing shifts in the location of peak temperature or

OH concentration and suspected a loss through the burner itself. To check this suspected loss, a calibration cup was designed to fit over the Hencken burner to measure the flow directly. The plastic cup built by the AFIT model shop and shown in Fig. 29 uses O rings to maintain an airtight seal. The results are shown in Fig. 42, which compares the actual flow rate directly from the line and through the burner to what should be delivered at that setpoint.

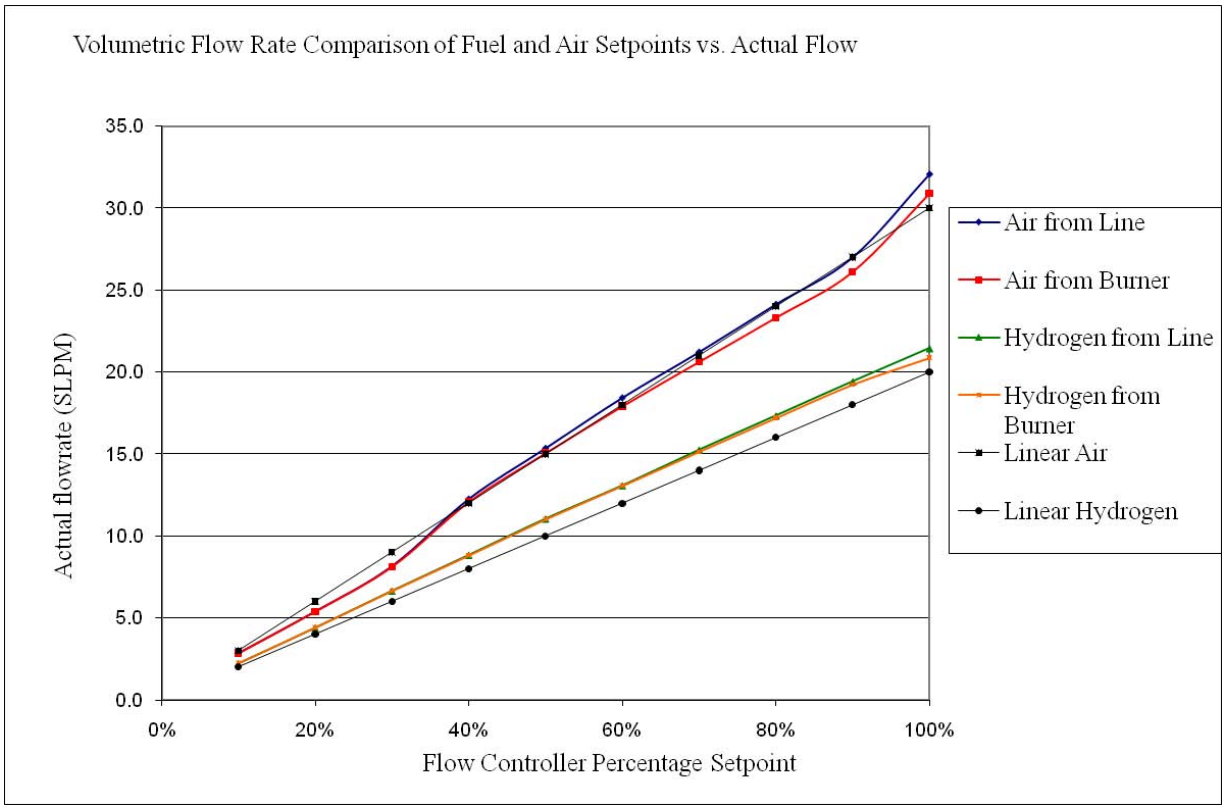

Figure 42. Difference between actual and set flow rates

The plot shows there is a flow loss through the burner. The loss is plotted versus flow controller setpoint in Fig. 43. Curvefit equations were applied to the calibration lines and used to calculate the MKS setpoint needed to deliver the flow of Tables 3 and 4.

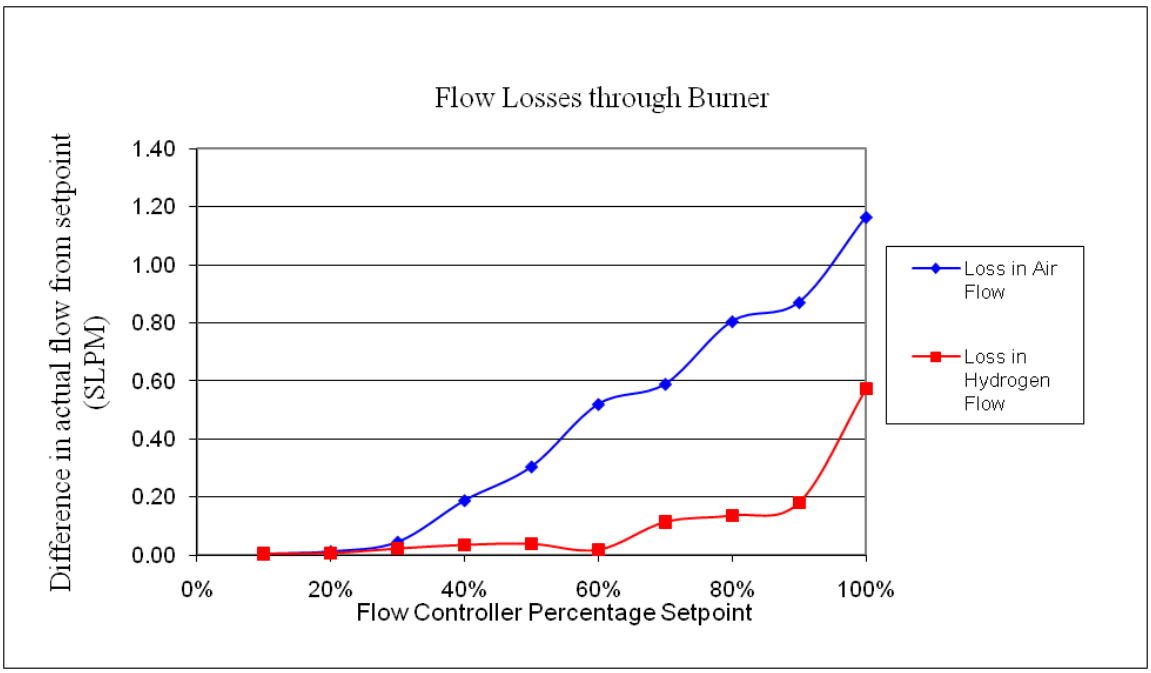

Figure 43. Losses through Hencken burner

Another possible source of error when calibrating a PLIF setup is the composition of oxidizer burned in the test unit. Early experimental runs showed a small shift in the peak of OH intensity even after correcting the flow rates. Theoretical databases show the peak OH concentration should occur at $\varphi = 0.95$. The experimental data was peaking closer to $\varphi = 0.98$. After examining the experimental setup, a problem was identified with the zero air being used in the COAL lab. It had a guaranteed O_2 content between 19.5 and 23.0%. Equation 4 assumes the simplified composition of air is 21.0% O_2 and 79% N_2 by volume, giving for each mole of O_2 in air there are 3.76 moles of N_2. If the actual content of the air used in the experiment is different, it will shift the results slightly since the true φ would be different than the calculated φ. Figure 44 illustrates this point by using 19.5, 21.0, and 23.5% in eq. 4 and showing how the results shift for one of the data sets. Knowing the actual oxygen content is important. This uncertainty can be significant when calibrating a LIF system. To eliminate this uncertainty, calibrated zero air was used

for the remainder of the test events. Future PLIF experiments should use calibrated zero air or emissions grade zero air where the oxygen content is known. The California Analytical Instruments (CAI) or Testo gas analyzer may also be able to analyze the gas within the COAL lab to give accurate concentrations. Swagelock® fittings have been ordered to adapt the Testo emissions probe to the air lines used in the lab. This may have been a source of uncertainty for past COAL lab researchers as well. Hankins reported a shift of approximately 3.15% in the peak of each OH concentration curve when performing LIF experiments.

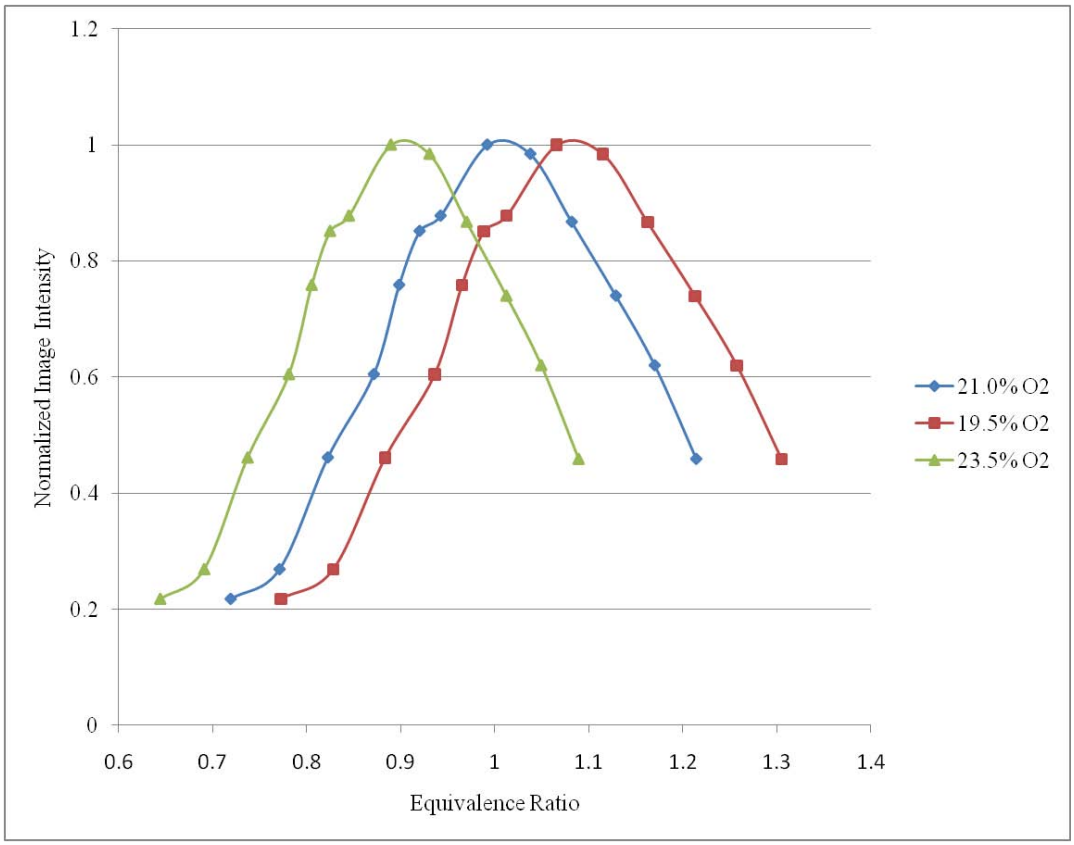

Figure 44. Effect of oxygen content

Once the flow rates were corrected, the process for non-simultaneous measurements involved passing a laser sheet from only one of the transitions, such as the $Q_1(5)$ line, and recording LIF signal for a range of equivalence ratio. The process was

then repeated with the second line. Since one dye laser can be used, previous AFIT students have performed PLIF thermometry in this manner in the past. The non-simultaneous measurements were used as a starting point to verify the setup was working and compare to past results. Several changes in methodology were implemented during this research, such as higher flow rates through the burner to reduce heat transfer, using an updated image math equation, using updated flow calibration techniques and using certified air.

Since only one line was being tested at a time, the fluorescence was recorded with both cameras for the non- simultaneous measurements helping to verify the accuracy of the 6% correction factor described earlier. The results for one of the runs are shown in Fig. 45.

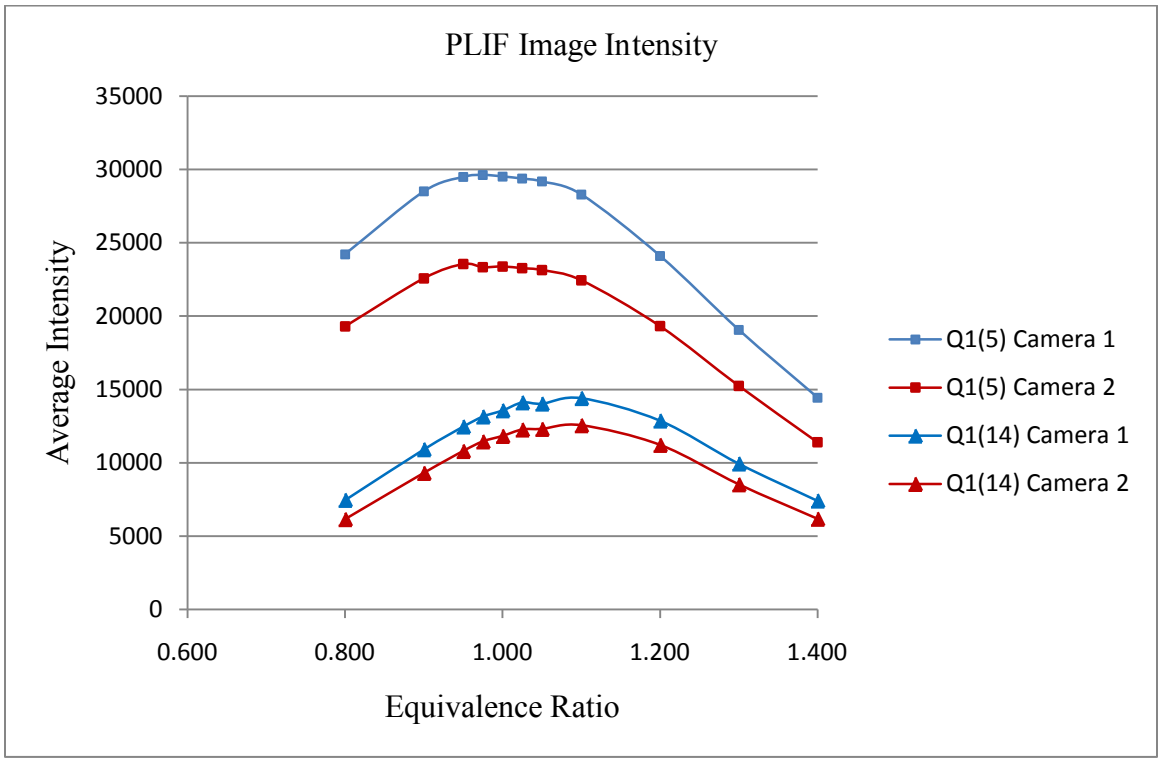

Figure 45. Non-simultaneous results

The average intensity in the ROI for each φ was then normalized by laser power, corrected for LIF efficiency, and adjusted with the correction factor for one of the cameras. Equation 15 was applied to subtract the effects of the background, laser, and flame. Finally, eq. 9 was used to calculate the temperature. The results were encouraging as shown in Fig. 46 – they were ~5% from equilibrium between φ = 0.8 and 1.2, an accuracy level that is valuable to combustion research.[27] Temperature measurements with < 3% error have been achieved with CARS,[44] but the experimental setup is more difficult than PLIF and the measurements are limited to point values only. The results were compared to past researchers in the COAL lab[27,28] and were similar to their results; error levels were also similar to other researchers[37,42,43] that have performed PLIF thermometry. This process was repeated several times to verify the results. Error bars on Fig. 46 indicate one standard deviation about the mean temperature value of the data set. As experienced by other researchers using PLIF thermometry, the results are most accurate around φ = 1.0 and least accurate for fuel rich or fuel lean conditions where LIF intensity decreases.

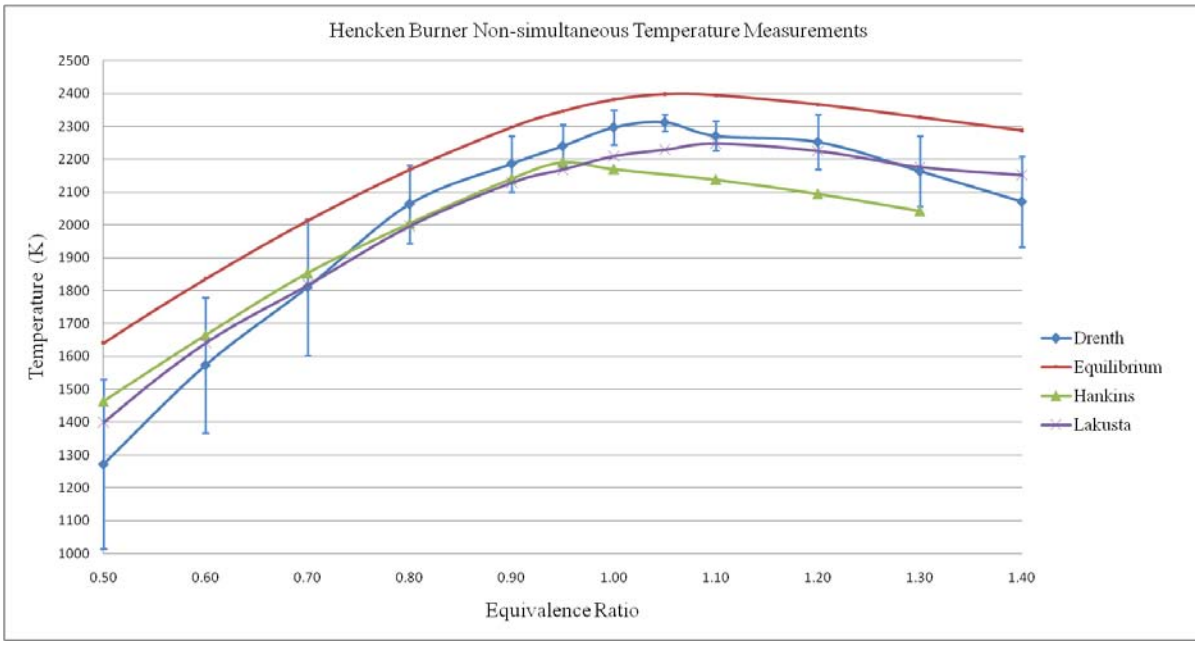

Figure 46. Non-simultaneous temperature measurements of Hencken flame

When doing PLIF studies on the Hencken burner and the UCC, it was important to have each camera looking at the same region and do image math on the same region. Using the same region was especially important with the Hencken burner as the cameras are looking across from each other. The result is illustrated in Fig. 47, where the effects of absorption can be seen as the laser sheet passes through the flame. The absorption of the laser beam as it passes through the flame affects the laser intensity in the ROI and may vary slightly for each line. Other sources of error in these measurements may include shot-to-shot variations in laser power and inability to tune the dye laser precisely at the line peak.

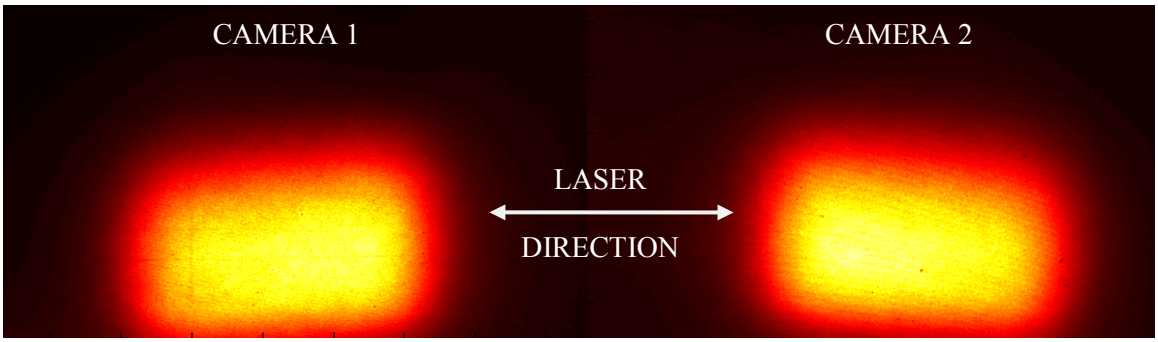

Figure 47. Decreased signal due to absorption

IV.1.3 Changes to experimental setup for two-line thermometry results

To have an accurate simultaneous two-line PLIF thermometry setup, the laser sheets produced from the two lines must overlap to study the same ROI. If they do not overlap, the properties of the flame may be different, especially in a small scale combustor like the UCC. The best way to get the beams in the same location in the ROI was to try to combine them before the sheet forming optics. A review of the literature revealed others have used a dichroic lens to combine the beams. A dichroic lens uses a coating to allow one beam to pass through, but reflects the other laser beam like a mirror. The coating is based on wavelength. This optic technique is not possible for this research due to wavelengths of the $Q_1(5)$ and $Q_1(14)$ line being so close together (282.750 and 286.456 nm respectively). Another possibility considered was a 50-50 beam splitter. The beam splitter allows 50% of the beam through and reflects the remaining. It was considered for this setup since it was simple to use and cost effective, but not pursued due to the penalty in laser power, potentially degrading the accuracy of the measurement. A thin film polarizer was also considered, similar in concept to the beam splitter but more efficient. After weighting the options, a polarizing beam splitter cube was chosen. This cube can combine equal wavelengths at opposite polarizations. PLIF is not impacted by

the input polarization so it was a good choice for this technique. A 1/2 wave plate was used to change the polarization of each line after it exits the dye laser. The cube was chosen since it is very efficient at combining beams (~90%) and easy to use. Figure 48 illustrates some of the options that were considered; the illustrations show beam separation versus combining.

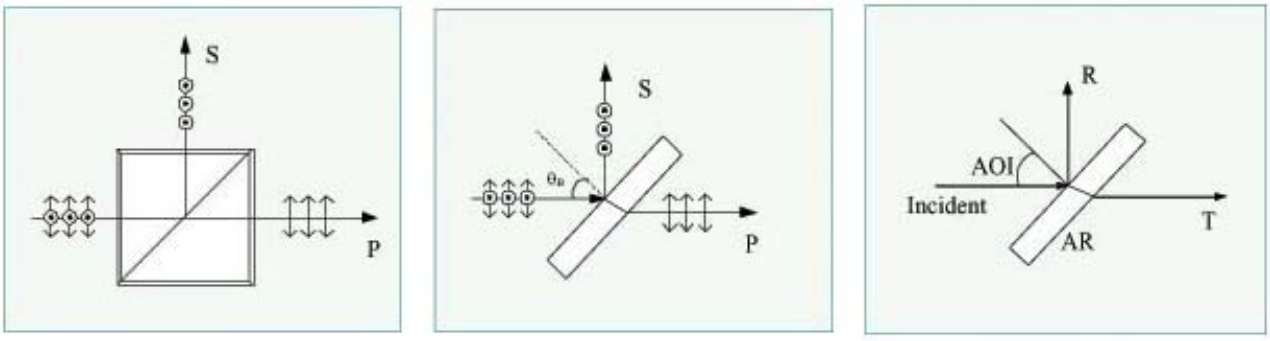

Figure 48. UV polarizing beamsplitter cube, high energy beamsplitter, thin film polarizer

The first cube used was a Lattice Electo Optics, Inc polarizing beamsplitter cube (PBU-283-10). The quoted damage threshold for this optic was 20 mJ/cm^2, but was damaged by one of the dye lasers while running at 75% of this value, shown in Fig. 49. The manufacturer claimed hotspots were responsible, but even after realignment of the laser and using burn paper to check for hotspots, the beam continued to damage the optic. A second cube was ordered from Rocky Mountain Instrument Co. (PC26U028). The two parts of the cube are optically fused, instead of using optical glue as in the LEO cube. The RMI cube was higher in cost but has a damage threshold of 100 mJ/cm^2.

Figure 49. Damaged LEO cube and Zap-It® Burn Paper showing hot spots

While waiting for the second cube to be manufactured, the optical setup of Fig. 22 was changed slightly. Instead of combining the beams before the sheet forming optics, two sets of sheet forming optics were used. As both lines are being formed into a sheet, the beams are slowly converged as shown in Fig. 50. The last 2" round mirror in the optic train was replaced with two 1"x2" mirrors that are placed next to each other and set at 43° and 45°. When the two lines approach the test section, they are perfectly overlapped for 6". This setup has an advantage to using the PBU cube in that there are no power losses through the cube. The big disadvantage and reason it was not pursued as the first option was the path through the quartz window of the UCC. The length required beams to be collinear for a significant distance for a region to be studied. If translated left or right, one of the beams would get blocked by the wall of the UCC. The window opening is only 12 mm wide and the ROI where the sheets must overlap is 210 mm downstream as shown in Fig. 51. The middle of the main channel was chosen to overlap the sheets and all results in the following sections refer to this ROI.

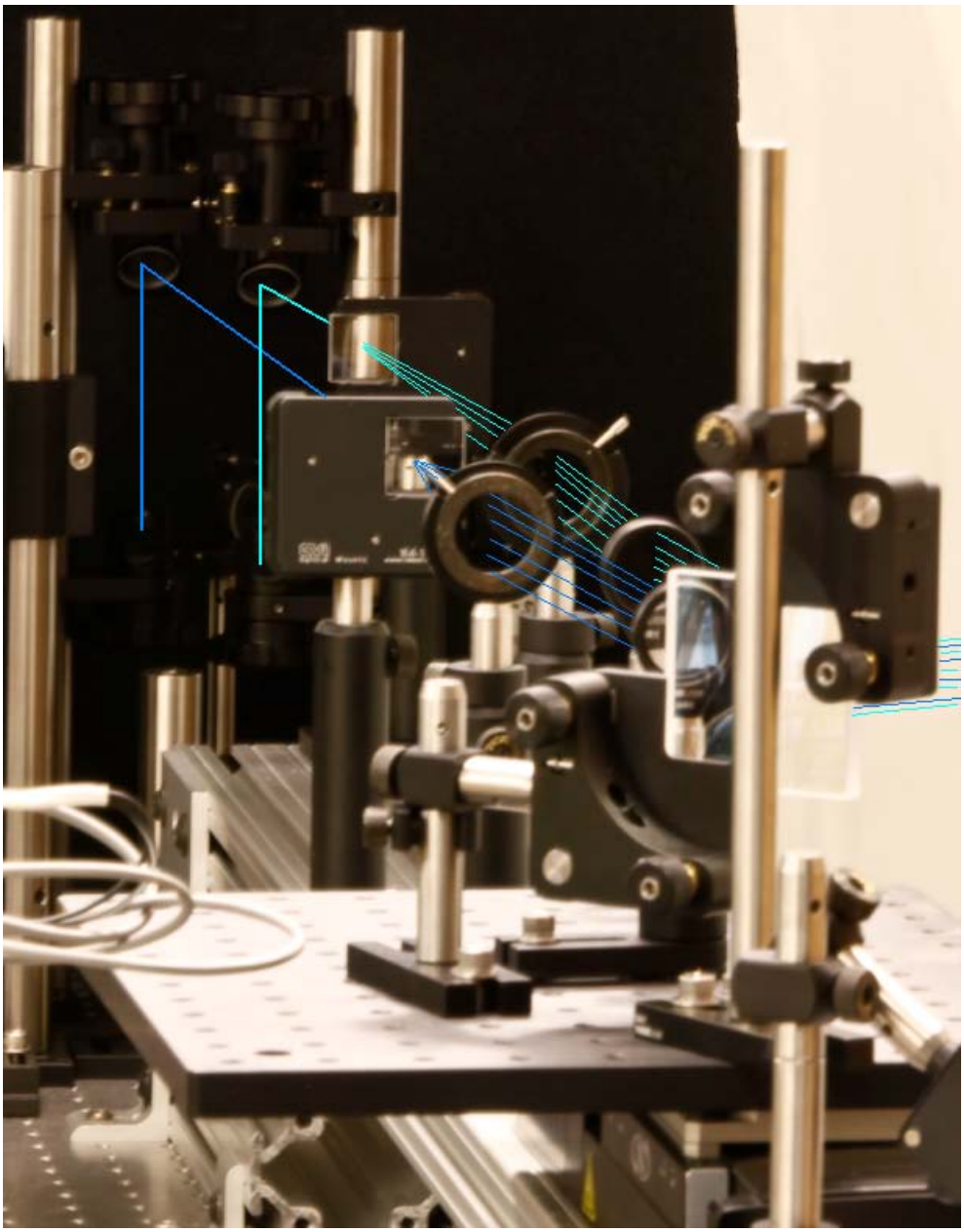

Figure 50. Sheet forming and overlapping optics

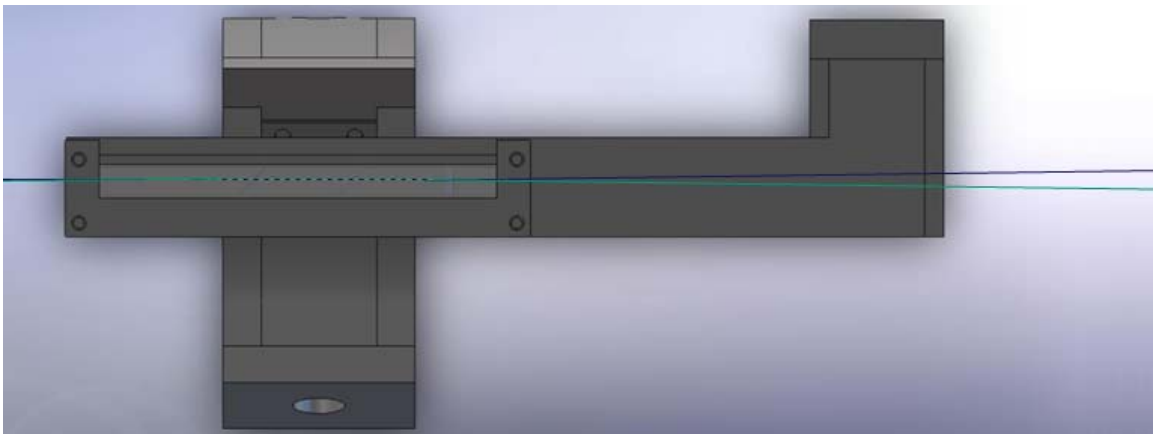

Figure 51. Top view of overlapping sheets in UCC

IV.1.4 Two-line PLIF thermometry results

Once the optic train was modified, simultaneous two-line PLIF experiment was performed on the Hencken burner. The testing procedure was the same as with the non-simultaneous measurements described above, with both lines recorded simultaneously and each camera recording the fluorescence of one line. The results are shown in Fig. 51 as well as the non-simultaneous for reference. The temperature measurement is based on the mean value of image intensity. To account for error in shot-to-shot noise, a 90% confidence interval was drawn about the mean intensity for the 20 images. The temperature was also calculated using these upper and lower confidence intervals to show the effect of shot-to-shot noise on the measurement and is represented by error bars in Fig. 50. Error bars also account for the run-to-run variation in laser power, recorded before each test run. The slight fluctuation near $\varphi = 1.05$ is from where the lasers were adjusted to re-peak their power. The results were similar to the non-simultaneous temperatures and the system was considered calibrated and ready for use in the UCC.

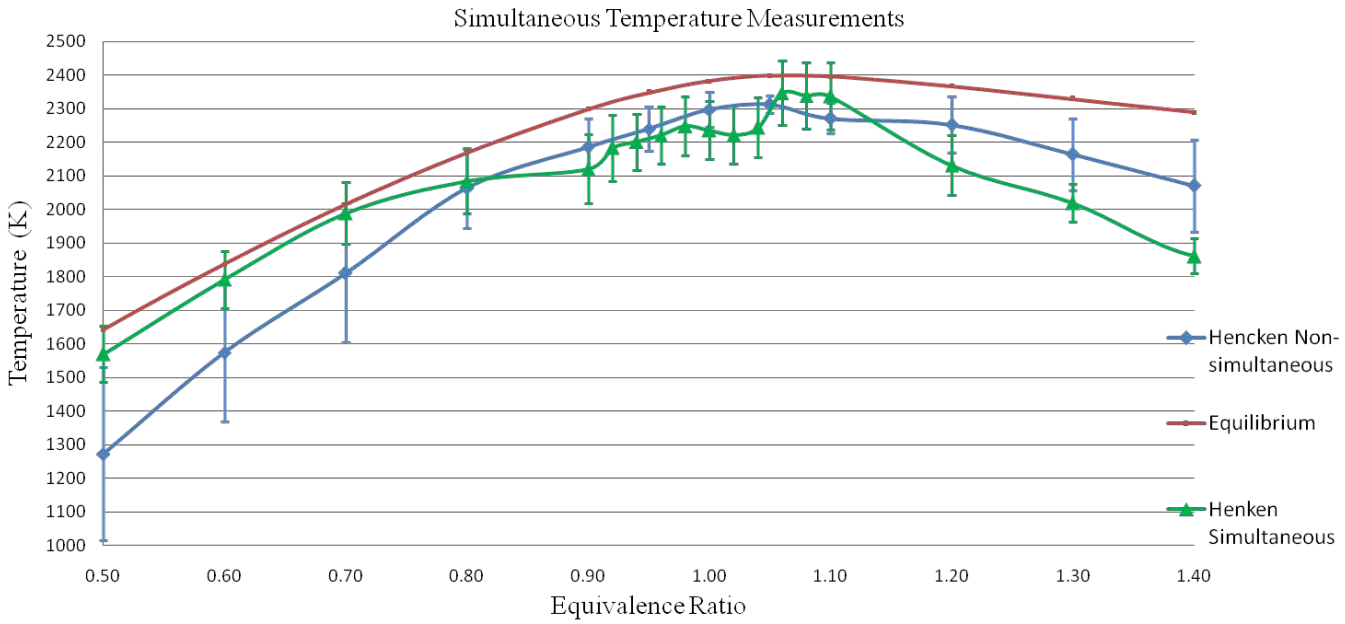

Figure 52. Simultaneous temperature measurements of Hencken flame

During this research, a 30 to 1 signal to noise (S/N) ratio was enjoyed for most of the runs in the Hencken burner and a 20 to 1 S/N for the UCC runs. High S/N level was partially due to the measures used to block laser scatter. Laser scatter can cause false signal since the camera cannot distinguish it from the fluorescent event. This introduced noise is especially true for the scatter of the 532 nm beam from the YAG before it enters the dye laser. The wavelength is close to the fluorescence and not filtered before entering the camera. To reduce scatter, a beam block was used to completely isolate the test area except for a small opening for the laser. This greatly reduced laser scatter as shown in Figs. 52 and 53.

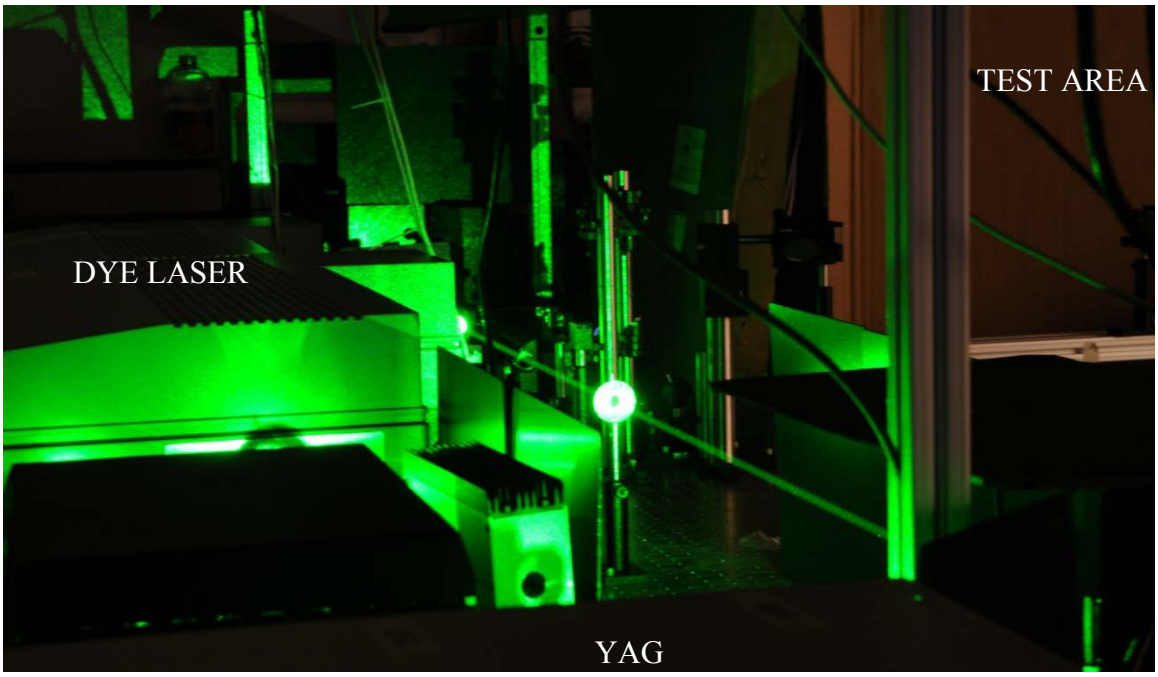

Figure 53. 532nm Laser scatter

Figure 54. Blocking of laser scatter

Since the face of the burner can cause scatter of the incoming laser beam, its stainless steel face was masked off with tape. Hankins[27] found there was a large amount of variance in the LIF signal near the burner surface caused by scatter. The stainless steel posts from the camera and filter holder were also masked since the opposite camera is looking at them and collects any reflections. Finally, the experiments were performed without room lights so gain could be maximized. Permanent aluminum laser blocks have been designed and ordered for future researchers to replace the current sections shown in Fig. 55.

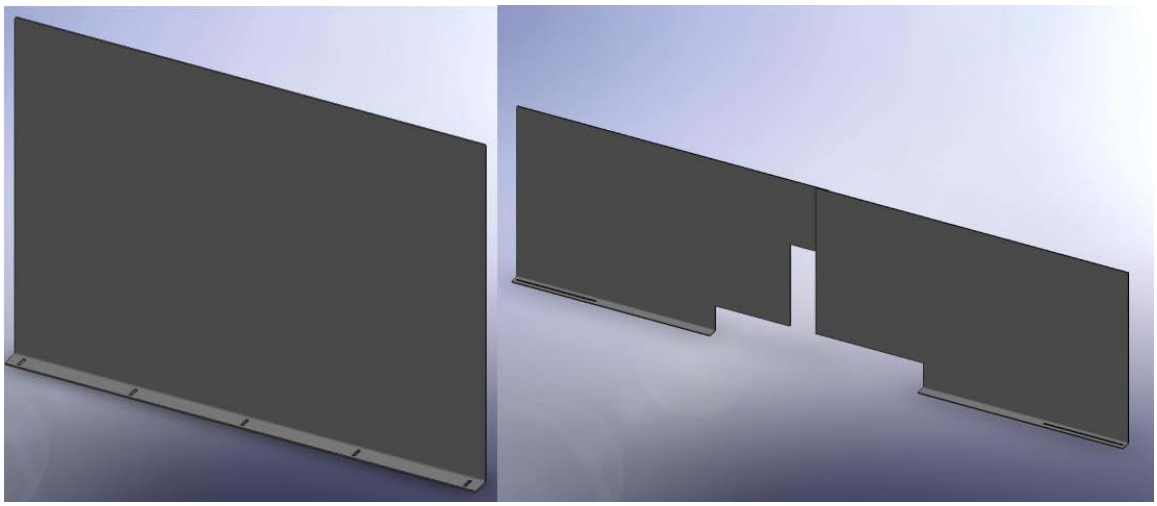

Figure 55. New laser shields

IV.1.5 Two-line PLIF thermometry results –cavity exit

The first area of the UCC studied for temperature measurement was the cavity exit of both the curved and straight sections. This region would represent the temperature of the combustion in the cavity around the engine. Most of the burning takes place here, the primary zone of the combustor. There was a large amount of OH due to the amount of burning in this location. The amount of OH produced continued to rise over cavity φ

instead of dropping off as with the Hencken burner as shown in Fig. 56. This behavior indicated there was a large amount of mixing with main flow air.

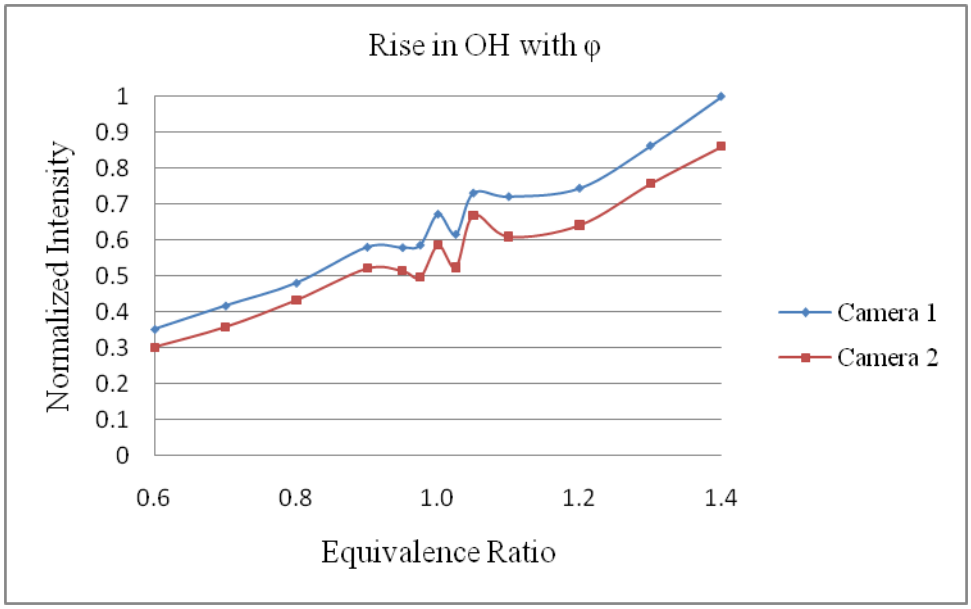

Figure 56. Rise in OH concentration with equivalence ratio

The ROI chosen was 2 cm from the exit plane. The straight section values were recorded first in a manner similar to the Hencken burner described above. The process was repeated with the curved cavity. A quick alignment check between straight and curved section runs was used to verify the same ROI would be used for both cavity sections for comparison. The results are shown in Fig. 57 with image averaged values used to calculate the temperature. Error bars represent shot-to-shot variations of the images based on a 90% confidence interval around the mean and run-to-run variations in laser power.

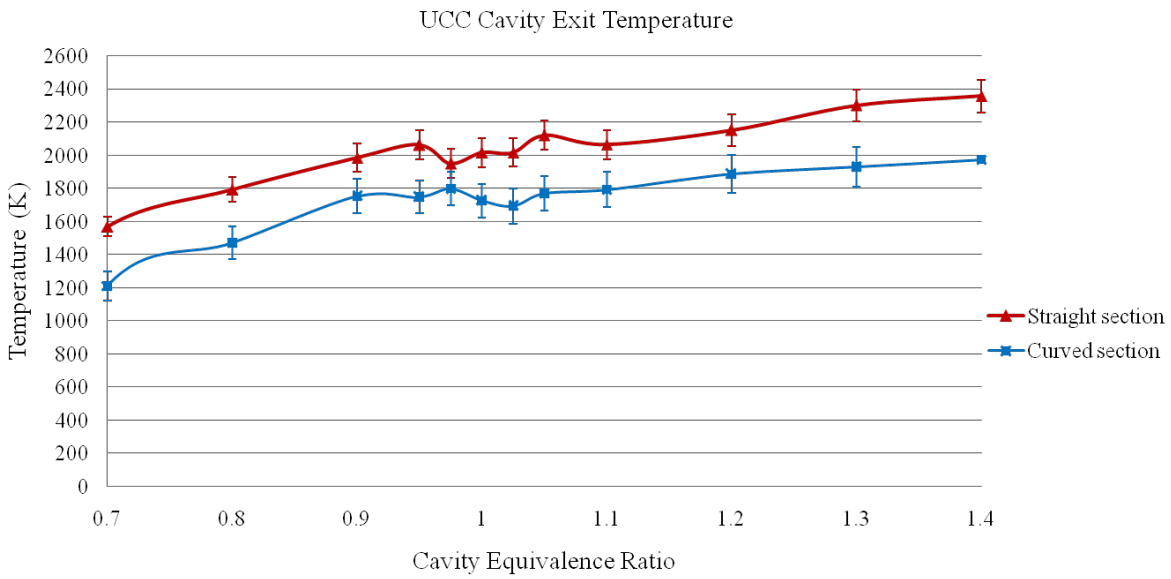

Figure 57. UCC cavity exit temperature for curved and straight sections

The difference in temperature between the two runs may be due to the difference in exit area between the curved and straight section. The curved section currently has a smaller cavity exit area, forcing more burning into the main section and lowering its temperature in the cavity exit relative to the straight section.

Since many combustion flows of interest are unsteady, objectives for PLIF thermometry often include temporally resolved (instantaneous) images. The measurement of instantaneous temperature measurement may be essential for verifying various combustion models or strategies. Short test times at some flow facilities such as hypersonic and high-enthalpy test sites may limit acquisition to a single image or data sets to small for successful averaging.[37] The temperature measurements described above in the Hencken burner and cavity exit were obtained from using 10 on-chip accumulations per image. Twenty images are taken for each φ and the results are averaged. The image-to-image variation was used to draw a 90% confidence interval

around the mean. This increases the overall signal to noise ratio and is common in PLIF thermometry. Essentially, each image gives the average intensity for 2 seconds of combustion (20 accumulations x 0.1 sec/accumulation). The largest source of error in instantaneous temperature measurements is signal-dependent shot noise. Shot-noise error can be reduced by averaging more pixels with their neighbors. Averaging more pixels reduces spatial resolution. Noise can also be reduced by increasing OH fluorescence signal through other means such as increasing laser power. To demonstrate the differences and relative accuracy of instantaneous versus time averaged measurements of this study, true single shot accumulations were made using one accumulation per image. This technique was applied 50 times per φ. The same ROI was used for each image and the same ROI was used for accumulated versus true instantaneous technique. The time between laser pulses and the duration of pulse is assumed less than the time scale of the flow. The results of one of the data sets is shown in Fig. 58 with the calculated temperature for each single shot contrasted with the solution with multiple accumulations per image. The figure shows this technique is possible but would increase uncertainty in the measurement. Increasing the number of single shots that are averaged would increase the accuracy of the measurement. Giezendanner-Thoben et. al[42] found single shot errors were 3.5-8.5% when measuring temperatures in a gas turbine model combustor but reduced to 1% when averaging 200 single shot measurements. The single shot versus accumulated comparison was only performed near stoichiometric conditions where OH signals were known to be high. It is assumed this error would increase in fuel rich or lean conditions.

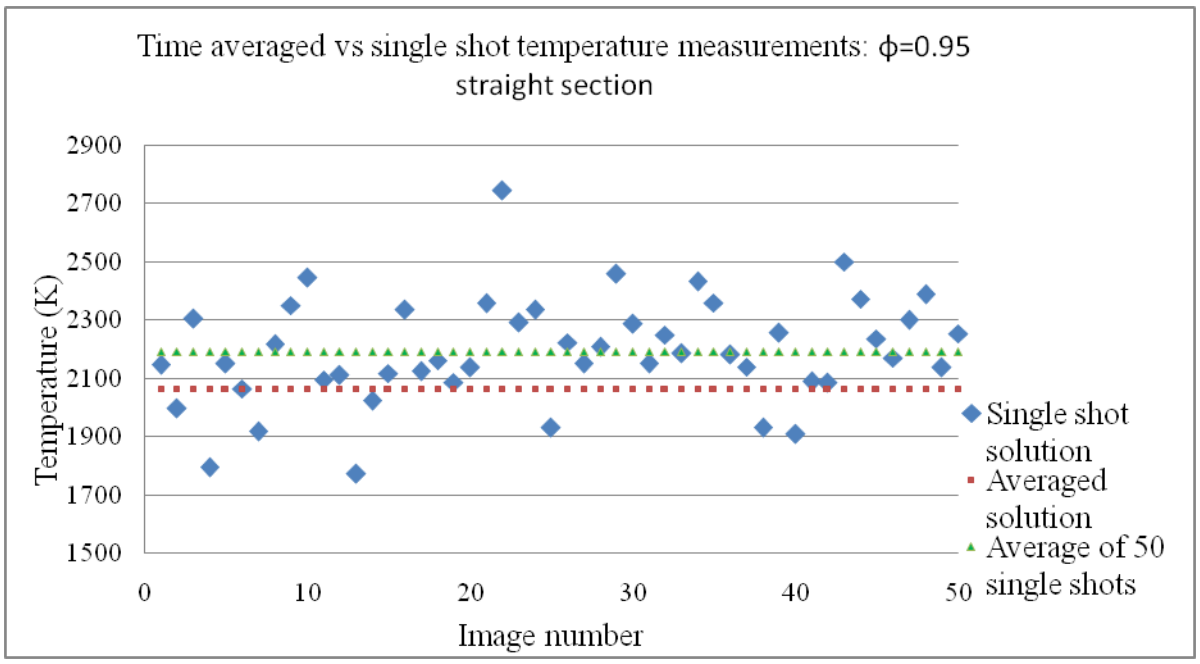

Figure 58. UCC cavity exit temperature – single shot versus accumulated average

IV.1.6 Two-line PLIF thermometry results –main section

The next two regions studied in the UCC were the main vane exit for the straight and curved section, after the RVC. In an actual engine, this region would represent the temperature going to the turbine. Figure 59 shows the alignment of the laser sheet in both the main vane exit and cavity exit as described in the previous section. The figure shows final alignment; during initial alignment, the UCC was moved down so a card could track the path of the two sheets through the entire combustor ensuring they were focused and overlapped.

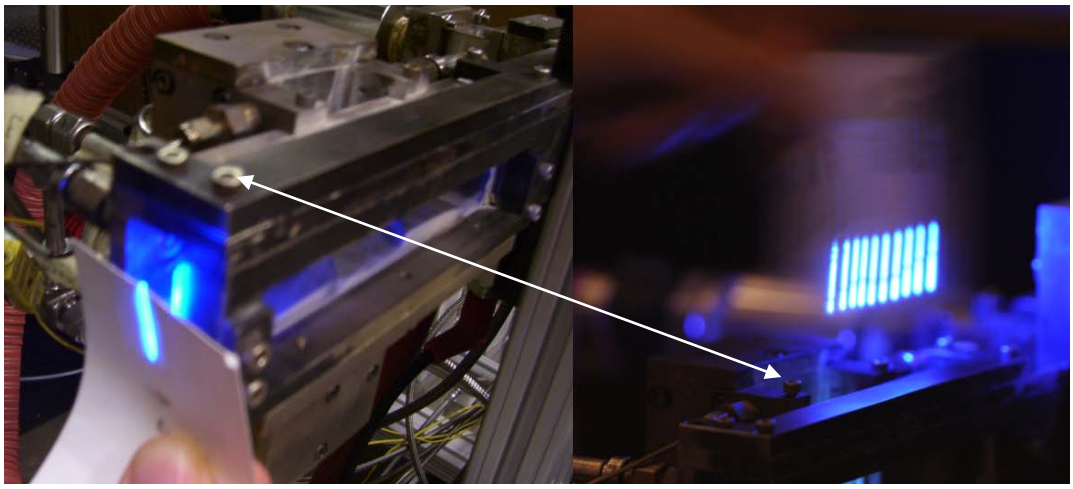

Figure 59. Aligning laser sheet in main section (left) and cavity exit (right)

The same methodology was used to study the temperature in this region. Unfortunately for this case, the temperatures measured using the ratio of intensity method did not produce realistic results. Temperatures were high – up to 5000K and nonlinear with φ. Each step of the procedure was examined closely for errors. The signal produced in this region was fairly linear and increased with φ as with the cavity exit as shown in Figs. 60 and 61. The error in the measurement was introduced when eq. 15 was applied. In the main flow, the laser background image produced without a flame was much larger in intensity in proportion to the test runs than in previous runs. When subtracting this out from the test runs, it subtracted too much intensity sometimes causing a negative intensity for fuel lean runs as shown in Fig. 62. The runs were repeated with similar results. During the second runs, the quartz window that the laser sheets pass through was removed during alignment and a laser only background image was taken without the window. This greatly reduced the intensity of the image versus with the window. It is suspected the window causes a small amount of surface scatter resulting in a high

intensity recorded on the camera. Once combustion starts, some of this scatter is absorbed during the combustion event leaving most of the intensity of the image due to OH fluorescence but is hard to quantify the amount of laser intensity to subtract. In the future, the quartz window should be antireflective (AR) coated for ~282 nm eliminating this problem.

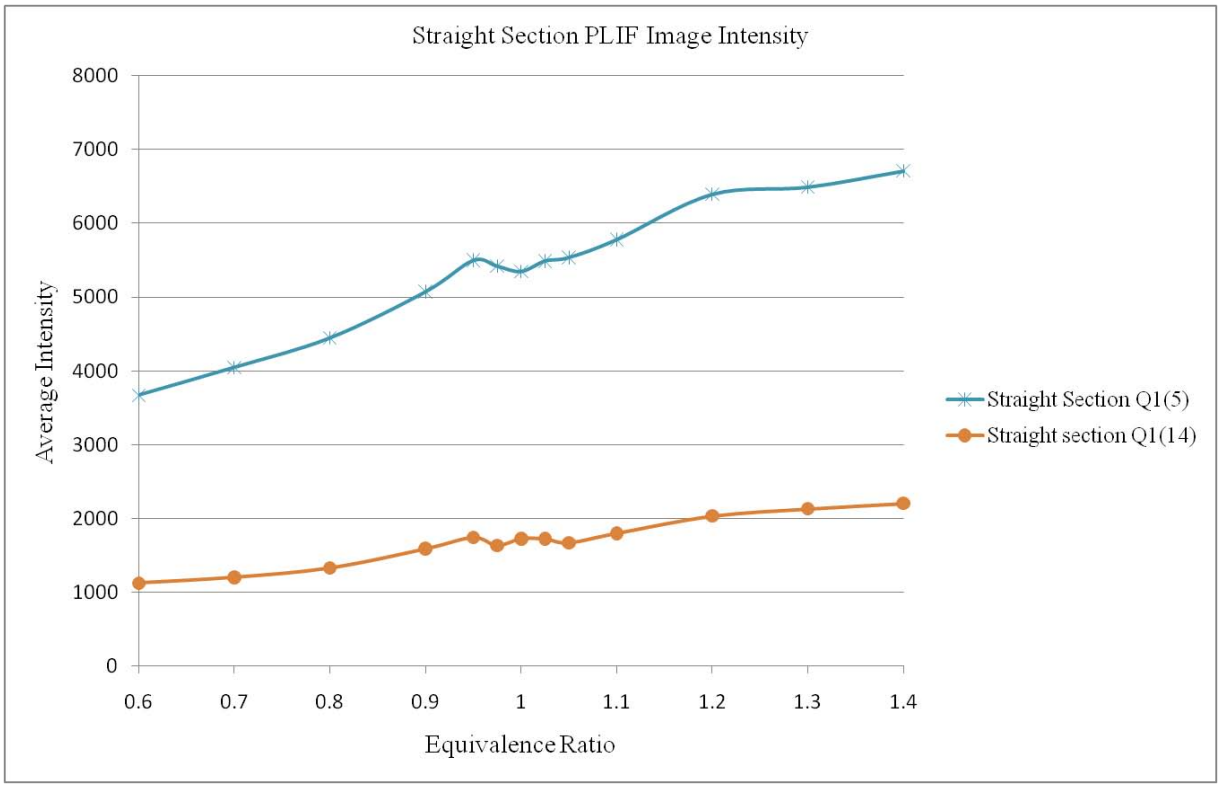

Figure 60. Image intensity versus equivalence ratio for straight section

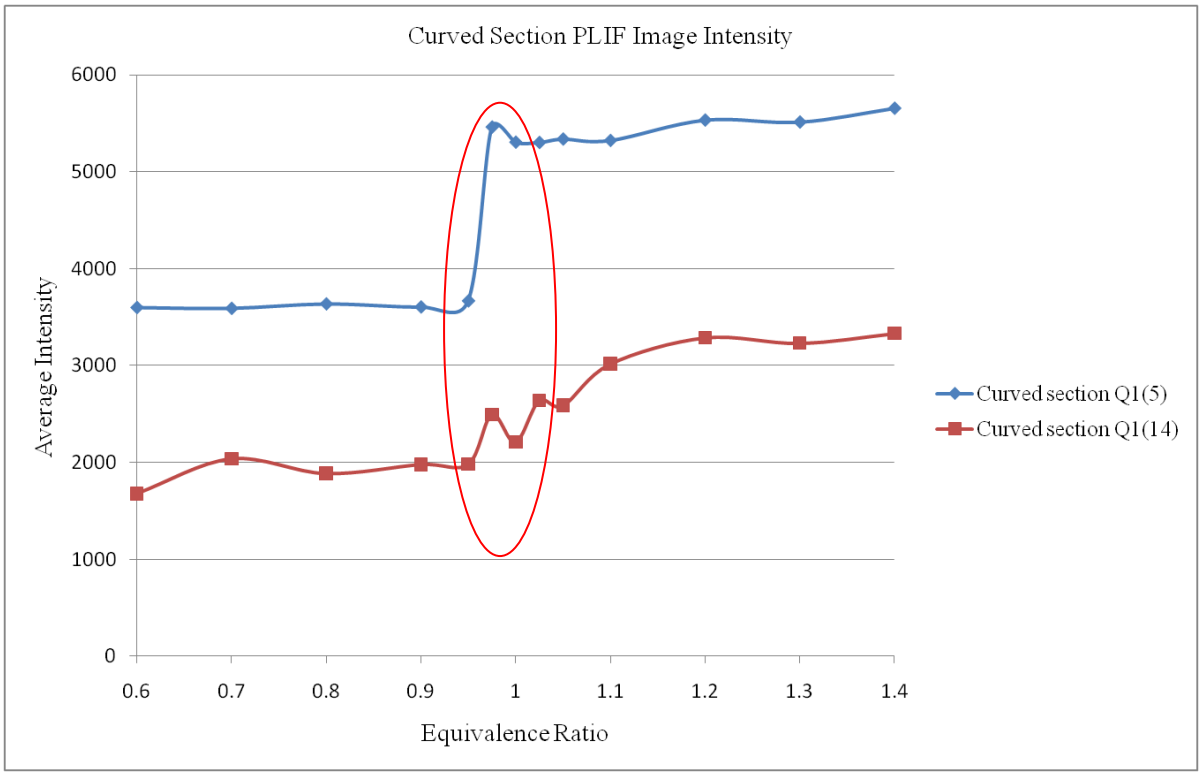

Figure 61. Image intensity versus equivalence ratio for curved section

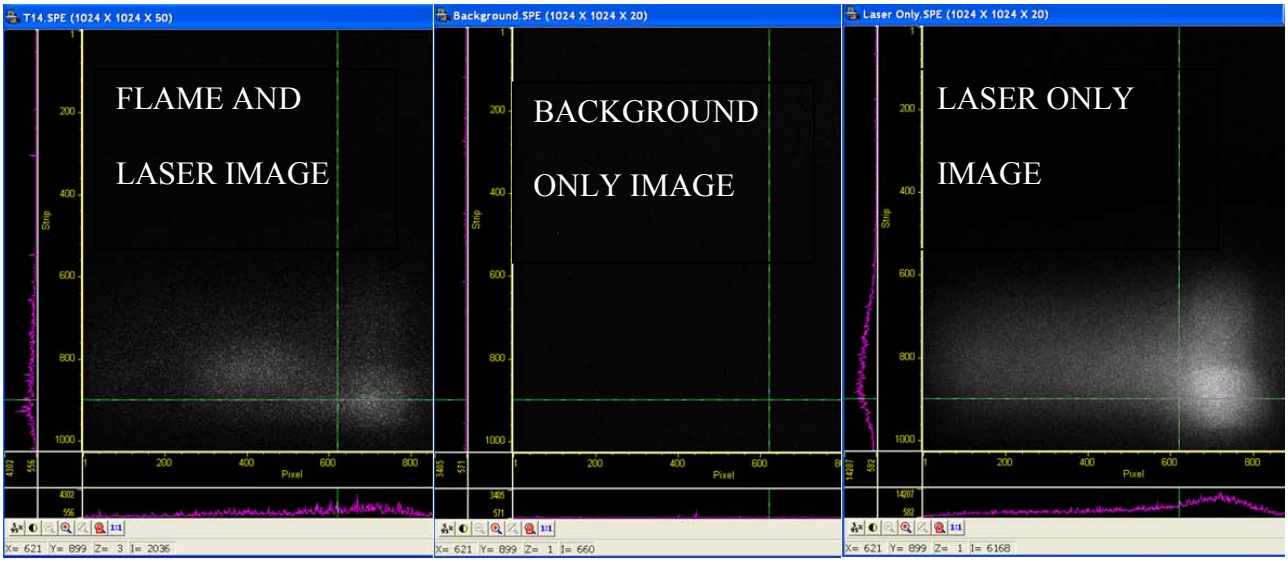

Figure 62. Image math errors due to large intensity in laser only image

The reflections due to this scatter may be compounded by the presence of PIV seeds remaining in the main channel. As mentioned in Ch. 3.1.2, PIV research was being conducted on the UCC at the same time as this PLIF research. Between tests, the main channel and quartz windows were thoroughly cleaned to remove residual seeds. However do to their small size (~2 μm), it was very difficult to remove all the seeds, especially near the RVC. The PIV seeds are inherently reflective, so that the laser sheet incident on the fluid flow will reflect off the particles and be scattered towards the camera. To show the negative effect of these reflections when performing PLIF, Fig. 63 shows the scatter due to PIV seeds as collected by the ICCD PLIF camera. The top part of the image is looking into the main channel through the quartz window. The holes are from a plastic alignment grid placed inside during alignment and focusing to make sure both cameras are focused on the same ROI. The laser sheet would be parallel to this alignment grid. The bottom section shows the actual laser background image with only the laser passing through. The alignment tool is removed for the background image. Figure 64 shows a picture of the UCC with arrows pointing to the location with highest buildup of seeds.

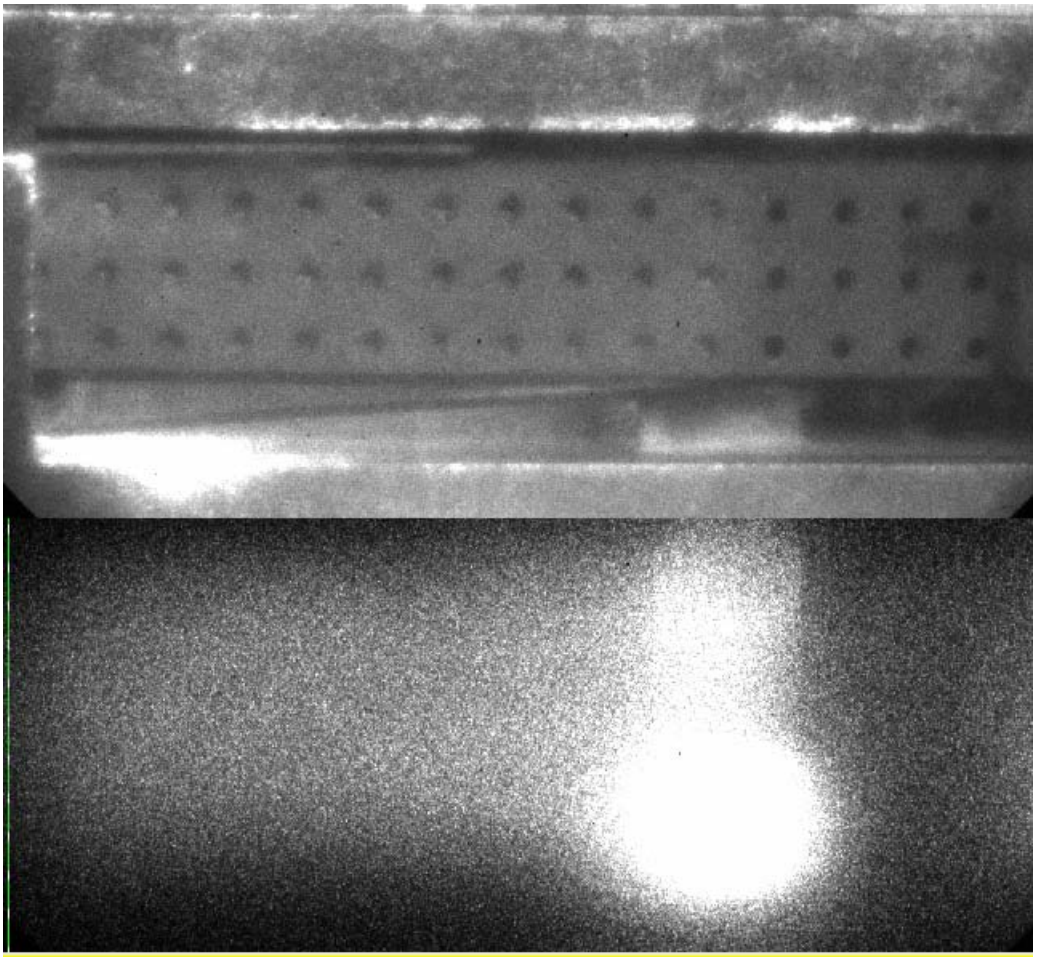

Figure 63. Location of scatter due to PIV seeding

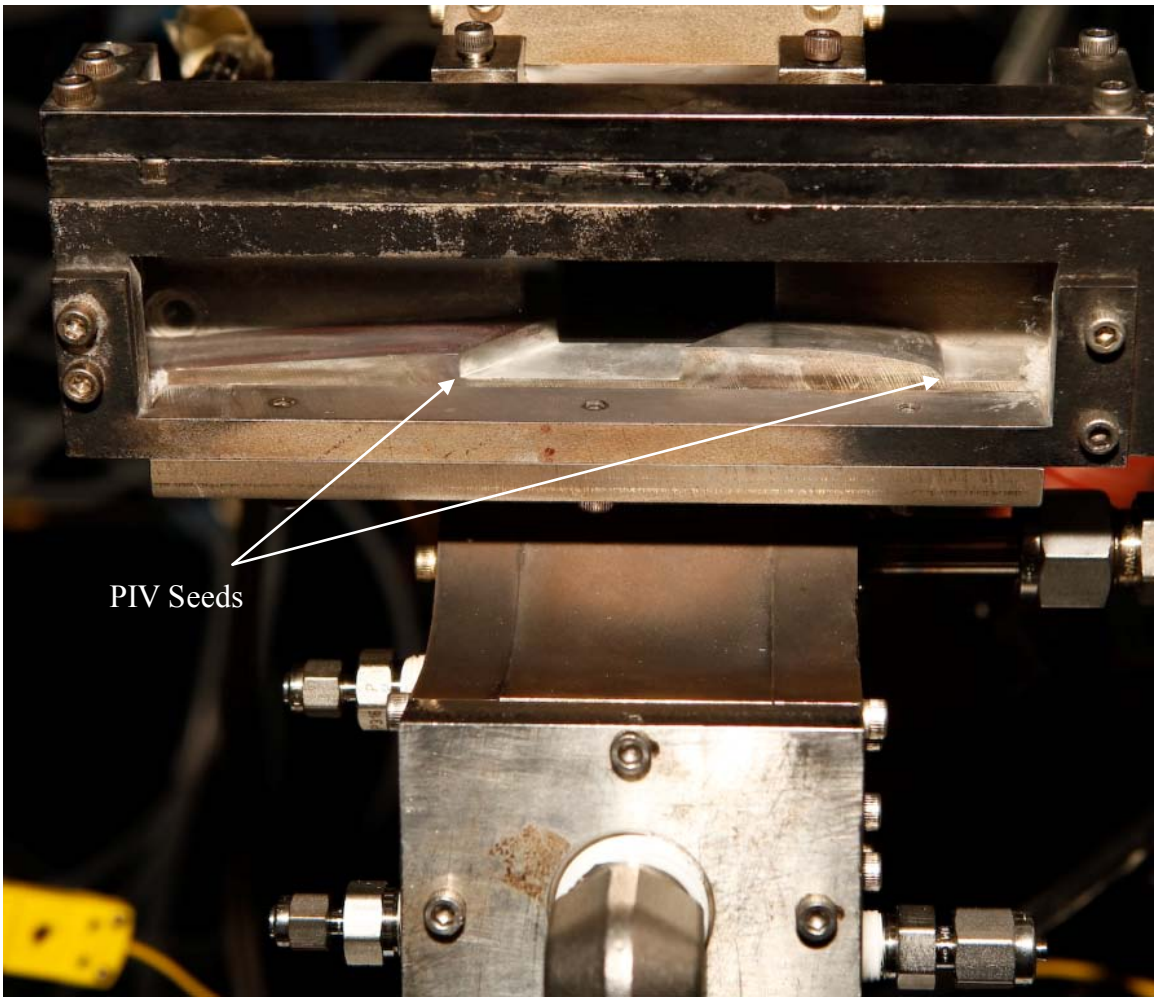

Figure 64. Location of PIV seeding

Figure 61 also illustrates another difficulty during this research and possible source of error. To peak the power of the dye laser, the doubling crystal is rotated slightly until the laser maximizes its output. As conditions change such as the room temperature, laser temperature, or condition of the dye, the laser may need to be re-peaked. Figure 61, which has not been corrected for power, shows the rise in LIF signal when the power is re-peaked mid test. The UVT auto tracking software can make these adjustments automatically but the auto trackers are not currently working on the dye laser forcing the

adjustments to be made manually through an adjustment wheel. During these test the power is checked just before starting the cameras for each run, so the correct value is used to normalize the signal. However, if the power continues to rise or fall after the power is adjusted before the test run, the correction may be off slightly. Ideally, the power would remain constant for the entire test run and be the same for both dye lasers. For the power levels and intensity ratios typical in these tests, a 10% error in recorded laser power would result in a 5% error in the temperature measurement. Since the images were taken almost immediately after checking power, the actual error is much less than this. Still, future students should continuously monitor power and having the auto trackers fixed may eliminate the issue altogether.

IV.2 PLIF to study the UCC

As discussed in section 2.7.3, OH PLIF has a range of uses besides temperature measurements, including acting as a flame marker for flame location studies. While taking images for PLIF thermometry, the images were also used to study flame locations and behavior. Analysis was done inside the main channel and at the cavity exit for both curved and straight section.

One of the first conclusions was that strong transitions (large population fractions) produce stronger LIF signals. Each line in the A-X band will produce slightly different fluorescent signal when exciting the molecule. In this study the $Q_1(5)$ line produced nearly twice the signal as the $Q_1(14)$ line as illustrated in Fig. 45. The $Q_1(5)$ line was therefore a better choice when studying the flame. The $Q_1(5)$ was able to distinguish pockets of the flame easier and was used to produce the images below.

One interesting result from the cavity exit was a comparison between the curved and straight exhaust planes. Figure 65 shows the straight section exhibiting a dual-flame region at the cavity exit possibly caused by a dual-vortex inside the cavity. Dual-vortex was also reported in the work of Hankins[27] and Lakusta.[28] The vortex was thought to be from the trapped vortex from the interaction of the main and cavity flows. The vortex is stronger on the side of the main flow exit. The curved cavity flow does not exhibit this dual vortex behavior. Its flame is concentrated in the middle of the cavity exhaust. It is possible the vortex is actually there but the flame is exhausted before separation as in the straight section. The location of the fuel and air injectors may influence the formation of this vortex since there are slight differences between the two sections in the spacing of the injectors due to curvature. This phenomenon should be researched further in future work.

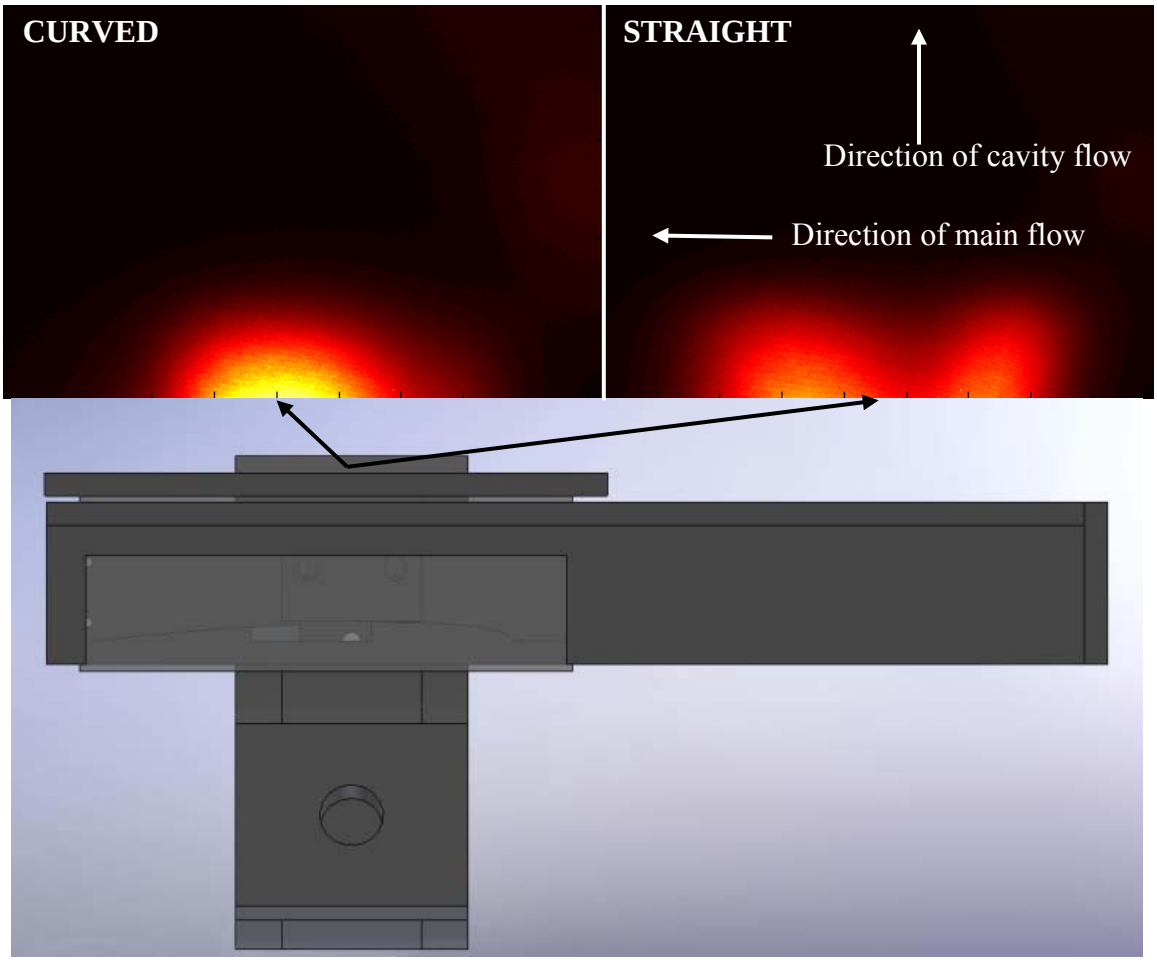

Figure 65. PLIF images of cavity exit for curved and straight cavity exit

Evidence of the effects of a trapped vortex can be seen inside the main section of the UCC. When taking single shot images and viewing them in small time increments, the images suggest there is swirl inside the UCC. Many images show pockets of OH burning and the images suggest the pockets were swirling and moving upstream. Figure 66 are single shot images showing some of these pockets. The top left is from the camera focus image for reference. The behavior was observed in the main flow when using both straight and curved cavity sections. This single shot imaging is where a large difference was seen between the strength of the two lines. The pockets are much easier to

distinguish for the $Q_1(5)$ line. Selecting an even stronger line to study these events may be useful for future researchers.

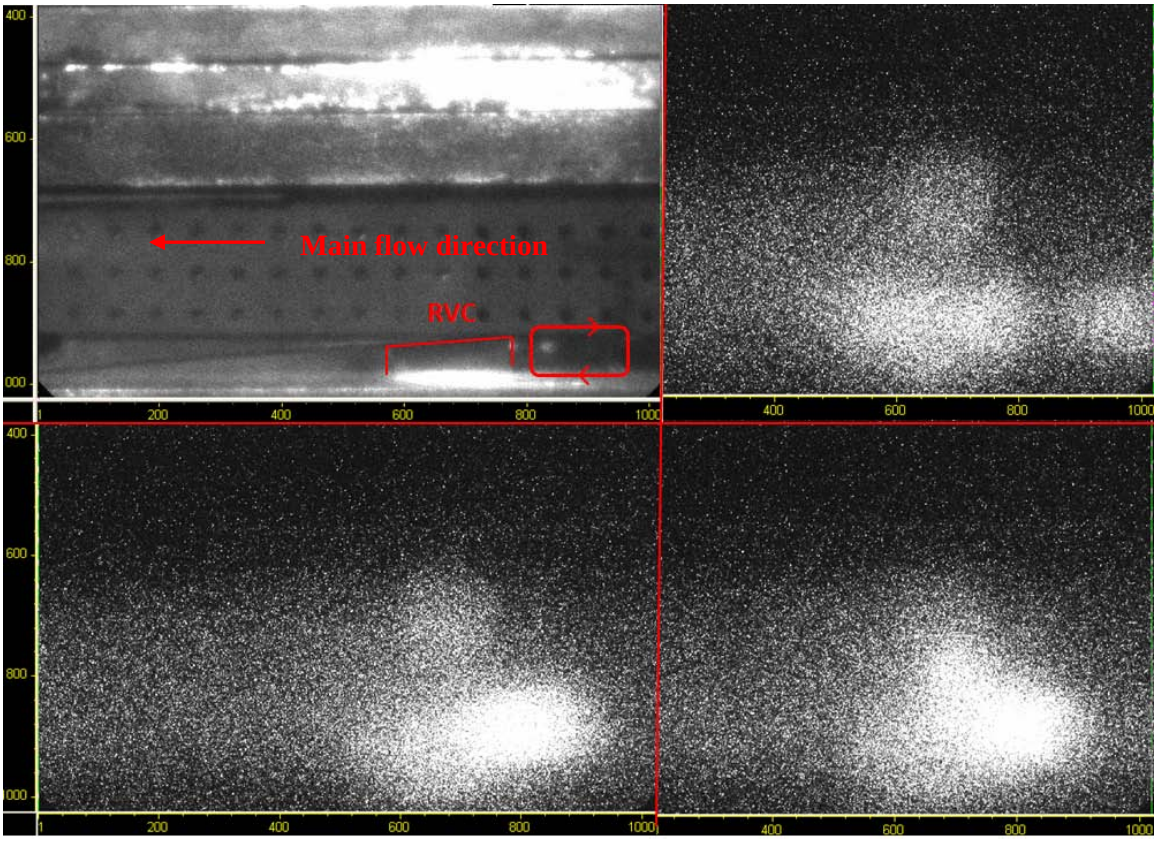

Figure 66. OH pockets revealing swirl in main channel

The levels of OH inside the main channel were also measured. Three regions were selected inside the main channel for interrogation when using both the curved and straight cavity sections. The region chosen was just downstream of the RVC as shown in Fig. 67.

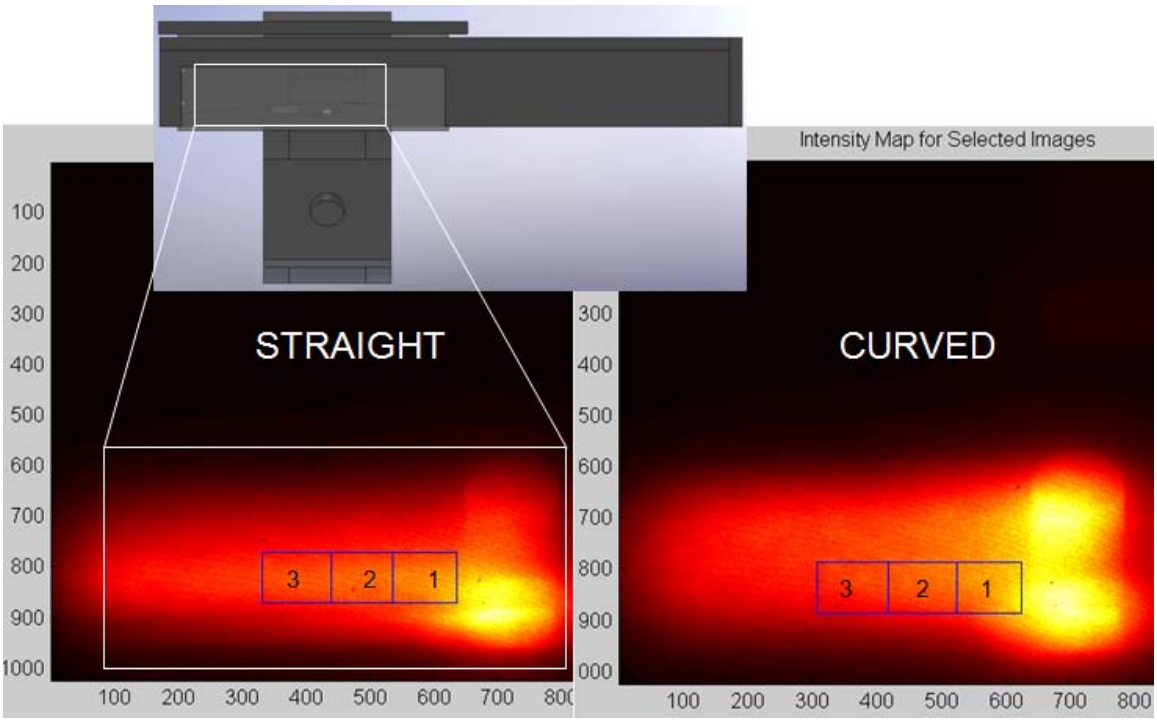

Figure 67. Regions where OH levels were measured in the main channel

The results are shown in Fig. 68 and indicate there are higher levels of OH exiting the main section exhaust when using the straight section. The levels rise with a steeper slope when using the straight section also. This may be due to the buoyancy forces at work in the curved cavity section. These forces may increase the burning rate inside the cavity and also increase the amount of mixing. The increased mixing is also suggested in Fig 68, just to the right of interrogation region one the curved section shows a more uniform distribution of OH than the straight section.

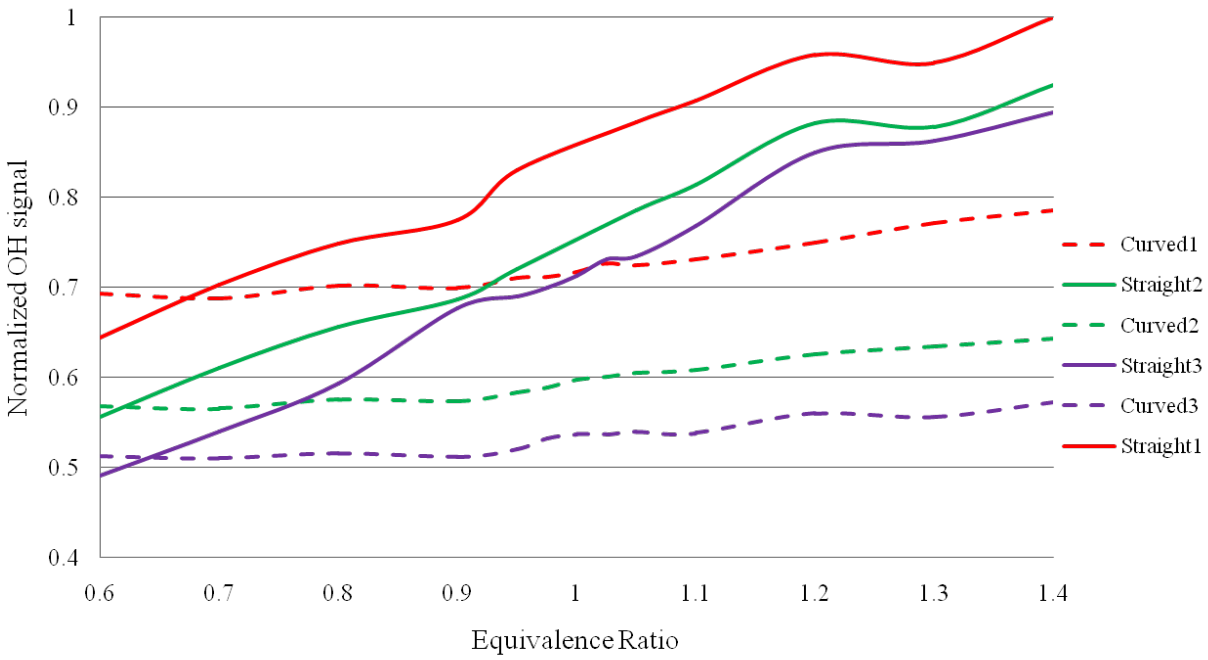

Figure 68. Levels of OH inside the main channel

IV.3 Synthetic fuel in the UCC

Before liquid fuel could be burned, the fuel lines needed to be rebuilt due to a recent COAL lab renovation. The liquid fuel system had not been used for nearly two years so some reassembly was required. Rebuild of the fuel system lines was performed using 1/4" OD stainless steel rigid tubing from the ISCO pump to the test section. A Mott 40 micron inline filter element was added just before the fuel pump and a 10 micron filter just before the injectors of the UCC. Extra filters have been ordered. These filters require changing periodically to protect the pump and injectors. A 48" flexible line has been ordered to improve flexibility by allowing the test section tubing be easily moved.

Once the fuel system was rebuilt, liquid fuel was used in the UCC. Synthetic fuel was used first. The results were encouraging. The synthetic fuel produced a strong flame as shown in Fig. 69. Even after burning the fuel in the UCC for 53 minutes, there were

minimal amounts of soot on the quartz windows allowing PLIF experiments inside the main vane using this fuel in the future. Emissions testing was performed and the results will be discussed in section 4.4.

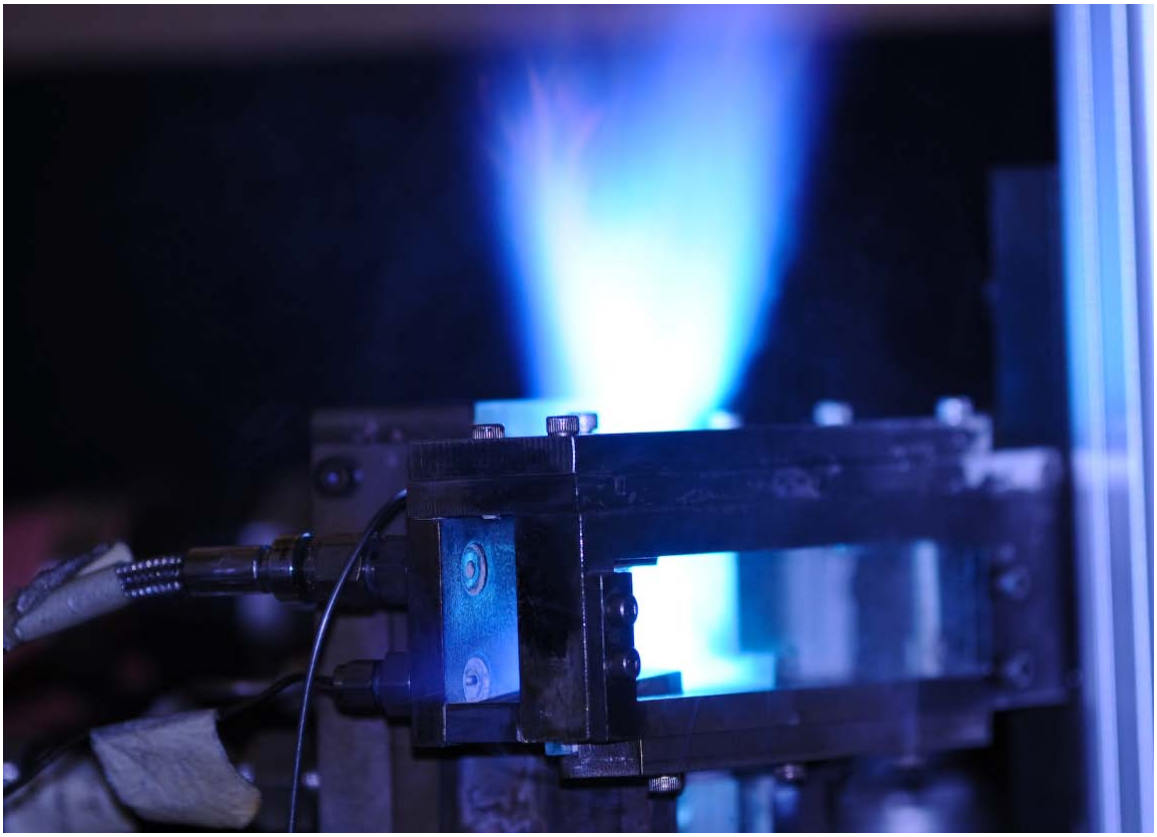

Figure 69. Synthetic fuel in the UCC

IV.4 Emissions Analysis

IV.4.1 Emissions Analysis – S-8 vs. JP-8

Emissions data was recorded at atmospheric pressure using a portable emissions analyzer described in section 3.1.6. Measurements were taken with the emissions probe placed one inch from the main vane exhaust plane. Once the combustor was at steady

state for a certain φ, the exhaust was sampled at 1 Hz for 1 minute. Pollutant emissions of concern in combustion design such as unburned hydrocarbons (UHC), carbon monoxide (CO), and nitrous oxide (NO_x) are presented in terms of EI. The 60 samples are averaged for each run; one standard deviation was ~12-20% of the mean value for each data set. Combustor efficiency is calculated using this data. Originally this research planned to compare the emissions data for burning S-8 and JP-8 over a range of equivalence ratios. Unfortunately, time constraints allowed only the synthetic fuel to be burned. However, in a previous study Hankins[27] performed emissions calculations using JP-8 and the results collected during this research will be compared to the previous study. Both data sets were performed using the straight section of the UCC, using the same air and fuel flow rates, same analyzer and with the same methodology.

UHC emissions are the result of incomplete combustion to include inadequate burning rates, poor fuel atomization, and decreased residence time. As seen in Fig. 70, more UHC is produced when using the traditional fuel. Both fuels show only small changes in UHC for changes in equivalence ratio.

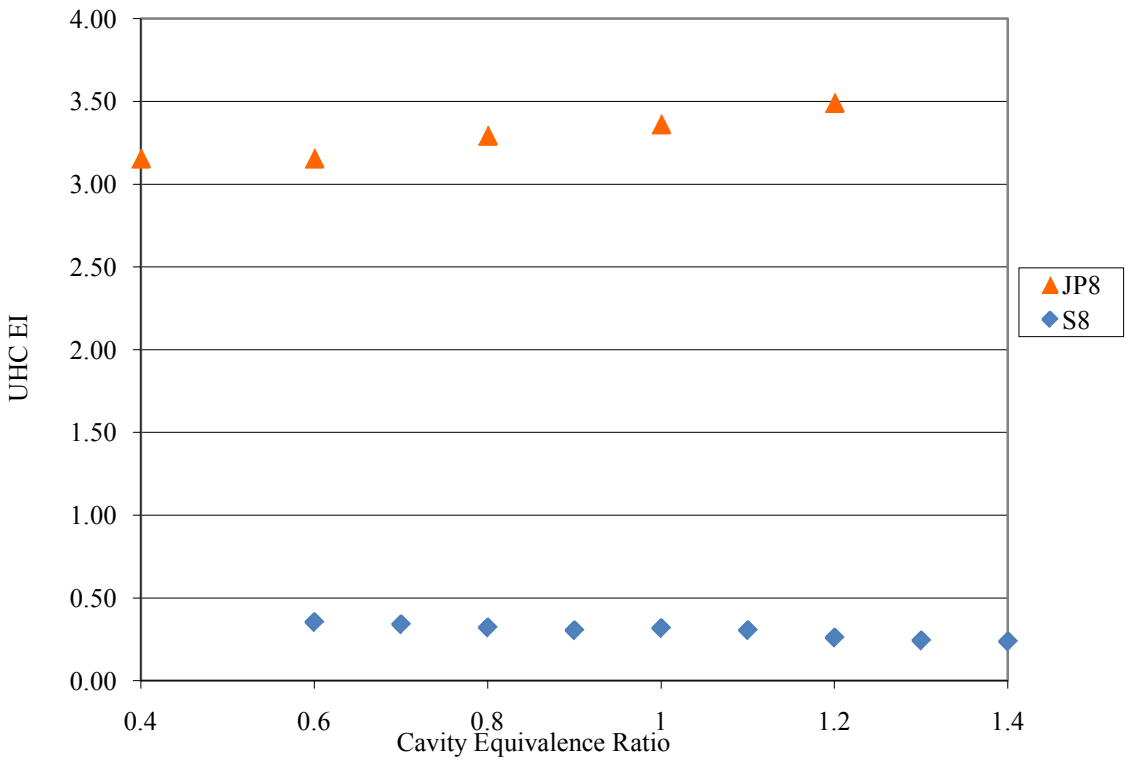

Figure 70. S-8 and JP-8 UHC EI

The creation of too much CO emissions is a concern for local/regional air quality. Carbon monoxide emissions were also reduced in this study using synthetic fuel, shown in Fig. 71. The amount produced also increases with equivalence ratio with a smaller slope for the synthetic fuel.

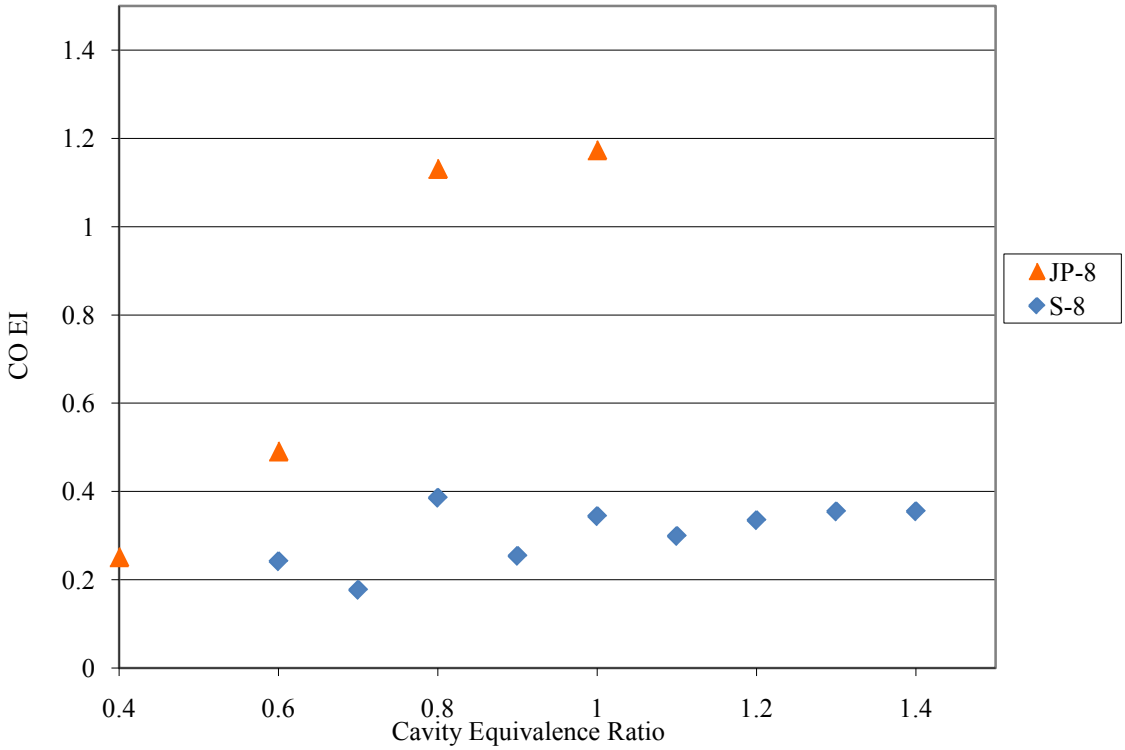

Figure 71. S-8 and JP-8 CO EI

NO_X are oxides of nitrogen produced during combustion, especially combustion at high temperatures and can lead to smog. The emissions of NO_X start as a similar rate, but the traditional fuel seems to increases emissions at a higher rate as equivalence ratio is increased as shown in Fig. 72. For all measurements, the synthetic fuel seems less sensitive to changes in equivalence ratio.

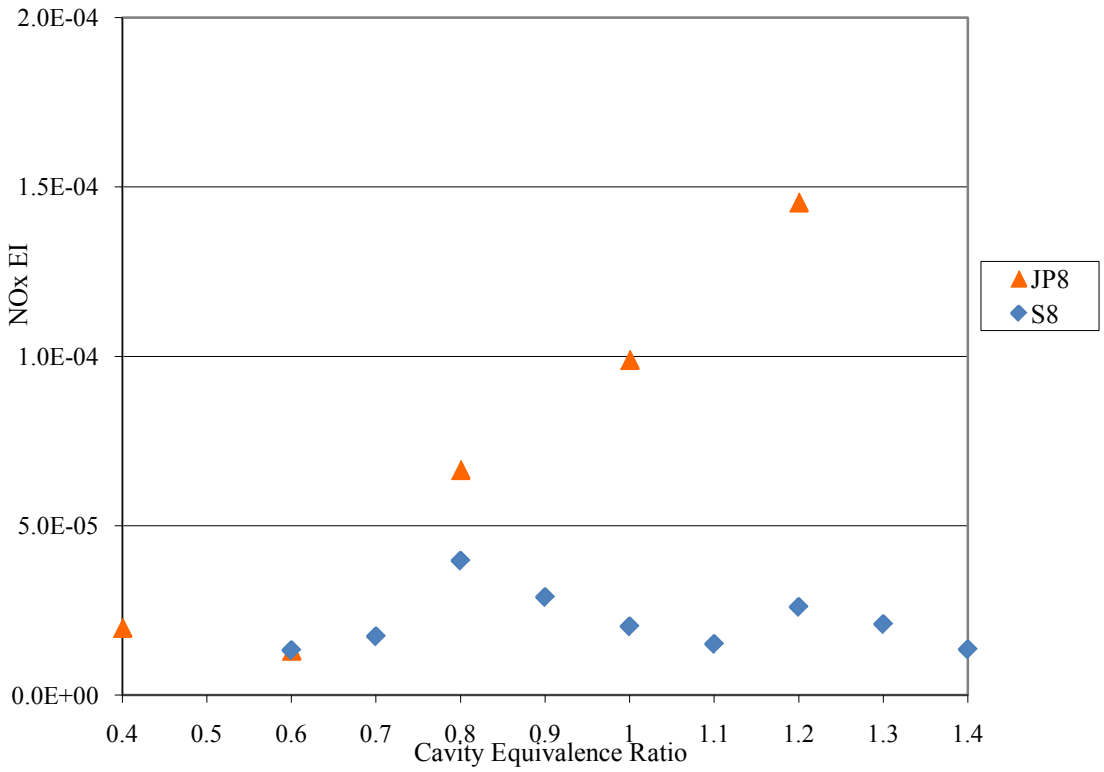

Figure 72. S-8 and JP-8 NOx EI

Overall, there are only small amounts of pollutants in the flow for both fuels. The emissions probe in both studies is placed one inch from the main vane exhaust plane. Since most of the burning occurs in the cavity section, only trace amounts of pollutants are carried downstream with the main flow. In the full-scale UCC, this is exactly why the UCC should reduce emissions. The products will remain in the cavity until combustion is complete. Since there are small amounts of pollutants at the main flow exit, and combustion efficiency is based on these measurements, both types of fuel have high efficiencies. The resulting efficiencies are therefore higher than would be expected for a full scale UCC. The values still give an effective comparison between fuels since the data was obtained in the same manner. The emissions indexes of UHC and CO were used to calculate combustor efficiency using eq. 8. As the quantity of these emissions is increased, efficiency decreases. Since JP-8 had slightly

higher emissions overall, its efficiency is lower as seen in Fig. 73. Due to the small amount of pollutants in the main flow, the measurements are at the accuracy limits of the Testo 350. As mentioned previously, it can measure UHC with an accuracy <400 ppm, actual levels measured in these tests were 275-410 ppm, and CO with an accuracy < 5 ppm, actual levels measured were 88-176 ppm.

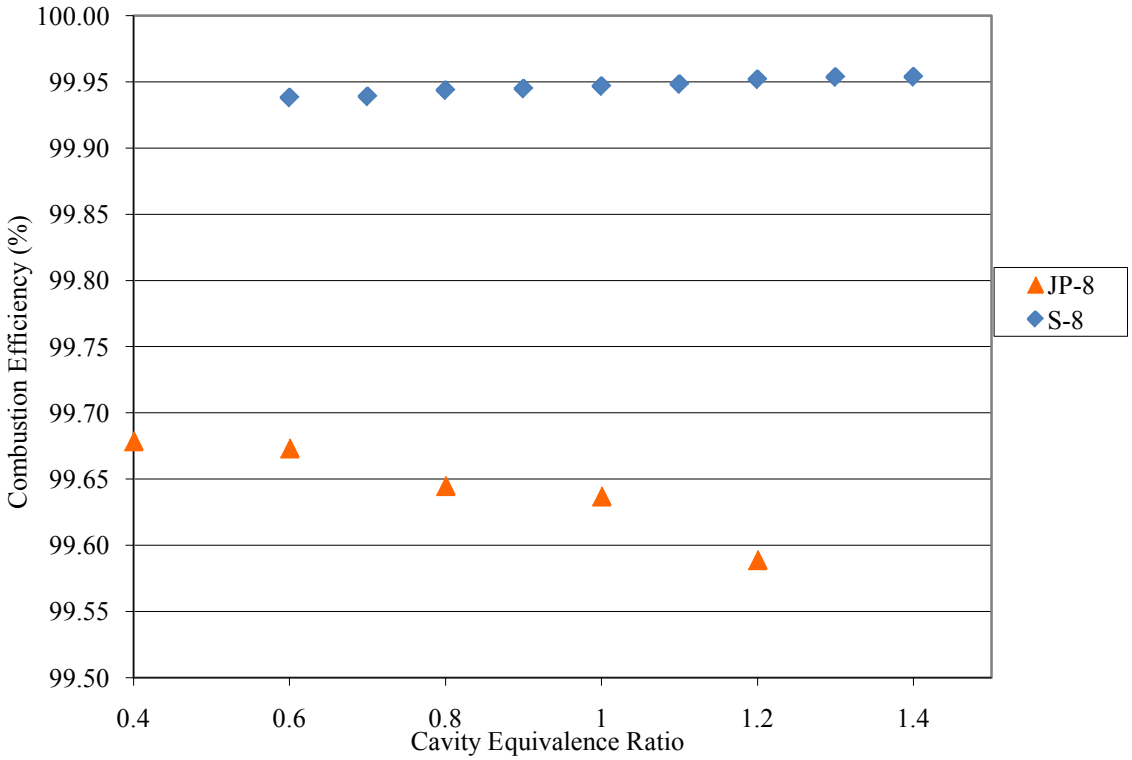

Figure 73. S-8 and JP-8 combustion efficiency

IV.4.2 Emissions Analysis – Straight vs. Curved Section using Propane

The emissions of the curved and straight sections were also compared. Due to concerns over the seal of the curved cavity section when using liquid fuel, propane was used for this comparison. The testing methodology was exactly the same as with the JP-8 and S-8 comparison.

The UHC EI was higher for the curved section than the straight. There was more than a factor of three reduction when switching from the curved to straight section as shown in Fig. 74. This trend continues for the CO EI as shown in Fig. 75.

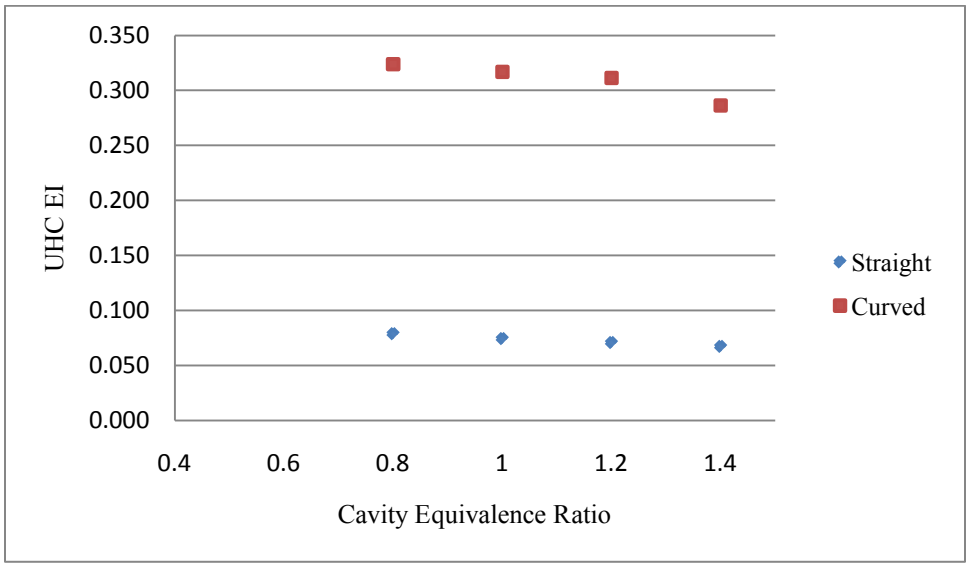

Figure 74. Curved vs. straight section UHC EI

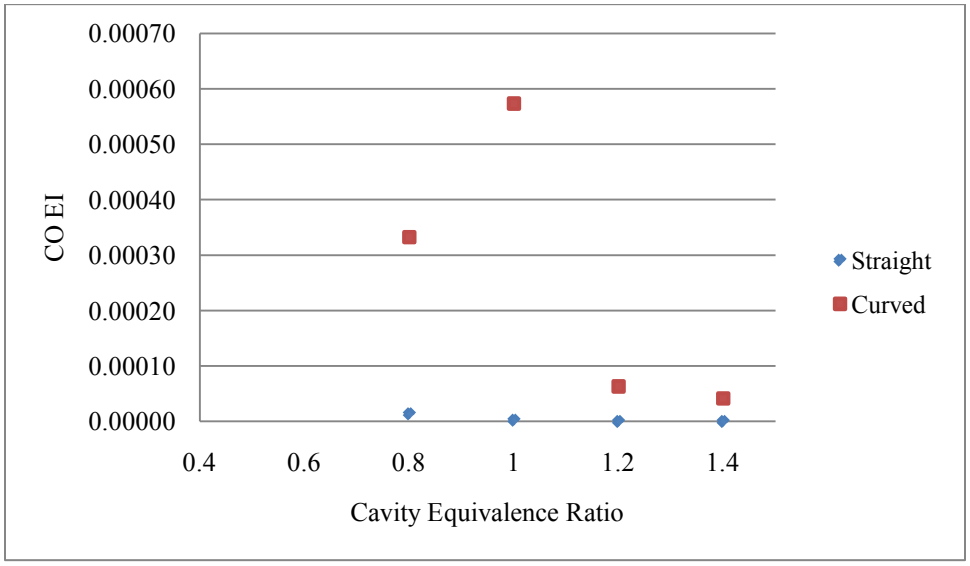

Figure 75. Curved vs. straight section CO EI

Since the CO EI and UHC EI were used to calculate combustion efficiency, the straight section is more efficient than the curved. This difference is likely due to the larger exit area for the straight section. This forces more of the burning in the main channel for the curved section. Since this is where the emissions are measured, the efficiency is lower. This difference will be discussed further in section 4.7. The efficiency curves for the two sections are shown in Fig. 76.

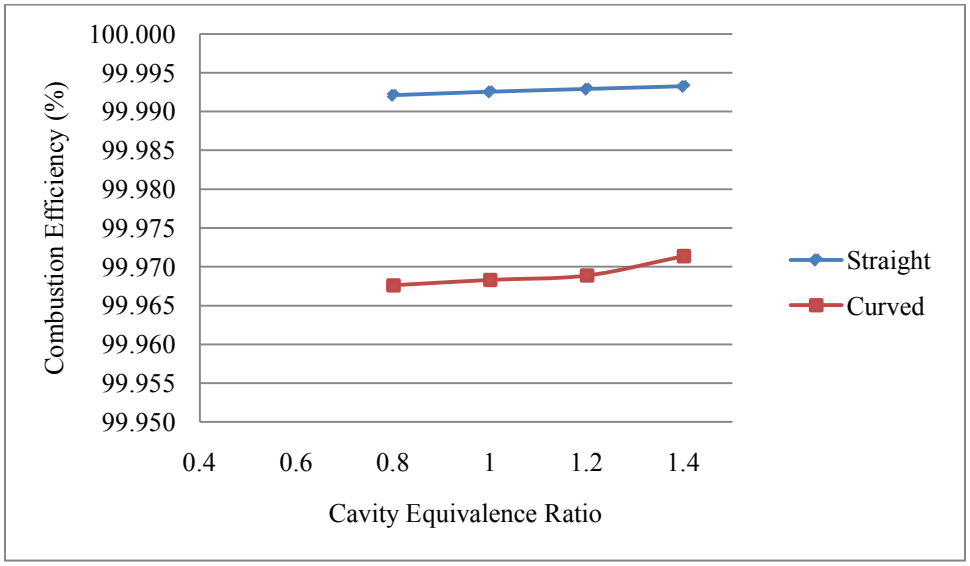

Figure 76. Curved vs. straight section combustion efficiency

There were other findings during the testing of liquid fuel. One is that the previously recommended starting conditions are too fuel rich resulting in pooling as shown in Fig. 77. The revised starting conditions will be discussed in the next section. Pooling becomes a safety issue due to the way the two sections of the UCC are held together. The UCC can be configured with the straight or curved cavity section. The straight section is mounted to the main section of the combustor with four hex screws, two 1/8" x 1/2" on the top near the exhaust and two 1/8" x 2" passing through the cavity

section and attach to the main wall as shown in Fig. 78. Ideally, there would be two more screws going through the cavity section to secure the bottom half of the cavity section to the main section, but this is not possible due to the location of the quartz viewing windows. This less than ideal seal combined with pooling during starting can make for a potentially dangerous situation. Fiberfrax® ceramic fiber paper is currently used as a gasket material and can withstand temperatures up to 1,111 K, but requires a tight seal to prevent blowout. The sealing method is more difficult when the curved section is mounted to the main. As with the straight, viewing windows do not allow a hole to be drilled on the bottom half of the rig to the main wall; on the top half pressure and temperature taps do not allow a hole to be drilled in that location either. Only the two 1/8" x 1/2" top screws hold the curved cavity section to the main. Although no issues were encountered when using the curved section with gaseous fuel, the curved section was not used with liquid fuel. In future research, two L brackets should be designed to help hold the two sections together, minimizing the chances for a fuel leak when burning liquid fuel. The location for these brackets is shown in Fig. 78. These brackets, combined with the updated starting conditions should eliminate issues when using liquid fuel in the UCC.

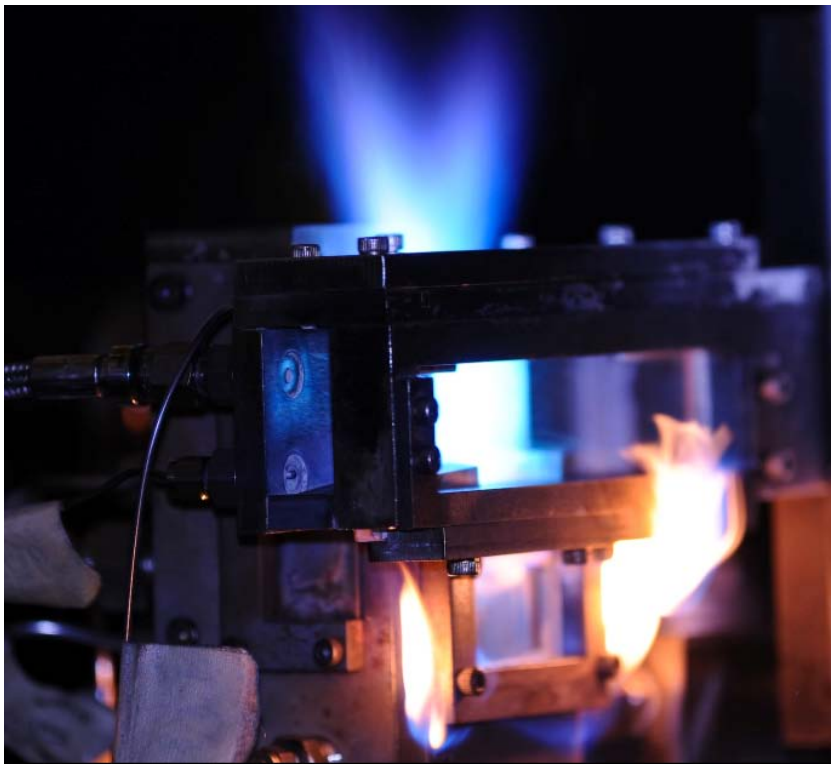

Figure 77. Results of pooling

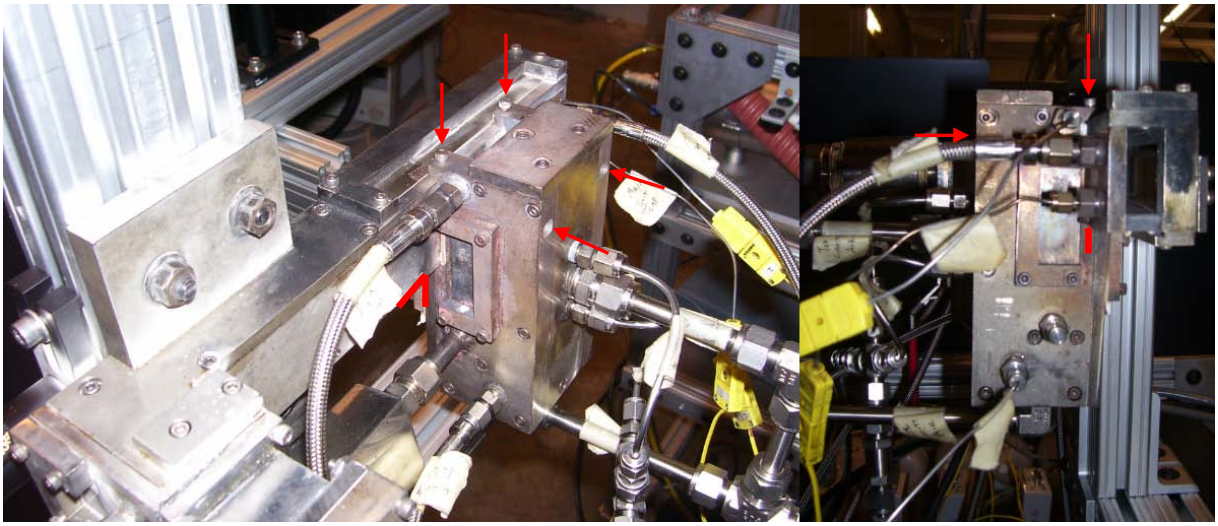

Figure 78. Flat cavity to main section - arrows indicate current mounting locations

IV.5 Improvements to igniter system

Hankins[27] was the first to burn fuel in the UCC. He reported several issues getting the UCC to light, especially when using liquid fuel. One of the issues was not have a

reliable ignition system. The UCC uses a torch ignition system – an ethylene-air mixture flows past an electrical arc produced by a spark plug making a torch. Lakusta[28] sought to improve the ignition sequence and removed the igniter from the UCC. He found lower flow rates helped maintain an ethylene torch. However, when he connected the igniter to the UCC, a steady torch could not be maintained without continuous use of the spark plug. Igniting the UCC was possible in this manner but using continuous spark plug creates pulses of flame instead of a steady torch. As the gas builds up in the cavity and the plug fires, the mixture detonates and then blows itself out. Furthermore, the 10,000 volt ignition system often creates enough electrical feedback during continuous operation to crash Lab-View. During this research, the igniter was again removed and tubes were mounted on the igniter to better represent being connected to the UCC. Lakuska's recommended conditions were used as a starting point, but it was shown that a steady torch could not be maintained under any flow conditions with the length of tube that connects the igniter to the UCC. A torch could be maintained in a shorter tube using low flow rates and fuel rich conditions. The UCC igniter tube was shortened to match. The igniter itself was also rebuilt by the AFIT model shop to be slightly smaller since there was interference with a pressure tap and the mounting bolts when using the shorter tube length. The spark plug in the new igniter was also set deeper into the cavity to allow the electrode to act as a flame holder. The new configuration was able to consistently start and maintain a steady torch within the UCC as shown in Fig. 64. To help minimize electrical interference when using the igniter, the ignition wire was separated from the wire bundle connecting all components of the UCC to Lab-View. The UCC test stand and Lab-View computer station were also electrically grounded helping to minimize the

amount of malfunctions when using the igniter. The starting conditions when using the igniter are given in Table 4.

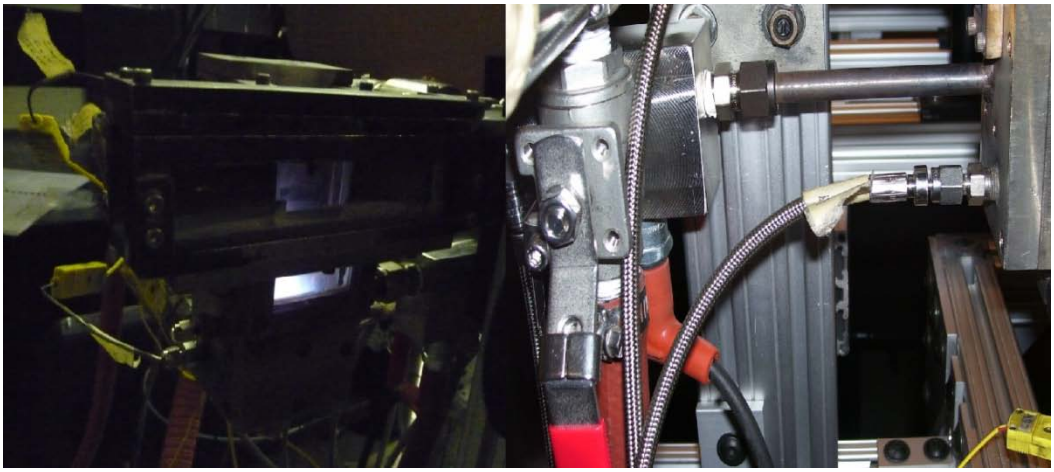

Figure 79. Using the new igniter and old length of igniter tube

IV.6 Revised starting conditions

As mentioned previously, past students could not maintain an ethylene torch in the UCC without constant spark plug operation. Now that a torch can be maintained in the combustor, the combustor should be easier to light using liquid fuels and the starting conditions revised. The following are updated UCC lighting procedures. The main and secondary Gaumer electric air heaters still play a major role in getting the combustor to light. Previous researchers found liquid fuel difficult to light when sprayed into a cold combustor. To alleviate this problem, each heater should be turned on 30 minutes prior to combustor start. The main and secondary air should be set at 1.95 kg/min and 0.195 kg/min respectively and the temperature set points should slowly be increased in Lab-View to keep the heaters from overheating. After the temperature set points for the air are met, the ethylene-air torch should be started. MFC set points are 5 SLPM for the air and 3.75 SLPM for the ethylene. Once the torch is started, the ethylene can be increased to

7.5 SLPM. After letting the torch run for 2 minutes, start the A syringe of the fuel pump in constant flow mode with a setting of 25 ml/min (φ = 1.4). It will take a moment for the pressure to build up and start spraying into the chamber. Once the fuel starts spraying, it will light and the igniter can then be turned off.

The major changes to this procedure are the mode of the pump during starting and the starting φ. The fuel pump has two modes of operation, constant pressure and constant flow. The fuel nozzles need a pressure above 2.07x105 Pa (30 psi) to provide a proper fuel spray for lighting. As a result, the fuel pump was previously operated in constant pressure mode delivering 3.45x105 Pa (50 psi) for starting. This results in a fuel rich condition with an equivalence ratio of approximately 3.0. Once lit, the fuel pump was immediately changed to 20 ml/min constant flow mode (φ = 0.3). The main problem was pooling using this method; any unburned fuel builds up in the bottom of the cavity or leaks out and creates an unsafe condition upon ignition. Table 5 displays optimal starting conditions for quick reference.

Table 5. Revised UCC starting conditions

	PREVIOUS RECOMMENDATION		NEW
Condition	**Lighting**	**After Light**	**Lighting**
Ethylene (slpm)	2.45	OFF	3.0 to start, then 6.0
Air (slpm)	25.0	OFF	5.0
Main Heater (ºF)	300 - 400	300 - 400	300 - 400
Secondary Heater (ºF)	200 - 300	200 - 300	200 - 300
Main Flow (kg/min)	1.3	1.3	1.95
Secondary Flow (kg/min)	0.13	0.7	0.195
Fuel Pump Mode	Const Press	Const Flow	Const Flow
Fuel Flow (ml/min)	25 - 35	20	25
Cavity φ	2.5 - 3.0	0.3	1.4

The starting flow conditions of this research were based on the flow curves created by Hankins[27] for the two syringes of the fuel pump and shown in Fig. 68. The 25

ml/min set point creates enough pressure to atomize in the fuel injectors and eliminates switching between flow modes. Syringe A should be used throughout the test if possible. Not only is its variance lower, it creates a higher pressure for the same flow set points helping the fuel injectors perform properly. If starting from a full syringe, the pump should be able to pump at 25 ml/min for 40 minutes before refilling or switching to syringe B.

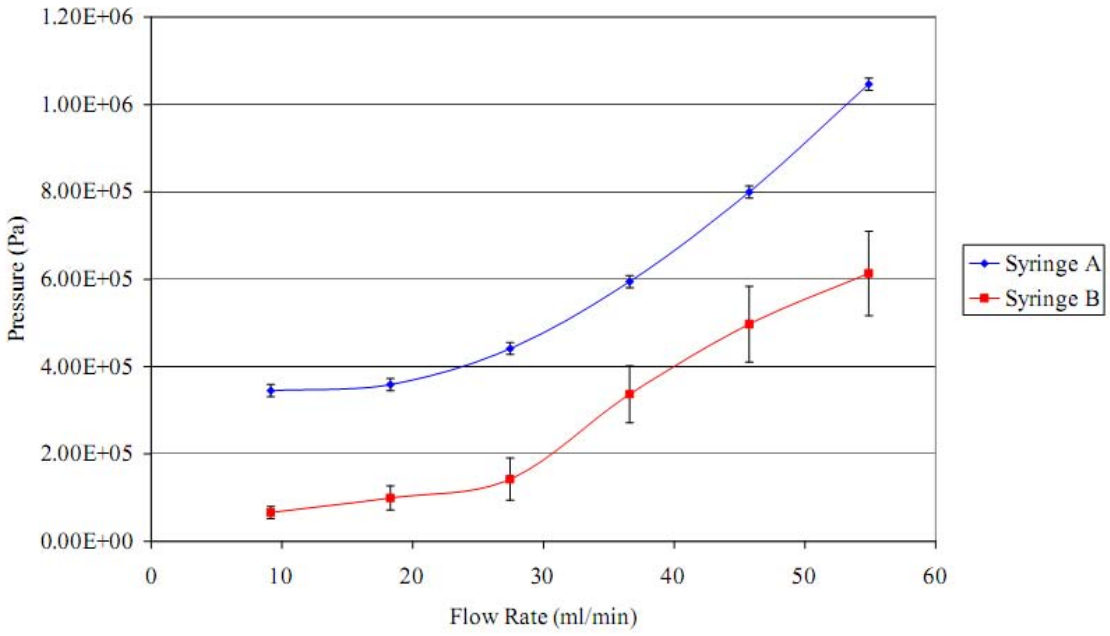

Figure 80. ISCO Pump syringe characteristics[27]

IV.7 Recommended changes to the UCC

As with any type of testing, laboratory experiments should strive to remain as operationally representative as possible. When making comparisons, test conditions should be the same for each trial. One major item of comparison in the UCC is between the straight cavity section and curved section. However, in its current setup, the geometries do not allow for an accurate comparison. The exit area for the straight section is more than twice the area for the curved section. This chokes the exit flow and forces

more burning in the main section. The exit area difference may be the reason higher exit temperatures were measured using PLIF thermometry in the cavity exit plane for the straight section than the curved. It also explains the higher emissions in the curved section. More burning taking place in the main channel when the curved cavity section is used equates to higher emissions since the emissions probe is sampling at the main exhaust plane. The concept of the UCC uses the cavity section as the primary combustion zone so the curved section exit area should be increased to match the curved and reduce the choking of the exit. Figure 81 illustrates the difference in the exit areas.

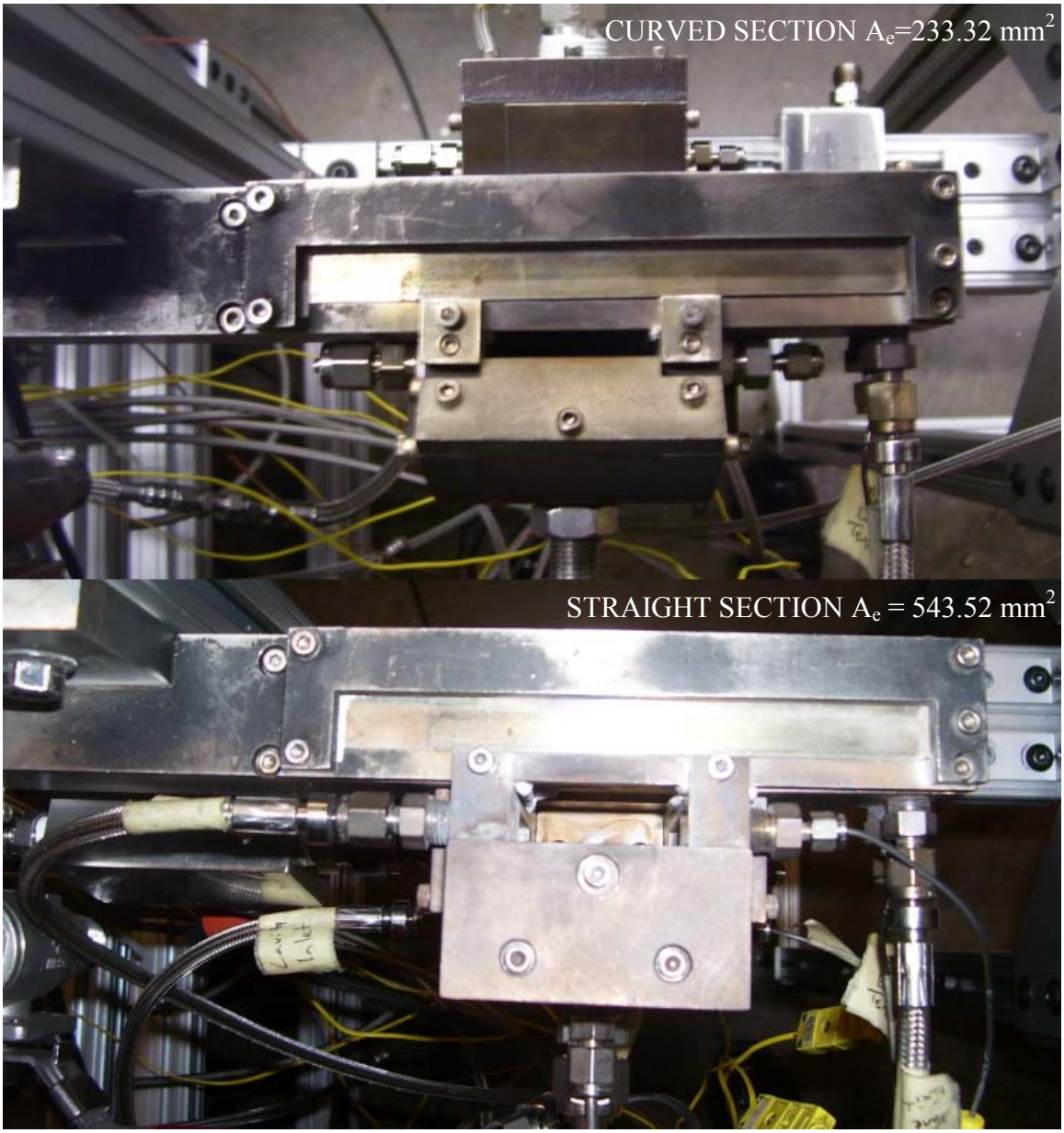

Figure 81. Exit area for straight and curved cavity sections

The issue can be easily fixed for future researchers. Wedges have been made to increase the exit area of the curved section. One piece that has yet to be built is the part that connects the curved to main section; this is circled in Fig. 82 and a top view can be seen in Fig. 81.

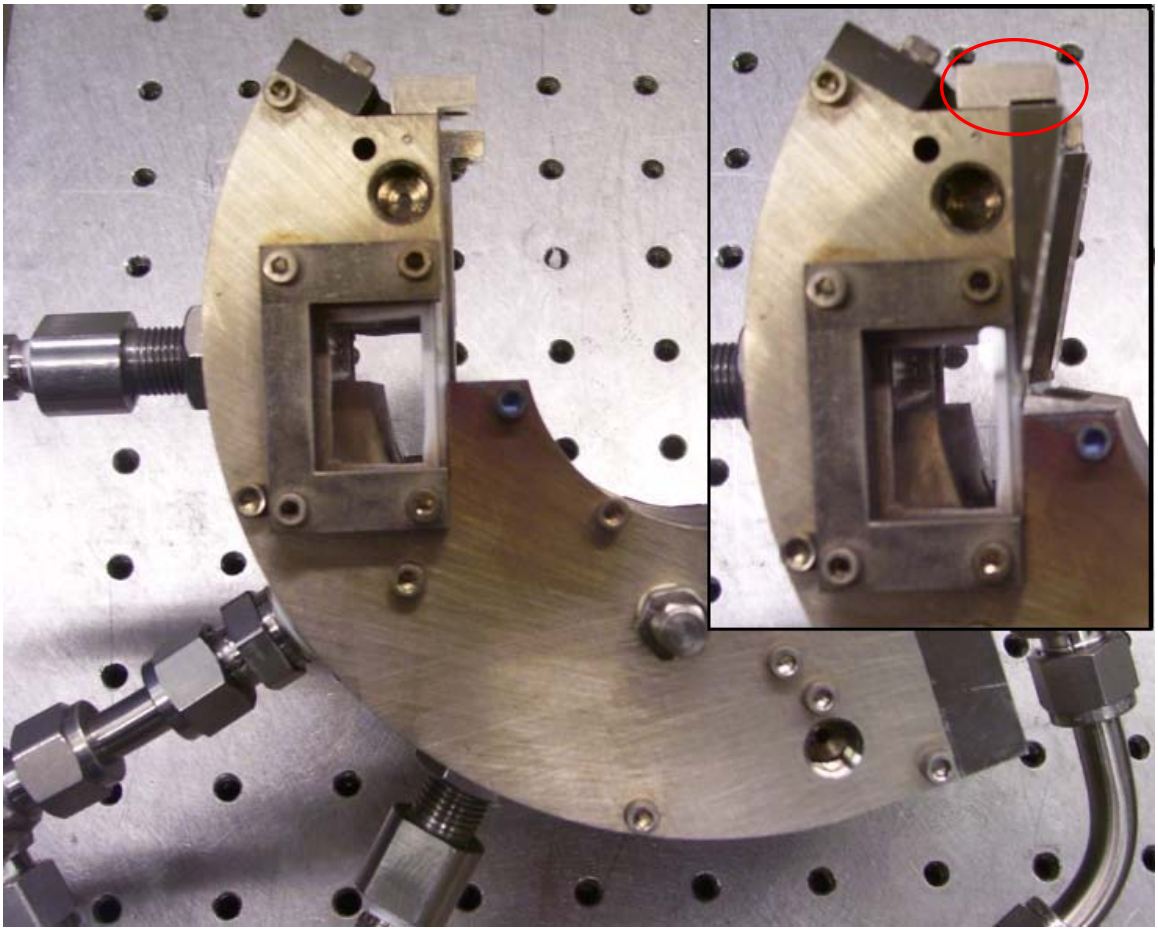

Figure 82. Wedge inserts to equalize exit areas

Currently the UCC model used in the COAL lab is a 1/6 section of the full combustor. This section allows for optical access into the combustor but may limit the representativeness of the data collected. For example, the emissions and temperature measurements were both studied in the main section, but most of the burning is taking place in the cavity and immediately exiting. In the actual combustor, the burning would continue in the cavity until fully burned before the hot products exit to the main flow. Increasing the size of the model to a 1/3 or even 1/2 section may better allow true emissions and main flow exit temperature to be studied. Figure 83 illustrates this concept.

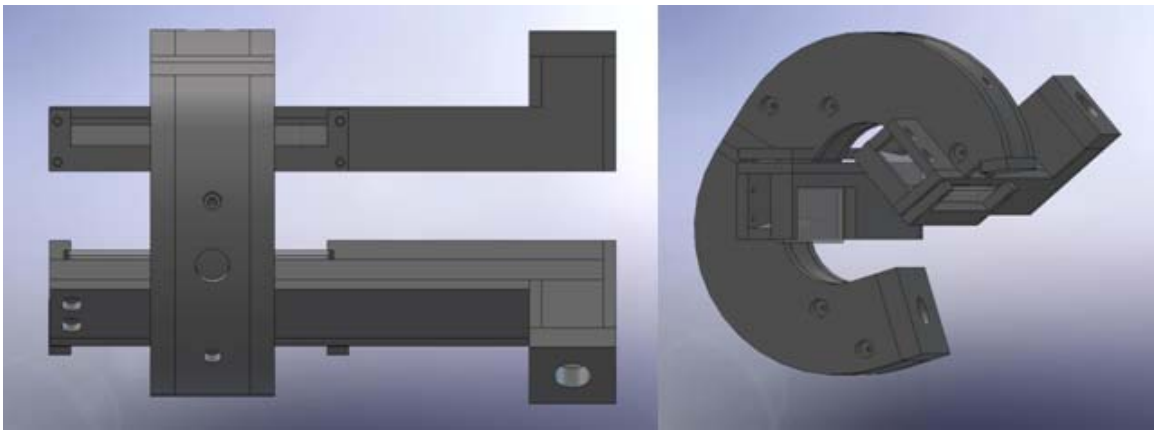

Figure 83. Generation two UCC model concept

IV.8 Dye pumps issues, findings and suggestions

There are several issues, findings and suggestions that were concluded from the many hours spent using the dye pumps of the dye lasers in the COAL lab. The dye pumps use a solution of dye and methanol in a stainless steel reservoir for the oscillator and amplifier pump. The oscillator creates the signal at the correct wavelength and the amplifier side of the laser increases the power of the beam. Mixing the dye solution is a tedious process since a small amount of dye can have a large effect on the output of the laser. If too much dye is added, the process must be repeated. After the mix is set and experiments start, the lasing properties of the dye will degrade with time. Rhodomine 590 dye was chosen for this research due to its long half-life. Even with a relative long half-life the solution was replaced on a bi-weekly basis. The reservoir holding the dye solution is covered with a lid, but the seal is not airtight. Methanol is susceptible to evaporation; as the methanol solution evaporates the dye is left behind increasing the concentration. Once the concentration changes, the lasing properties will also change, sometimes drastically enough that it must be flushed. To help reduce this problem, a sealing material should be placed over the reservoirs underneath the lid to minimize this evaporation. The

manufacturer is aware of these issues and may produce a screw on lid as a future upgrade. A second recommendation to combat this issue is to mark the level just after the solution has first been added to the containers after a dye change. If any evaporation is noticed, adding methanol to fill the container to the mark should maintain the needed dye and methanol ratio to peak wavelength power output.

The two dye pumps currently being used have drastic performance differences. Continuum is currently changing the design of their dye pump. When the dye pump stopped working on one of the dye laserss during this research, it was replaced with a new style pump. The new pump is a prototype to the final design. Continuum has offered to update it with any changes when the design is finalized. The new pump seems better in every way. It circulates the solution fast enough that it produces visible bubbling on the surface when looking into the reservoir. The old pump's flow rate does not disturb the surface. Since the weaker pump cannot circulate the dye fast enough through the amplifier cells, the maximum power available is limited. The old pump has also oscillated in speed during test runs making the power oscillate as well. The new style pump should be purchased to replace the old one when funds are available. Since one pump is old and performance is limited, and the other is a prototype, both should be closely monitored. If the pump stops working, the entire dye laser can be damaged. The solution acts as a cooling system for the optics. Without the cooling, the inputted laser energy from the YAG may quickly damage the internal optics.

V. Conclusions and Recommendations

V.1 PLIF Thermometry

Calibration is very important in a PLIF experiment, especially when using the Hencken burner, used as a baseline for calibrating species concentrations and temperatures in an unsteady flame. To ensure the desired amount of flow is needed for a set equivalence ratio, the flow rates delivered to the Hencken burner should be calibrated. This research has shown there is a loss of flow through the Hencken burner. The recommendation is to continue calibration using the calibration cup to capture theses loses. The current calibration tool is a Bios Definer 220, limited to calibrate maximum flow rates of 30 SLPM. When using a 50 SLPM mass flow controller extrapolation was necessary to predict the actual flow rates of the flame, and may introduce error. Purchasing a larger gas calibrator, such as the Bios Definer 1020 can calibrate flows from 5-500 SLPM would eliminate this error. A larger calibrator could also be used to more accurately determine the flow rates in the UCC from the main and secondary air lines. The oxygen content of the zero air should also be known to best calibrate PLIF thermometry using the Hencken burner. Changes from the simplified atmosphere assumption will equate to changes in the equivalence ratio. Future researchers should test the air with the Testo or CAI gas analyzers to eliminate this error or have the zero air professionally analyzed to measure its contents.

LIF experiments require complex equipment such as the source YAG laser, dye laser, dye pumps, cameras, computer and software. Moving from one to two line experiments required doubling the amount of equipment except for the YAG laser. The dye pumps proved to be the weakest link in this complex experimental setup. Two of the pumps were

sent in for repair during this research. When a dye pump malfunctions, the dye laser can easily be damaged since it acts as the cooling system and the YAG may continue to pump laser energy into it if the problem is not immediately noticed. Due to the backlog of pumps needing repair, Continuum has sent a prototype pump that has been upgraded and uses more reliable components. These pumps should be closely monitored in future research. One pump is the old style known to have reliability issues. The second pump is a prototype whose reliability is unknown. Having an extra pump on hand in the COAL lab would also be recommended to help the flow of future research since losing a pump will stop two-line PLIF experiments.

Changing dye solution in the dye pumps is a tedious task and reduces the time spent running experiments. This process is necessary as the dye breaks down with lasing or when the properties otherwise change such as through evaporation. Placing a plastic seal over the dye reservoir will greatly reduce the amount of evaporation from the system. If evaporation is still suspected, use a ruler to mark the fluid level just after initially mixing the dye. Keeping a log of the amount of dye needed to maximize output is recommended. There will be slight differences between the two lasers and the oscillator and amplifier side of each laser.

Repairing the auto-trackers may help the dye lasers maintain a constant power setting over the course of a data set reducing variability in the data. Future researcher should also incorporate a method to continuous monitor the laser power method instead of checking it between runs as in this work.

V.2 UCC operation

The quartz window the laser passes into the UCC main cavity is not AR coated causing laser scatter inside the combustor. Laser scatter creates false signal for PLIF experiments, especially where the scatter reflects off PIV particles. An AR coating should reduce the problem. Between PIV and PLIF experiments, the UCC should be completely disassembled and scrubbed to remove all traces of seeding.

The starting conditions have been revised and the igniter remodeled. This update should make starting the UCC more reliable and safer in the future. Even though pooling should be less of an issue, L brackets should be added to both straight and curved section to help seal the rig.

V.3 Future work

Before additional comparisons are made between the two sections, the exit areas should be matched. Changing to a generation two design may allow more detailed studies and would allow the RVC to draw combustion products from the cavity flow.

Once the windows are AR coated, PLIF thermometry should be attempted in the main vane exit. PLIF should continue to be used as an effective way to study the UCC. Using strong transitions such as the $Q_1(5)$ line when using PLIF for non temperature measurement studies will help better resolve combustion structures. The $Q_1(9)$ line is also considered an ideal line to study flame structures.

Two-line simultaneous PLIF thermometry is now possible in the COAL lab. Accuracies of ~95% have been observed when measuring flame temperatures in a near adiabatic Hencken flame. This tool should be used in the future to further study interactions inside the UCC.

Initial studies using synthetic fuel are promising. Reductions in harmful emissions were shown when compared to a previous study using JP-8. Comparisons should be done between JP-8 and S-8 fuels in future studies to verify these results. Once the exit area are equal and L brackets have been added to help seal the rig, emissions studies should continue for both curved and straight sections. Future studies should use the CAI analyzer to probe the main flow exhaust to obtain readings that are more accurate at these low pollutant levels. If the Testo 350 is used in future studies, both the main and cavity exit flow should simultaneously be probed since the COAL lab has two analyzers available.

Appendix A

COAL LAB LASER FUNDAMENTALS

Laser Startup Procedure

Safety

1. Secure entrances to the laboratory
2. Activate laser warning lights
3. Check to ensure that all personnel have the proper PPE
4. Check to ensure that all personnel have proper safety training
5. Check to ensure that all beam paths are initially blocked

YAG Laser Start (from a complete Power Down)

1. Check water level – see Fig. A-1
2. Turn key switch on and flip breaker switch up on YAG power supply
3. Press the *enable* button on the YAG keypad
4. Allow amber simmer lights on the YAG keypad to stop blinking
5. Allow YAG laser to warm up for 20 minutes

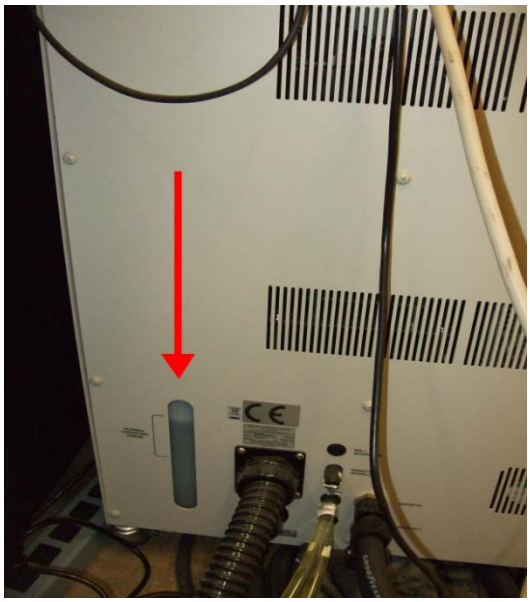

Figure A-1. YAG water level

Dye Lasers Start

1. Check methanol level in dye pumps, refill if necessary to 5-10 mm below the bottom of the tube
2. Turn on dye laser by switch on the back, verify that the dye pump also powers on

Tuning

YAG Laser Tuning

1. Turn *osc* or *amp* flash lamp energy to 5 on the YAG keypad
2. Double click *Trigger* software on the computer desktop
3. Click *File* the *Open* and open text file- ex: *AFIT 1 YAG 1 Camera*
4. Click *Program* button to load settings- it's the button between *H* and *Reset*
5. Click *Enable* on Channel A of *Trigger* software (if not already enabled)
6. Click *Enable* on Channel C of computer control software to turn on Q-switch
7. After checking beam path, turn up *osc* flashlamp energy to full power
8. Set delay in Channel C of *Trigger* software to 180 microseconds and click Apply and Enable
9. Open Wavemeter software, click start, and set signal to *Pulsed*
10. Maximize power output by rotating crystal shown in Fig. A-2

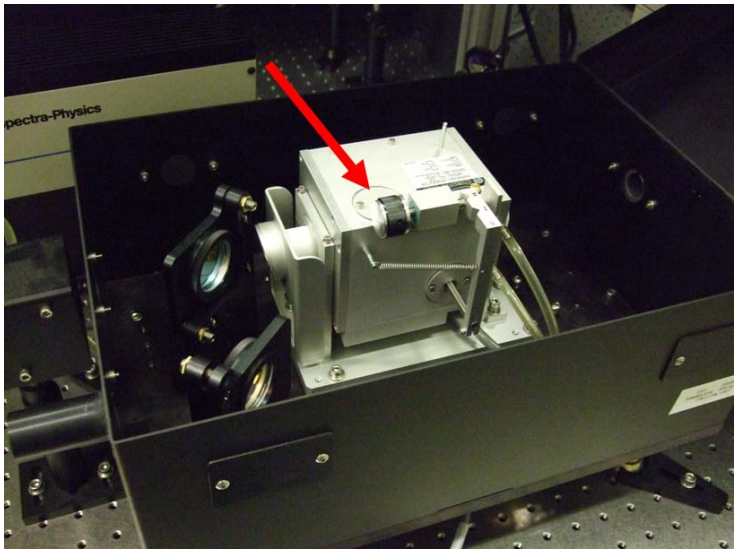

Figure A-2. Rotating doubling crystal

Dye Laser Tuning

1. Input desired wavelength into Continuum ND6000 software, the dye laser frequency is doubled so twice the excitation wavelength should be entered
2. For easier and more accurate adjustment of the concentration of both oscillator and amplifier dye solvent a highly concentrated mixture of MeOH and the user specified dye is made. This solvent can be added incrementally to either of the circulators during initial alignment and calibration or at a later time to adjust dye concentration during experimental use. This concentration of this mixture is not overly specific (~1-2g/L) and is made by adding 1g of granular solvent to 500mL of HP MeOH and agitating thoroughly.
3. Drain used methanol from dye pump shown in Fig. A-3 and properly dispose of it
4. Add 400 mL of new methanol to oscillator and amplifier containers of dye pump

5. Slowly add dye concentration to oscillator container in 2 mL increments until beam is properly shaped, the total concentration is approximately 105 g/L.
6. Slowly add dye concentration to amplifier container in 2 mL increments until maximum power is achieved, the total concentration is approximately 65 g/L.

Figure A-3. Dye pump for dye laser

7. Check wavemeter reading and adjust dye laser wavelength to desired wavelength using ND6000 software

Laser Shutdown

1. Turn “osc” and “amp” flashlamp energy to 0 on YAG keypad
2. Allow water to keep running for at least 10 to 15 minutes
3. Push “Stop” on YAG keypad
4. Turn off dye pump
5. Turn key switch off and flip breaker switch down on YAG power supply

Appendix B

Using MATLAB for PLIF Image Math

This MATLAB program reads average image intensity of a certain region from a Win-View SPE file. The program asks the user to select the .SPE files to be evaluated and specify the region of interest to find the average intensity of. The number of images stacked up in each SPE file, the height and width of the region of interest, and the size of the entire SPE image are all implicitly specified in the code
• Region of interest size must be specified (default 100x100)
• Number of stacks must be correct (default 20)
• Image size must be correct (default 1024x1024)
Created by COAL Lab Intern Mike Boehler, 419-688-1703, boehler.4@osu.edu

```
clear all
close all
clc

%% Open Images
pwd1=pwd;

[FileName,PathName,FilterIndex] = uigetfile('*.spe','Select Images to
Evaluate','MultiSelect','on');
cd(PathName);
FV=strvcat(FileName);
l=length(FV(:,1));
if l>1
  FN=sort(FileName);
elseif l==1
  FN=FileName;
end
FV=strvcat(FN);
nstacks=input('Enter number of images stacked in each SPE file (Default
20): ');
if isempty(nstacks)
  nstacks=20;
end

stop=false;
h = waitbar(0.0,'Please wait...','CreateCancelBtn','stop=true;
delete(h); clear h');
set(h,'Name','Averaging SPE Image Stacks...');

for i=1:l
  waitbar((i-1)/l,h,['SPE File ' num2str(i)]);
  if stop break; end
  fid=fopen(FV(i,:),'r');
  header=fread(fid,2050,'uint16');
  for j=1:nstacks
    ImMat=fread(fid,[1024,1024],'uint16');
    z(:,:,j)=ImMat;
```

```
  end
  Z(:,:,i)=mean(z,3);
  fclose(fid);
end
if exist('h') delete(h); end

for i=1:l
  ZZ(:,:,i)=[Z(:,:,i)]';
end

im=mean(ZZ,3);

%% Specifiy Region
Y=1;N=0;
input1=input('Select center of region of interest? (Default N) Y/N: ');
if isempty(input1)
  input1=N;
end

ntries=1;
while (ntries<2)

  clc
  close all

  figure
  imagesc(im); colormap(hot); title('Intensity Map for Selected
Images');

  if input1==1
    [x,y] = ginput(1);
    x=round(x); y=round(y);
    dx=100;dy=100;
    x1=x-dx/2; x2=x+dx/2;
    y1=y-dy/2; y2=y+dy/2;
  elseif input1==0
    % • Specify the corners of the region of interest explicitly
    % below:
    %x1=482;x2=582;y1=507,y2=607;
    x1=input('x1=  ');
    x2=input('x2=  ');
    y1=input('y1=  ');
    y2=input('y2=  ');
    dx=x2-x1;dy=y2-y1;x=(x2+x1)/2;y=(y2+y1)/2;
  end

  rectangle('Position', [x-dx/2 y-dy/2 dx dy], 'edgecolor', 'b');

  Xcenter=x;
  Ycenter=y;
  Xrange=[x1,x2];
  Yrange=[y1,y2];
```

```
  input2=input('Select another center for region of interest? (Default
N) Y/N: ');
  if isempty(input2)
    input2=N;
  end
  if input2==1
    ntries=ntries;
  elseif input2==0
    ntries=ntries+1;
  end

end

%% Calculations
for i=1:l
  total(i)=sum(sum(Z((x1:x2),(y1:y2),i)));
  avg(i)=total(i)/((dx+1)*(dy+1));
  sigsum=0;
  for j=x1:x2
    for k=y1:y2
      sigsum=sigsum+((Z(j,k,i))-avg(i))^2;
    end
  end
  sigma(i)=(sigsum/((dx+1)*(dy+1)))^.5;
end

%% Results
clc

Xcenter=x
Ycenter=y
Xrange=[x1,x2]
Yrange=[y1,y2]

format long g

averages=avg' %average intensity for region of interest
sigmas=sigma' %standard deviation
disp('Results are in alphebetical order according to filename')
disp(FV)

%% Return to Original Directory
cd(pwd1);
```

Appendix C

Optics

Before using optics in the COAL lab, a basic understanding of optics is needed. Some optics are easily damaged and if not used properly also can damage the source laser system.

Cleaning Optics

For best beam quality, the surface of all optics being used should be clean. Cleaning should be done upon initial installation of the optic and when necessary upon suspicion of dust or other surface contamination. All optical surfaces used in this experiment can be cleaned with a methanol solvent. However, as is the case for some filters, certain solvents can ruin the optic. Attention should be paid to this before using a new solution as a lens cleaner. To effectively clean the surface of an optic, methanol and optical cleaning wipes may be used to wipe away any impurities. Due to residue that can be left behind by the methanol, a particular method is described:

1. Gather the optic to be cleaned, a small ball driver, a small bottle of methanol with a dropper, and optical wipes; the methanol and ball driver may be found in the ball driver rack on the optics table, the optical wipes may be found in RAMAN drawer #4. The necessary supplies are display in Fig. C-1.

Figure C-1. Supplies for cleaning an optic

2. Place the optic on a wipe as in Fig. C-2 with the side to be cleaned facing up. In the case of mirrors, only the reflecting surface needs to be cleaned . An arrow drawn on the side of the optic points to the reflective side of a mirror or the curved side of a lens.

Figure C-2. Prepping optic for cleaning

3. Place another sheet of the optical wipes on top of the optic and off centered to a side. Place a drop of methanol on top of the sheet on the side of the optic that the sheet is off centered to. Using the ball driver to hold the lens in place from one

side, lightly drag the top sheet across the optic in the direction to pull the drop of methanol over the entire surface of the optic as in Fig. C-3.

Figure C-3. Drop and drag cleaning method

4. Upon inspection, no smudges or specs should be seen, leaving a nice clean optic.

To ensure that dust and other particles do not collect on the surface during the testing period, cover optics installed and in use with a plastic bag

Installation and Alignment

Several basic components are used to install an optic including the optic itself, an optic mount, a post, a post holder, and a base. Discretion may be made as to which type of each to use. The optic is first placed and secured in the mount with care taken to not over tighten the set screw. Be sure the side to be used of the optic is facing away from any adjustment screws or other obstructions on the mount. Blocking and scattering of a reflected or passed through line could occur if care is not made here. For mirrors, make sure the reflective side is facing toward the oncoming beam. For lenses, make sure the beam first hits the curved surface of a lens, then if another lens follows, the flat surface. In this way, the curved surface of the first lens should face the laser, and with multiple lenses the flat surfaces of lenses should face each other and the curved surfaces of lenses

face each other. If the flat surface of the first lens is facing the laser, reflections could bounce back into the laser and damage it.

The mount is secured to a post and inserted into a post holder that is attached to a base. The base is placed on the table and may be secured in the desired location. The set screw on the post holder may be used to fix the rotation of the lens and the height. Once the desired height has been established, a collar may be secured on the post directly above the post holder to hold the height constant when the post holder set screw is loosened for other adjustments to be made.

When installing bases on the table, care should be taken to the alignment of the beam. To ensure adjustments in the needed direction can be made, consecutive bases should be installed with the sliding screw channels oriented in opposite directions. The beam should be kept straight and level between optics and only make 90° turns at mirrors. To check the alignment of the beam between two optics, a business card can be taped to a post attached to a base. Placing the card directly behind the first optic and then moving the card along the same line of holes on the table to directly in front of the next optic will reveal if the beam walks off the center mark at all. Once the bases of the optics have been secured with the beam in generally good alignment, minor adjustments can be made with the set screws on the optic mounts. The alignment should be checked between every optic to ensure the beam does not walk at all.

To adjust the vertical height of the beam to the height needed in the test section, a simple installment of two mirrors on one post may be made. The first mirror reflects the beam to the needed height and the second mirror reflects the beam back to its original

direction. This arrangement is often referred to as a periscope and an example is shown in Fig. C-4.

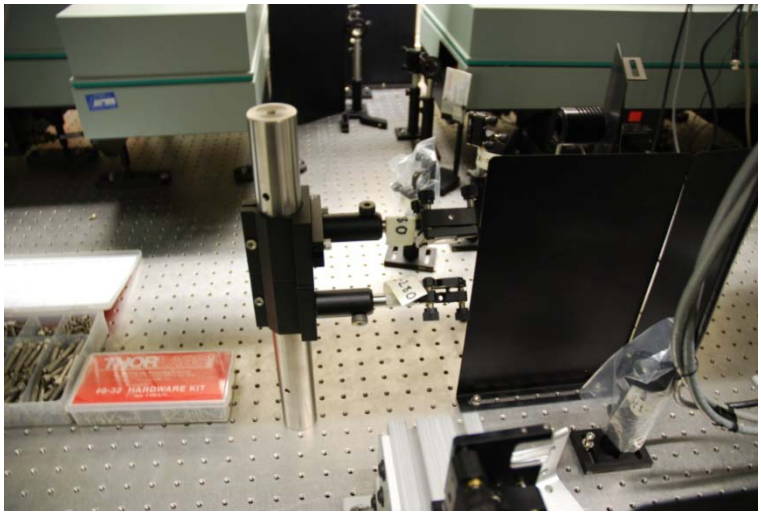

Figure C-4. Periscope to change laser height

In order to create a laser sheet to investigate a plane in the test section, a cylindrical lens is installed just before the test section. The curved surface of the lens is verified to be facing the oncoming beam, if not, the flat surface facing the beam could reflect it back to the laser and cause damage. After the cylindrical lens creates a laser sheet, a spherical lens is used to focus the sheet. The flat side of the spherical lens faces the oncoming beam. To determine which side is curved and flat, an arrow is drawn on the side of the spherical lens that point to the curved face. The lenses should be positioned at approximately the focal length of the lens away from the test section to focus it, however the focus length of each lens is rated for a certain wavelength and may vary, so some adjustment will probably need to be made until a focused sheet is achieved.

Besides optics, certain other components should also be installed. Irises should be placed in the middle of long sections of beams to clean up the beam and remove soft edges. While most the beam is reflected when using a mirror, some of the beam may still

pass straight through the mirror as illustrated in Fig. C-5. Beam dumps should then be installed behind the mirror to contain it. Beam dumps should especially be used early in the beam path where laser energy is high. Furthermore, beam shields should be installed on the table where possible to block any scattered light from damaging eyes or being picked up by a camera. The use of an iris and beam dump is shown in Fig. C-5.

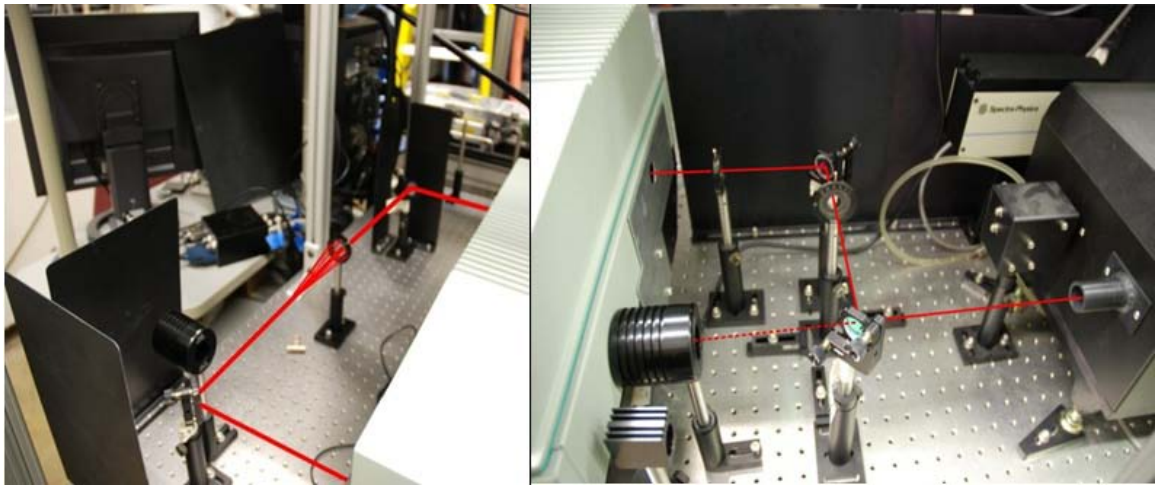

Figure C-5. Proper use of iris and beam dump

Appendix D

Hencken Burner Operations

Installation

1. The Hencken burner is mounted on a superstructure box containing mass flow controllers and solenoid valves as shown in Fig. D-1.

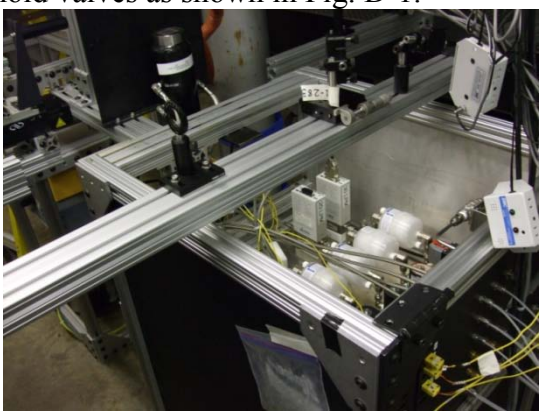

Figure D-1. Superstructure box

2. The mass flow controllers are connected to the Hencken burner with stainless steel flex lines and are installed to the base inside the structure. Connect the lines for the fuel, air, and co-flow to the burner
3. Upstream of the mass flow controllers, line filters are installed to prevent any solid particles from getting to the mass flow controller and causing damage. This arrangement is shown in Fig. D-2

Figure D-2. Filters and mass flow controllers

4. Solenoid regulators in Fig. D-3 are installed upstream of the filters inside the structure that block or pass all of the flow, an explosion proof solenoid is used for flammable gas lines.

Figure D-3. Solenoid regulators

5. Lines run from the box structure to a set of valves mounted on the wall of the lab.
6. The lines running along the ultimately connected to gas tanks in the tank farm.

Startup

1. Turn on the equipment switch on in Fig. D-4 located on the main control console

Figure D-4. Equipments switch

2. Turn the MKS controller panel power switch of Fig. D-5 on.

Figure D-5. MKS four channel readout

3. Turn on the main controlling computer shown in Fig. D-6 located in the middle of the lab. This computer controls Lab-View.

Figure D-6. COAL lab workstation

4. On the computer, open the Lab-View file: *Combustion Lab- Drenth.vi*, located on the desktop.
5. Click *run* from the top toolbar.
6. Verify that the valve on the black pressurized air tank of Fig. D-7 is on to supply instrument air.

Figure D-7. Instrument air control valve

7. Verify the regulator on the side of the black tank is set to approximately 80 psi.
8. Get the keys to the tank farm located on a hook on the main control console displayed in Fig. D-8.

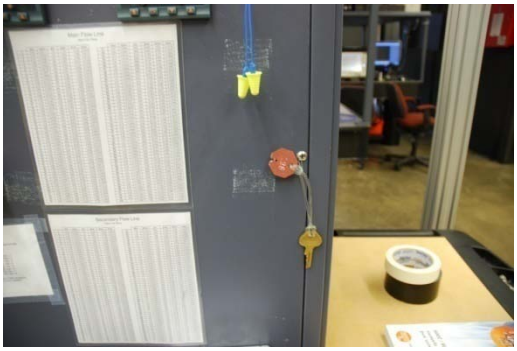

Figure D-8. Location of tank farm key

9. After opening the tank farm in Fig. D-9 and opening the valves on the air, nitrogen, and hydrogen tanks. Verify that enough pressure is in each tank for the extent of the experiment.

Figure D-9. Tank farm

10. On the side wall next to the black tank, open the valves for the air, nitrogen, and hydrogen.
11. Verify that the three mass flow controllers needed for the experiment are connected properly and the indicator lights are all green as displayed in Fig. D-10; if a light is red, turning the equipment switch off and on again may fix it.

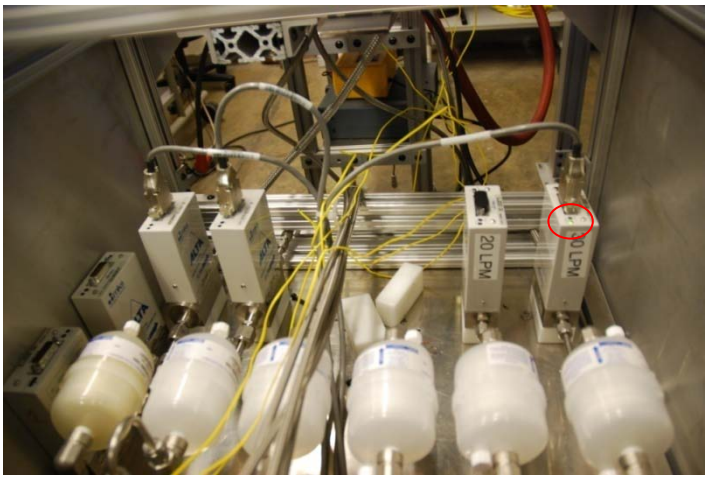

Figure D-10. MKS mass flow controller status light

12. With no flow on, zero the mass flow controllers by pressing the zeroing button on the top of each one with a small screwdriver.
13. On the MKS controller panel, set the desired percentages of the total flow rate for each mass flow controller by holding the set point switch up and turning the set screw, with the display knob turned to the appropriate channel.
14. In the Lab-View file, click the *Zero Air* and *Nitrogen* solenoid valve buttons to open the valves before the mass flow controllers and allow pressure to go to the mass flow controllers.

15. On the MKS controller panel, turn on the channel switches for the air and nitrogen line mass flow controllers.
    CAUTION: The mass flow controllers can be damaged if turned on without pressure going to them for extended periods of time, be sure that air is flowing through the mass flow controller before leaving it running.
16. In the Lab-View screen, click the *Hydrogen* solenoid valve button to open the valve for the hydrogen line.
17. On the MKS controller panel, turn on the channel switch for the hydrogen line.
18. After the hydrogen switch is turned on, ignite the gases with a sparker over the Hencken burner; a laminar flame should ignite similar to Fig. D-11.

Figure D-11. Hencken flame

Shutoff

1. Set the toggle switches for each channel to off on the MKS control panel, the flame will go out
2. Close the solenoid valves in the Lab-View program
3. Close the valves on the side wall
4. Turn off the flow from the gas tanks in the tank farm
5. Turn off the MKS controller
6. Stop the Lab-View program
7. Turn off the Equipment switch

Bibliography

1 BP. "BP Statistical Review of World Energy June 2008." 2008

2 Karbuz, S. "US military energy consumption – facts and figures." Energy Bulletin (2007): 10-20.

3 AIAA Position Paper, "Versatile Affordable Advanced Turbine Engines (VAATE) Initiative," AIAA Air Breathing Propulsion Technical Committee, Reston, VA, January 2006.

4 Anthenien, R. A., Mantz, R. A., Roquemore, W. M., & Sturgess, G. "Experimental Results for a Novel, High Swirl, Ultra Compact Combustor for Gas Turbine Engines." *2nd Joint Meeting of the United States Section of the Combustion Institute*. Oakland CA, 2001.

5 Edwards, T. "Advancements in Gas Turbine Fuels From 1943 to 2005." Transactions of the ASME.

6 Mattingly, J. D. *Elements of Gas Turbine Propulsion.* New York: McGraw-Hill, Inc. 1996.

7 Liu, F., & Sirignano, W. A. "Turbojet and turbofan engine performance increases through turbine burners." *38th Aerospace Sciences Meeting and Exhibit.* Reno NV, 2000.

8 Zelina, J., Sturgess, G. J., & Shouse, D. T. *The Behavior of an Ultra-Compact Combustor (UCC) Based on Centrifugally-Enhanced Turbulent Burning Rates*. 2004.

9 Zelina, J., Sturgess, G. J., Manour, A., & Hancock, R. D. *Fuel injector design for an ultra-compact combustor.* No. ISABE-2003-1141. 2003.

10 Anisko, J. *Numerical Investigation of Cavity-Vane Interactions Within the Ultra Compact Combustor*. MS thesis, AFIT/GAE/ENY/06-M01. Graduate School of Engineering and Management, Air Force Institute of Technology (AU), Wright-Patterson AFB OH, March 2006.

11 Zelina, J., Shouse, D. T., & Neuroth, C. *High Pressure Tests of a High-g Ultra-Compact Combustor*. 2005.

12 Thornburg, H., Sekar, B., Zelina, J., and Greenwood, R. "Numerical Study of an Inter-Turbine Burner (ITB) Concept with Curved Radial Vane." *45th AIAA Aerospace Sciences Meeting and Exhibit*. AIAA-2007-649. Reno NV, January 2007.

13 Koether, S. J. *Validation of the AFIT Small Scale Combustion Facility and OH Laser-Induced Fluorescence of an Atmospheric Laminar Premixed Flame.* MS thesis, AFIT/GAE/ENY/07-S03. Graduate School of Engineering and Management, Air Force Institute of Technology (AU), Wright-Patterson AFB OH, September 2007.

14 Dittman, E. R. *Design, Build and Validation of a Small Scale Combustion Chamber Testing Facility*. MS thesis, AFIT/GAE/ENY/06-M06. Graduate School of Engineering and Management, Air Force Institute of Technology (AU), Wright-Patterson AFB OH, March 2006.

15 Sirignano, W.A., Delplanque, J.P., and Liu, F. "Selected Challenges in Jet an Rocket Engine Combustion Research." *33rd AIAA/ASME/SAE/ASEE Joint Propulsion Conference.* AIAA-97-2701. Seattle WA, 1997.

16 Sirignano, W.A. and F. Liu. "Performance Increases for Gas-Turbine Engines Through Combustion Inside the Turbine." *Journal of Propulsion and Power*, Volume 15,No. 1. January-February 1999.

17 Zelina, J., Ehret, J., Hancock, R. D., Shouse, D. T., and Roquemore, W. M., "Ultra-Compact Combustion Technology Using High Swirl for Enhanced Burning Rate," 38th AIAA/SAE/ASME/ASEE Joint Propulsion Conference & Exhibit, AIAA-2002-3725, Indianapolis, IN, July 2002.

18 Mawid, M. A., Thornburg, H., Sekar, B., Zelina, J., "Performance of an Inter-Turbine Burner (ITB) Concept with Three-Different Vane Cavity Shapes," *42nd AIAA/SAE/ASME/ASEE Joint Propulsion Conference & Exhibit.* AIAA-2006-4740. Sacramento CA, July 2006.

19 Hsu, K-Y, and Goss, L. P., "Characteristics of a Trapped-Vortex Combustor," *Journal of Propulsion and Power,* Vol. 14, No. 1. 1998.

20 Roquemore, W. M., Shouse, D., Burrus, D., Johnson, A., Cooper, C., & Duncan, B., et al. "Trapped vortex combustor concept for gas turbine engines." *39th AIAA Aerospace Sciences Meeting & Exhibit.* Reno NV, 2001.

21 Lewis, G. D. "Swirling flow combustion -- fundamentals and application." *AIAA/SAE 9th Propulsion Conference.* Las Vegas Nevada, 1973.

22 Yonezawa, Y., Toh, H., Goto, S., & Obata, M. "Development of the jet-swirl high loading combustor." *AIAA/SAE/ASME/ASEE 26th Joint Propulsion Conference,* Orlando FL, 1990.

23 Quaale, R. J. *Experimental Results for a High Swirl, Ultra Compact Combustor for Gas Turbine Engines*. MS thesis, AFIT/GAE/ENY/03-5. Graduate School of

Engineering and Management, Air Force Institute of Technology (AU), Wright-Patterson AFB OH, 2003.

24 Moenter, D. S. *Design and Numerical Simulation of Two-Dimensional Ultra Compact Combustor Model Sections for Experimental Observation of Cavity-Vane Flow Interactions*. MS thesis, AFIT/GAE/ENY/06-S07. Graduate School of Engineering and Management, Air Force Institute of Technology (AU), Wright-Patterson AFB OH, September 2006.

25 Anderson, W. S. *Design, Construction, and Validation of the AFIT Small Scale Combustion Facility and Sectional Model of the Ultra-compact Combustor.* MS thesis, AFIT/GAE/ENY/07-M01. Graduate School of Engineering and Management, Air Force Institute of Technology (AU), Wright-Patterson AFB OH, March 2007.

26 Greenwood, R. T. *Numerical Analysis and Optimization of the Ultra Compact Combustor*. MS thesis, AFIT/GAE/ENY/05-M10. Graduate School of Engineering and Management, Air Force Institute of Technology (AU), Wright-Patterson AFB OH, March 2005.

27 Hankins, T. B., *Laser Diagnostic System Validation and Ultra-Compact Combustor Characterization*. MS thesis, AFIT/GAE/ENY/08-M14. Graduate School of Engineering and Management, Air Force Institute of Technology (AU), Wright-Patterson AFB OH, March 2008.

28 Lakusta, P. J., *Laser-Induced Fluorescence and Performance Analysis of the Ultra-Compact Combustor*. MS thesis, AFIT/GAE/ENY/08-J03. Graduate School of Engineering and Management, Air Force Institute of Technology (AU), Wright-Patterson AFB OH, June 2008.

29 Hunecke, K. Jet Engines. Biddles, Ltd. Great Britain, 1997.

30 Society of Automotive Engineers, Inc., "Aerospace Recommended Practice: Procedure for the Analysis and Evaluation of Gaseous Emissions from Aircraft Engines." ARP1533, Warrendale, PA: 2004.

31 Turns, S. R. *An Introduction to Combustion* (2nd Ed.). New York: McGraw-Hill, Inc., 1996.

32 Zamorano, M. "B-52 synthetic fuel testing: Center commander pilots first Air Force B-52 flight using solely synthetic fuel blend in all eight engines". *Aerotech News and Review*. 22 December 2006.

33 Beatriz, R., Bartsch, T., "The United States Air Force's Process for Alternative Fuels Certification." American Institute of Aeronautics and Astronautics AIAA 2008-6412, 2008

34 Isleb, C., US military energy consumption- facts and figues http://www.energybulletin.net/node/29925#, 10 June 2009

35 Eckbreth, A. C. In Gupta A. K., Lilley D. G. (Eds.), *Laser Diagnostics for Combustion Temperature and Species*. Abacus Press, Tunbridge Wells Kentucky, 1998.

36 Eckbreth, A. C., Bonczyk, P. A., & Verdieck, J. F. "Combustion diagnostics by laser raman and fluorescence techniques." *Progress in Energy and Combustion Science, 5*, 253-322. 1979.

37 Seitzman, J. M., R. K. Hanson, P. A. DeBarber, and C. F. Hess. "Application of quantitative two-line OH planar laser-induced fluorescence for temporally resolved planar thermometry in reacting flows." Applied Optics, Vol. 33, No. 18. June 1994.

38 Tamura, Masayuki, Pamela A. Berg, Joel E. Harrington, Jorge Luque, Jay B. Jefferies, Gregory P. Smith, and David R. Crosley. "Collisional Quenching of CH(A), OH(A), and NO(A) in Low Pressure Hydrocarbon Flames." *Combustion and Flame*. Vol 114, pp. 502-514. 1998.

39 Kostka, S., Roy, S., Lakusta, P. J., Meyer, T.R., Renfro, M.W., Gord, J.R., Branam, R. "Comparison of line-peak and line-scanning excitation in two-color laser-induced-fluorescence thermometry of OH". *Applied Optics*, 16 October 2009.

40 Spectra-Physics Lasers & Photonics. *Quanta-Ray Lab-Series Pulsed Nd:YAG Lasers User's Manual.* Mountain View CA, 2001.

41 Reynolds, William C. "STANJAN: Equilibrium solver." Stanford University CA, 1995.

42 Giezendanner-Thoben, R., Meier, U., Meier, W., Heinze, J., Aigner, M., "Phase-locked two-line OH planar laser-induced fluorescence thermometry in a pulsating gas turbine model combustor at atmospheric pressure." *Applied Optics*, 1 November 2009.

43 Devillers, R., Brunequx, G., Schulz, C. "Developments of a two-line OH-laser-induced fluorescence thermometry diagnostics strategy for gas-phase termperature measurments in engines." *Applied Optics. Vol. 47, No. 31 1 November 2008.*

44 Hancock, R. D., Bertagnolli, K. E., Lucht, R. P. Nitrogen and Hydrogen CARS Temperature Measurements in a Hydrogen / Air Flame Using a Near-Adiabatic Flat-Flame Burner. *Combustion and Flame 109, pp. 323-331*. 1997.

VI. Vita

Captain Aaron C. Drenth graduated from George-Little Rock High School in George, Iowa. He received an ROTC commissioning scholarship in February 1999. Graduating from South Dakota State University with a Bachelor of Science in Mechanical Engineering, he was commissioned as a Second Lieutenant in May 2004.

His first assignment was to the 28th Test and Evaluation Squadron, Eglin AFB, Florida where he served as an operational and flight test engineer. There he coordinated live fire tests of air-to-ground weapons such as AGM-65H/K Maverick, GBU-31/38/54 JDAM, and GBU-10/12 LGBs from F-16C/D, F-15E, B-2, and B-52 aircraft. In September 2008, he entered the Graduate School of Engineering and Management, Air Force Institute of Technology. Upon graduation he will be assigned to the United States Air Force Academy, as an Instructor in the Engineering Mechanics Department.

REPORT DOCUMENTATION PAGE

Form Approved
OMB No. 074-0188

1. REPORT DATE *(DD-MM-YYYY)*	**2. REPORT TYPE**	**3. DATES COVERED** *(From – To)*
20-11-2009	Master's Thesis	Sept 2008 – Dec 2009

4. TITLE AND SUBTITLE

Laser-Induced Fluorescence And Synthetic Jet Fuel Analysis In The Ultra Compact Combustor

5a. CONTRACT NUMBER

5b. GRANT NUMBER

5c. PROGRAM ELEMENT NUMBER

6. AUTHOR(S)

Drenth, Aaron C., Captain, USAF

5d. PROJECT NUMBER

5e. TASK NUMBER

5f. WORK UNIT NUMBER

7. PERFORMING ORGANIZATION NAMES(S) AND ADDRESS(S)

Air Force Institute of Technology
Graduate School of Engineering and Management (AFIT/EN)
2950 Hobson Way, Building 640
WPAFB OH 45433-8865

8. PERFORMING ORGANIZATION REPORT NUMBER

AFIT/GAE/ENY/09-D03

9. SPONSORING/MONITORING AGENCY NAME(S) AND ADDRESS(ES)

Air Force Office of Scientific Research
Dr. Julian Tishkoff
4015 Wilson Boulevard, Room 713 Arlington, VA 22203-1954

10. SPONSOR/MONITOR'S ACRONYM(S)
AFOSR

11. SPONSOR/MONITOR'S REPORT NUMBER(S)

12. DISTRIBUTION/AVAILABILITY STATEMENT

APPROVED FOR PUBLIC RELEASE; DISTRIBUTION UNLIMITED.

13. SUPPLEMENTARY NOTES

14. ABSTRACT

The Ultra Compact Combustor is currently under investigation at the Air Force Institute of Technology and Air Force Research Laboratory's Propulsion Directorate. This combustor is a small-scale, axi-symmetric, atmospheric pressure, laboratory combustor with an outer circumferential cavity in which the flame is stabilized by a highly accelerated swirled flow. This ultra-compact combustor (UCC) will enable aero gas turbine reheat cycle engines and significantly shorten conventional aero gas turbine engines. The experiments of this work utilized the AFIT small-scale combustion diagnostics facility, investigating a sector model of the UCC. The objectives of this research was to perform an addition to and validation of the COAL lab laser diagnostic system and to begin the characterization of a small-scale model of an UCC using hydrogen, and both traditional and synthetic jet fuels. Validation of the laser system was accomplished by using two-line planar laser induced fluorescence (PLIF) on a laminar premixed hydrogen-air flame produced by a Hencken burner. OH species concentrations were measured. Flame temperatures were determined with a two-line fluorescence technique using different transitions in the (1,0) band of the OH (A-X) electronic transition system. Comparisons are made to existing research to prove accuracy. Operational procedure of the Hencken burner and UCC were modified as necessary. The ignition system was modified and UCC starting conditions have been updated. Emissions data was collected using synthetic jet fuel and compared to traditional jet fuel. Future work will involve using PLIF to further study the cavity-vane interactions of the UCC.

15. SUBJECT TERMS

Combustion, Combustors, Laser Diagnostics, Ultra-Compact Combustor, Laser-Induced Fluorescence, Hencken

16. SECURITY CLASSIFICATION OF:			**17. LIMITATION OF ABSTRACT**	**18. NUMBER OF PAGES**	**19a. NAME OF RESPONSIBLE PERSON**
a. REPORT	**b. ABSTRACT**	**c. THIS PAGE**			Richard Branam, Lt Col, USAF
U	**U**	**U**	**UU**	163	**19b. TELEPHONE NUMBER** *(Include area code)* (937) 255-6565, ext 7485 (richard.branam@afit.edu)

Standard Form 298 (Rev. 8-98)
Prescribed by ANSI Std. Z39-18